International Collaborations on Engineered Barrier Systems: Experimental and Modeling Investigations Report

Fuel Cycle Research & Development

FCRD-UFD-2014-000058

Prepared for
U.S. Department of Energy
Used Fuel Disposition Campaign

Jonny Rutqvist, Carl Steefel,
Fei Chen, Jim Houseworth, Victor Vilarrasa, Hui-Hai Liu, Jens Birkholzer
Lawrence Berkeley National Laboratory

Carlos F. Jové Colón
Sandia National Laboratories

Mei Ding
Los Alamos National Laboratories

December, 2013

SAND2014-0069 P

Prepared by:
Sandia National Laboratories
Albuquerque, New Mexico 87185

Sandia National Laboratories is a multi-program laboratory managed and operated by Sandia Corporation, a wholly owned subsidiary of Lockheed Martin Corporation, for the U.S. Department of Energy's National Nuclear Security Administration under contract DE-AC04-94AL85000.

FCT DOCUMENT COVER SHEET

Revision 2
12/20/2012

APPENDIX E

FCT DOCUMENT COVER SHEET [1]

Name/Title of Deliverable/Milestone/Revision No. International Collaborations on Engineered Barrier Systems: Experimental and Modeling Investigations Report (M2FT-14SN0806054)

Work Package Title and Number DR Argillite Disposal R&D - SNL, FT-14SN080605

Work Package WBS Number 1.02.08.06

Responsible Work Package Manager Carlos F. Jove Colon (Name/Signature)

Date Submitted: 12/11/2013

Quality Rigor Level for Deliverable/Milestone[2]	☒ QRL-3	☐ QRL-2	☐ QRL-1 Nuclear Data	☐ Lab/Participant QA Program (no additional FCT QA requirements)

This deliverable was prepared in accordance with Sandia National Laboratories
(Participant/National Laboratory Name)

QA program which meets the requirements of

☒ DOE Order 414.1 ☐ NQA-1-2000 ☐ Other

This Deliverable was subjected to:

☐ Technical Review

Technical Review (TR)
Review Documentation Provided

☐ Signed TR Report or,
☐ Signed TR Concurrence Sheet or,
☒ Signature of TR Reviewer(s) below

Name and Signature of Reviewers

Charles R. Bryan

☐ Peer Review

Peer Review (PR)
Review Documentation Provided

☐ Signed PR Report or,
☐ Signed PR Concurrence Sheet or,
☐ Signature of PR Reviewer(s) below

Charles R. Bryan

NOTE 1: *Appendix E should be filled out and submitted with the deliverable. Or, if the PICS:NE system permits, completely enter all applicable information in the PICS:NE Deliverable Form. The requirement is to ensure that all applicable information is entered either in the PICS:NE system or by using the FCT Document Cover Sheet.*

NOTE 2: *In some cases there may be a milestone where an item is being fabricated, maintenance is being performed on a facility, or a document is being issued through a formal document control process where it specifically calls out a formal review of the document. In these cases, documentation (e.g., inspection report, maintenance request, work planning package documentation or the documented review of the issued document through the document control process) of the completion of the activity, along with the Document Cover Sheet, is sufficient to demonstrate achieving the milestone. If QRL 1, 2, or 3 is not assigned, then the Lab / Participant QA Program (no additional FCT QA requirements) box must be checked, and the work is understood to be performed and any deliverable developed in conformance with the respective National Laboratory / Participant, DOE or NNSA-approved QA Program.*

AKNOWLEDGEMENTS

The authors acknowledge our gratitude to Yifeng Wang (SNL), Ernest Hardin (SNL), Peter Swift (SNL), Kevin McMahon (SNL), David Sassani (SNL), Glenn Hammond (SNL), Charles R. Bryan (SNL), William Spezialetti (DOE NE-53), Prasad Nair (DOE NE-53), Mark Tynan (DOE NE-53), and Tim Gunther (DOE NE-53), for their helpful discussions on various topics covered in this report.

SUMMARY

International research collaborations on deep geological disposition of nuclear waste are a key aspect of the nation's strategy to investigate disposal design concepts in geologic settings considered by other countries. Leveraging on such international partnerships translates to gains of scientific knowledge and is also a cost-effective strategy towards the development and enhancement of the Used Fuel Disposition (UFD) R&D activities. Several international partners operate underground research laboratories (URLs) to conduct short- and long-term field experiments in different types of host rock (clay/argillite, granite, salt). Such URL sites provide a unique opportunity to engage in field- and laboratory-scale research activities analyzing the performance of the engineered barrier systems (EBS) though multifaceted experiments targeting coupled processes (e.g., THMC). These types of experimental observations serve as the basis for the validation of coupled processes models and in parallel also provide crucial information on model constraints and input data needs.

This report centers on results obtained on THM simulations, reactive transport model development, and engineered barrier system (EBS) material characterization studies. These activities include modeling of field experiments at the Mont Terri URL, Switzerland, and the Horonobe URL, Japan. It also includes a characterization study of heterogeneous media represented by cement – Opalinus Clay interactions in a backfilled borehole. Related to cement interactions, modeling tools have been used to describe phase equilibria relations and 1D reactive transport modeling of cement – clay interactions. Modeling of coupled THM processes in the EBS is part of the international DECOVALEX-2015 project which is an acronym for the 6th and current phase of the ongoing "Development of Coupled Models and their Validation against Experiments" from 2012 to 2015. The Colloid Formation and Migration (CFM) international activity is described in the report "Natural System Evaluation and Tool Development - International Collaborations: FY13 Progress Report (FCRD-UFD-2013-000628)" by Wang et al. (2013).

The involvement in DECOVALEX-2015 where LBNL is a key participant in Task B includes:

- Subtask B1: HE-E Heater Test – Studies of bentonite/rock interaction to evaluate sealing and clay barrier performance, in a micro-tunnel at the Mont Terri URL, Switzerland – Coupled THM modeling of the HE-D experiment using the TOUGH-FLAC model:
    - Good agreement has been obtained for the temperature-time profiles between simulation and field data. Reasonably good agreement between simulated and measured pressure is achieved for a given value of permeability and pore compressibility.
    - Comparisons of thermal modeling results between different participating teams (and different coupled models) are in good agreement with observed temperatures.
    - These comparisons illustrate the importance of anisotropic heat conductivity of Opalinus Clay.
    - In the buffer material study (modeling a column experiment on granular MX-80 bentonite), temperature and relative humidity (RH) predictions are in reasonable agreement with measurements.

- Subtask B2: EBS Experiment – Studies of the thermo-hydro-mechanical-chemical (THMC) behavior of the EBS under heating conditions in both the early resaturation and post-closure stage of the repository and its interaction with the clay host rock (vertical emplacement hole) at the Horonobe URL in Japan:
    - 1D TH and THM benchmark modeling test using TOUGH2 and ROCMAS, respectively. In this step, simulations were conducted using properties and boundary conditions stipulated by the JAEA to become familiarized with the problem and for comparison of code results. Later, a realistic model of the experimental design will be constructed and a predictive thermal load analysis will be performed.

Modeling Reactive diffusive transport of the DR-A (diffusion and retention) borehole experiment in Opalinus Clay:

- Development of a new reactive diffusion model to simulate the DR-A borehole test:
    - DR-A test: a single borehole drilled in Opalinus Clay that contains a constant ionic strength cocktail of anions, cations, and non-reactive tracers (tritium (HTO)).
    - The new model for diffusive transport includes an explicit Electrical Double Layer (EDL) model (CrunchEDL code)
    - Preliminary simulations show that the anion exclusion effect seems to lessen when the ionic strength is increased. This requires lower diffusion coefficients in the EDL for the anions to capture this effect.
    - FY14 work will focus on refining the EDL-explicit model to the current DR-A experiment, focusing on evaluating the anion exclusion effect with increasing ionic strength based on the rapid out-diffusion of iodide and bromide.

Cement-Clay Interactions in Engineered Barrier Systems in Opalinus Clay:

- Opalinus Clay interaction (CI) Experiment at Mt Terri, Switzerland. Phase 12 of the experiment began in 2007 by filling two boreholes with ordinary portland cement (OPC), bentonite, and low-pH cement to characterize cement – Opalinus Clay interactions.
- After a few years, sampling boreholes were drilled transecting the interfaces between the cement and host rock:
    - A small-angle neutron scattering (SANS) study on OPC concrete – Opalinus Clay sample was conducted for the characterization of pores form the nano- to micron-scale.
    - SANS analysis targeted three sample regions: cement phase, interface, and Opalinus Clay rock.
    - Sufficient difference to resolve distinct pore structures for these three regions makes this technique highly suitable to provide a statistical description of heterogeneous media in an intact core sample.
- 1D reactive transport modeling using the open-source massively parallel code PFLOTRAN: Results from diffusion modeling are in good agreement with the expected change in pH for cement – clay pore water interactions. The CI collaborative project has a modeling phase for which this tool can be applied to cement – clay interactions and migration of the hyperalkaline reactive front.
- Evaluation of cement equilibrium phase relations and generation of activity phase diagrams using the CHNOSZ package in the R language platform.
- The CI collaboration activity will not continue in FY14.

CONTENTS

FIGURES

TABLES

ACRONYMS

BBM	Basic Barcelona Model
CIEMAT	Centro de Investigaciones Energéticas, Medioambientales y Tecnológicas
CFM	Colloid Formation and Migration
CI	Cement – Opalinus Clay Interaction (Mt. Terri URL)
DOE	Department of Energy
EBS	Engineered Barrier System
EDL	Electrical Double Layer
FEPs	Features, Events, and Processes
FLAC	Fast Lagrangian Analysis of Continua
GWB	Geochemist's Workbench®
JAEA	Japan Atomic Energy Agency
LANL	Los Alamos National Laboratory
LBNL	Lawrence Berkeley National Laboratory
LQD	Low-Q Diffractometer
NBS	Natural Barrier System
NEA	Nuclear Energy Agency
OBIGT	OrganoBioGeoTherm
OECD	Organization for Economic Cooperation and Development
OPA	Opalinus Clay Rock (Mt. Terri URL)
OPC	Ordinary Portland Cement
R&D	Research and Development
SANS	Small-Angle Neutron Scattering
SNL	Sandia National Laboratories
THM	Thermal-Hydrological-Mechanical
THMC	Thermal-Hydrological-Mechanical-Chemical
TOUGH	Transport of Unsaturated Groundwater and Heat
UFD	Office of Used Fuel Disposition Research and Development
URL	Underground Research Laboratory

1. INTRODUCTION

Recognizing the benefits of international collaboration in the common goal of safely and efficiently managing the back end of the nuclear fuel cycle, DOE's Office of Nuclear Energy (NE) and its Office of Used Fuel Disposition Research and Development (UFD) have developed a strategic plan to advance cooperation with international partners (Birkholzer et al., 2013; UFD, 2012). The strategic plan lays out two interdependent areas of international collaboration. The first area is cooperation with the international nuclear community through participation in international organizations, working groups, committees, and expert panels. Such participation typically involves conference and workshop visits, information exchanges, reviews, and training and education. The second area of international collaboration is active R&D participation of U.S. researchers within international projects or programs (UFD, 2012). By active R&D, it is meant here that U.S. researchers work closely together with international scientists on specific R&D projects relevant to both sides. With respect to geologic disposal of radioactive waste, such active collaboration provides direct access to information, data, and expertise on various disposal options and geologic environments that have been collected internationally over the past decades. Many international programs have operating underground research laboratories (URLs) in clay/shale, granite, and salt environments, in which relevant field experiments have been and are being conducted. Depending on the type of collaboration, U.S. researchers can participate in planning, conducting, and interpreting experiments in these URLs, and thereby get early access to field studies without having *in situ* research facilities in the United States.

UFD considers this second area, active international R&D, to be very beneficial in achieving the program's long-term goals of conducting "experiments to fill data needs and confirm advanced modeling approaches" (by 2015) and of having a "robust modeling and experimental basis for evaluation of multiple disposal system options" (by 2020). Advancing opportunities for active international collaboration with respect to geologic disposal has therefore been the primary focus of UFD's international strategy in the recent year (Birkholzer et al., 2013; Birkholzer, 2012).

Here we report LBNL, SNL, and LANL activities related to international collaborations on THM simulations, reactive transport model development, and engineered barrier system (EBS) material characterization studies. These activities include modeling of field experiments at the Mont Terri URL, Switzerland, and the Horonobe URL, Japan. They also includes a characterization study of heterogeneous media represented by cement – Opalinus Clay interactions in a backfilled borehole. The Colloid Formation and Migration (CFM) international activity is described in the report "Natural System Evaluation and Tool Development - International Collaborations: FY13 Progress Report (FCRD-UFD-2013-000628)" by Wang et al. (2013). Dr. David Sassani (SNL) participated as an Associated Group in the Second Annual Workshop for FIRST – NUCLIDES in Antwerp, Belgium, November 5 through 7, 2013. The first results of this program were presented from this 3- year European Union Collaborative Project on the instant release fraction for high burn-up fuels. Topics covered sample preparation and characterization techniques, fission gas releases, leaching studies, and model development. Dr. Sassani was the only US representative in the workshop that had about 75 participants from

about 10 countries. Abundant interactions with technical staff from the wide variety of institutions provided opportunities for discussion and time to review the US DOE Used Fuel Disposition Campaign progress on used fuel degradation. It should be noted that Dr. Sassani's participation in this workshop was on the capacity of an Associated Group and there is no R&D participation associated with this activity.

Sections 2 and 3 below present activities related to THM and reactive transport modeling, respectively. These activities address key Features, Events and Processes (FEPs), which have been ranked in importance from medium to high, as listed in Tables 7 and 8 of the *Used Fuel Disposition Campaign Disposal Research and Development Roadmap* (FCR&D-USED-2011-000065 REV0) (Nutt, 2011). Specifically, they address FEP 2.2.01, Excavation Disturbed Zone (EDZ) for shale; FEP 2.1.04.01, Buffer/Backfill; FEPs 2.1.07.02, 03, 04, 09, Mechanical Processes; FEPs 2.1.08.03, 07, 08, Hydrologic Processes; and FEP 2.1.11.04, Thermal Processes, by studying coupled processes in the EBS and its interaction with the natural barrier system (a shale formation); and FEPs 2.1.09.52, 53, 54, Chemical Processes—Transport, by investigating reactive-diffusive radionuclide transport in bentonite and/or a shale formation.

Section 4 describes the cement – Opalinus Clay interaction (CI) experiment at Mont Terri and the small-angle neutron scattering (SANS) characterization study performed at LANL. In addition, tools for thermodynamic analysis and reactive transport modeling are also advanced for the evaluation of cement – clay interactions. This research addresses issues outlined by Nutt (2011) on the "State of the Art" related to cementitious materials in the EBS. For example, as stated in Nutt (2011), "As an example, considerable effort has been undertaken in other countries to understand radionuclide transport properties in bentonite buffers, while less work has been performed to understand the effects of cementitious materials in deep geologic environments." Also, an alkaline plume from cementitious materials leaching from the disposal gallery can potentially interact with the host rock. These investigations address the following FEPS ranked medium through high in Nutt (2011): Buffer/Backfill Materials: 2.1.04.01 (high); Chemical Processes-Transport: 2.1.09.01, .03, .07, .09, .13 (medium-high); seals: 2.1.05.01 (medium).

2. MODELING COUPLED THM PROCESSES IN EBS

LBNL and SNL (Natural System – Bedrichov Tunnel Tests) are participating research teams in the international DECOVALEX-2015 project. DECOVALEX is a unique international research collaboration, initiated in 1992 for advancing the understanding and mathematical modeling of coupled thermo-hydro-mechanical (THM) and thermo-hydro-mechanical-chemical (THMC) processes in geological systems—subjects of importance for performance assessment of radioactive waste repositories in geological formations. DECOVALEX-2015 is an acronym for the 6th and current phase of the "Development of Coupled Models and their Validation against Experiments" project that is ongoing from 2012 to 2015. In DECOVALEX-2015, LBNL participates in Task B which includes:

Subtask B1) HE-E Heater Test: Studies of bentonite/rock interaction to evaluate sealing and clay barrier performance, in a micro-tunnel at the Mont Terri URL in Switzerland; and

Subtask B2) EBS Experiment: Studies of the thermo-hydro-mechanical-chemical (THMC) behavior of the EBS under heating conditions in both the early resaturation and post-closure stage of the repository and its interaction with the clay host rock, in a vertical emplacement hole at the Horonobe URL in Japan

The model simulations related to these two tasks are carried out using the TOUGH-FLAC simulator (Rutqvist et al., 2002; 2011), which is based on linking the TOUGH2 multiphase flow and heat transport simulator (Pruess et al., 2011) with the FLAC3D geomechanical simulator (Itasca, 2009). The TOUGH-FLAC simulator has been further developed within the UFD campaign and has since been applied to issues related to nuclear waste disposal in clay host rocks, involving bentonite-backfilled emplacement tunnels. As part of this effort, the Barcelona Basic model (BBM) has been implemented for advanced modeling of bentonite backfill behavior (Rutqvist et al., 2013a). The most recent model development involved implementation of a dual-structure model for clay mechanical behavior and an extension to coupled THMC processes related to clay swelling. LBNL is also involved in coupled THM modeling of the Mont Terri URL FE experiment, which is a major large scale field experiment, simulating a full-scale bentonite backfilled repository tunnel. The recent work related to these model developments and modeling of the Mont Terri FE experiment were presented in two recent UFD milestone reports (Davis et al., 2013; Liu et al., 2013).

2.1 Task B1: MONT TERRI URL HE-E HEATER TEST

The Mont Terri URL HE-E Heater Test focuses on THM behavior of bentonite barriers in the early nonisothermal resaturation stage and their THM interaction with Opalinus clay (Figure 2.1). The objective is to better understand the evolution of a disposal system of high level waste in the early post-closure period with emphasis on the thermal evolution, buffer resaturation (*in situ* determination of the thermal conductivity of bentonite and its dependency on saturation), pore water pressure in the near field, and the evolution of swelling pressures in the buffer. Because the test is conducted in a micro-tunnel (at 1:2 scale), it is considered a validation, not a demonstration experiment. The heating test involves two types of bentonite buffer materials (Figure 2.1, left). The heater-buffer interface is heated to a maximum temperature of 135^{o}C and a temperature of 60–70^{o}C is expected at the buffer-rock interface. A dense instrumentation network was in place in the host rock surrounding the micro-tunnel from a previous experiment testing the impact of ventilation on the clay host rock. This netwrok has been improved for the purpose of the HE-E Heater Test (up to 40 piezometers in total); various sensors have also been placed in the buffer material. The heating phase was initiated in late summer of 2011 and is being continued for at least three years.

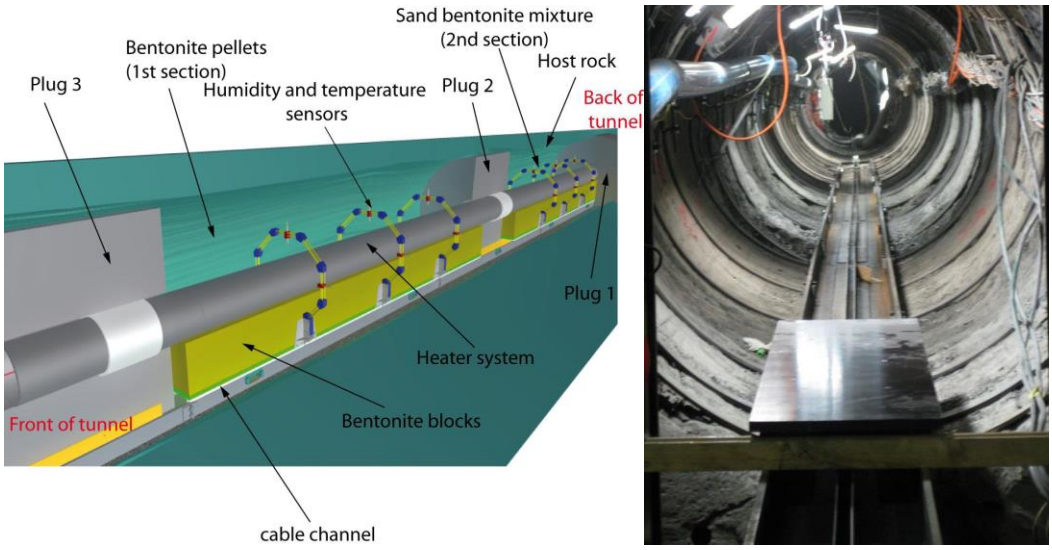

Figure 2.1. Schematic setup of HE-E heater test at Mont Terri and photo of micro-tunnel (Garritte, 2012).

In DECOVALEX-2015 (Task B1), eight international research teams are participating in the modeling of the HE-E experiment. Task B1, which is running over 3 years, is divided into the following steps:

- Step 1a: Opalinus clay study including HE-D experiment, literature study, processes understanding and parameter determination.
- Step 1b: Buffer material study including CIEMAT column cells, literature study, processes understanding and parameter determination.
- Step 2: HE-E predictive modeling using as-built characteristics and true power load. Modeling is 2D (axisymmetric, plane strain or combination) and 3D.
- Step 3: HE-E interpretative modeling when data are made available.

Step 1a started in 2012 with the modeling of the previous HE-D experiment for *in situ* characterization of THM material parameters for the Opalinus Clay. The DECOVALEX-2015 project is currently in Step 1b, which is a study of buffer material properties through modeling of laboratory experiments on buffer material samples. The buffer material study is mainly focused on modeling and analysis of a THM column experiment conducted by CIEMAT, Spain.

In the following subsections, we present the results of the modeling of the HE-D experiment and the current status on the modeling of CIEMAT column experiment.

2.1.1 Modeling of the HE-D Experiment

The HE-D experiment was conducted between March 2004 and June 2005 by *in situ* heating of Opalinus Clay from two heaters placed in a horizontal borehole (Figure 2.2) (Wileveau, 2005; Gens et al., 2007). Around this heating borehole, approximately 30 temperature sensors, 10 water pressure sensors, and 3 extensometers were placed, which allowed for monitoring the evolution

of the variables induced by the heating (Wileveau, 2005; Gens et al., 2007). Approximately one month after installation, the heaters were switched on with a total power of 650 W (325 W per heater). The heaters were then left under constant power for 90 days. Afterwards, the power was increased threefold, to 1950 W (975 W per heater), and maintained at that level for a further 248 days. At the end of this second heating stage, the heaters were switched off and the clay was allowed to cool. Temperature, pore pressure, and deformation were measured for the duration of the experiment. In Figure 2.2, the positions of the main temperature and pore pressure sensors with respect to the heater axis are indicated.

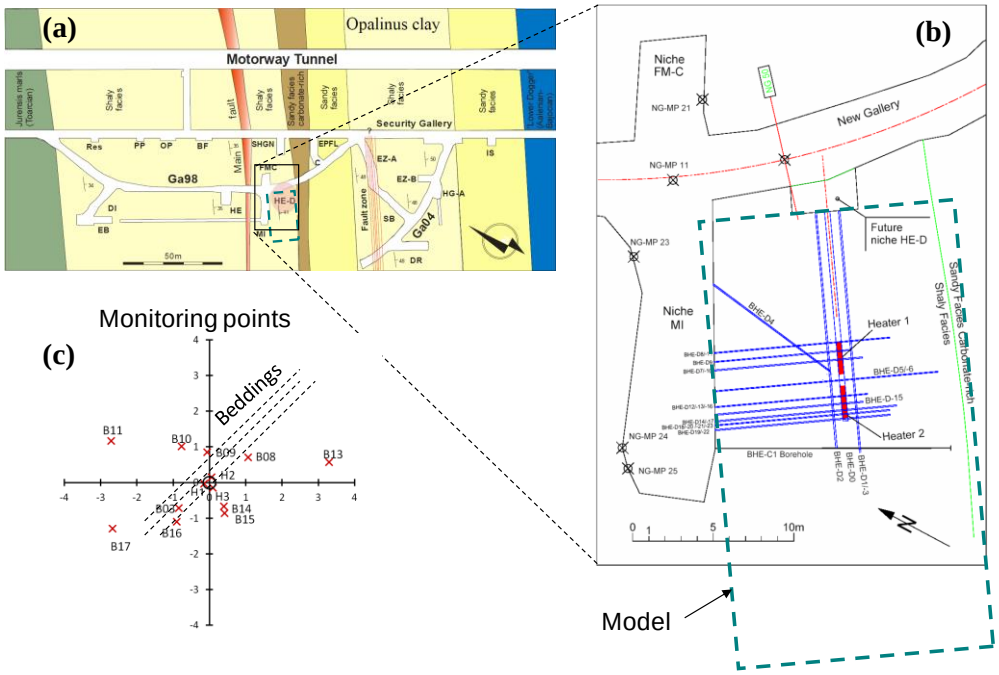

Figure 2.2. Layout of the HE-D experiment including (a) location in the Mont Terri URL, (b) monitoring points, and (c) top view of experiment including monitoring borehole layout (Wileveau, 2005; Rutqvist et al., 2013b).

2.1.1.1 Model Setup

The key of the HE-D modeling is to accurately represent the anisotropic THM behaviour of the Opalinus Clay when it is heated. Opalinus Clay is an argillaceous rock sedimented in marine conditions (Middle Jurassic) with sedimentation planes that results in anisotropic properties. Typical properties of the Opalinus Clay are a low permeability of approximately 5×10^{-20} m^2, a porosity of 0.16 and a bulk density of approximately 2450 kg m^{-3} (Wileveau and Rothfuchs, 2007). The mechanical properties of Opalinus clay are usually described as a transversely isotropic elastoplastic material. The heat conductivity tensor can also be considered as transversely isotropic (Garitte et al., 2013).

We modeled the HE-D experiment using the TOUGH-FLAC simulator employing an anisotropic material model that considers the beddings of the Opalinus Clay. To accurately model

anisotropic thermal and hydrological behavior in TOUGH2, the mesh is inclined along with the beddings. Anisotropic mechanical behavior is simulated using a so-called ubiquitous joint model, available in FLAC3D, with properties derived from published work (Corkum and Martin, 2007).

We constructed a 3D TOUGH-FLAC model with a 45° inclined mesh as shown in Figure 2.3. The model dimensions (16×16×28 m) are equivalent to those used by Gens et al. (2007) in their modeling of the HE-D experiment. We used the thermal heat load according to the electric power supplied, and conducted sensitivity studies to back-calculate the *in situ* THM properties of the Opalinus Clay. The rock mechanical properties for the Opalinus Clay were taken from Corkum and Martin (2007). These included parameters for the FLAC3D ubiquitous joint model defining anisotropic strength properties, a bulk modulus of 4.17 GPa, and a shear modulus 1.92 GPa. The thermal expansion coefficient was set to 1.4×10^{-5} °C^{-1} which is a representative isotropic average value of the Opalinus Clay (Gens et al., 2007). In the simulation presented here the permeability was set to an isotropic value 5×10^{-20} m^2 according to previous simulations by Gens et al. (2007), although permeability at the Mont Terri is anisotropic by a factor of about 4. Finally, we assigned an isotropic permeability of 5×10^{-20} m^2, and pore compressibility of 1×10^{-9} Pa^{-1}, based on Gens et al. (2007).

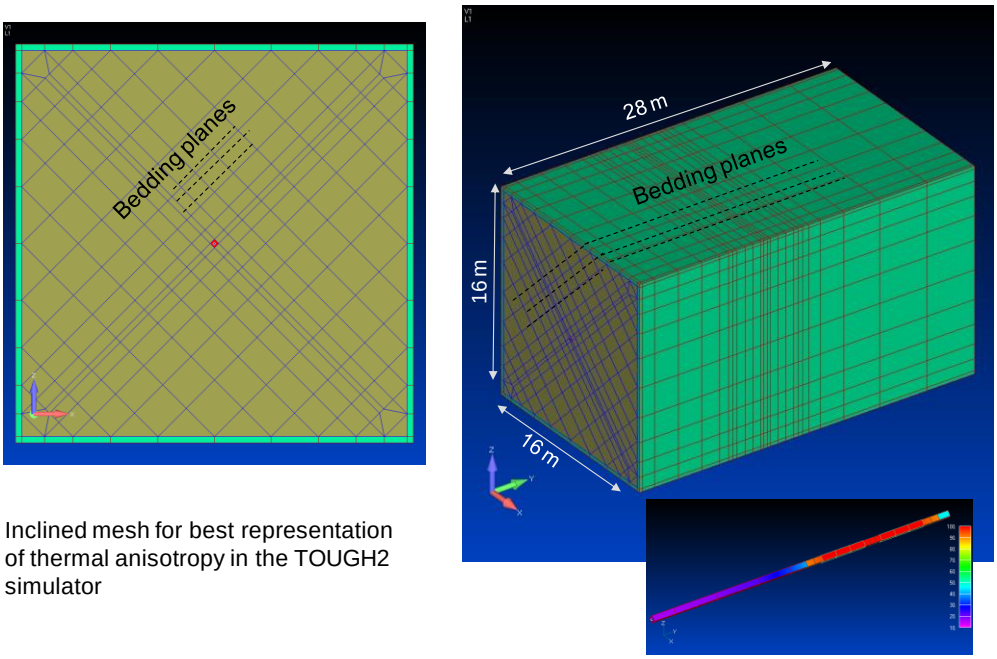

Inclined mesh for best representation of thermal anisotropy in the TOUGH2 simulator

Figure 2.3. TOUGH-FLAC model for the analysis of coupled THM processes at the HE-D experiment.

The initial hydraulic and thermal conditions for the model simulation were pore fluid pressure of 2 MPa and a temperature of 15°C within the host rock. The 2 MPa of pore pressure is not under hydrostatic conditions, and the process is affected by the existing tunnel system at the site. A stress field was applied based on the best estimated Mont Terri *in situ* stresses. The vertical stress

was set to 7 MPa, whereas the maximum and minimum horizontal stresses were respectively set to 5 MPa and 2 MPa (parallel to the bedding).

2.1.1.2 Results with Comparison to Field Data

The modeling shows that the heating of the rock mass is the driving force for the THM responses in the HE-D experiment. Temperature changes strongly affect hydraulic and mechanical responses whereas thermal processes are not significantly impacted by the hydraulic and mechanical processes. Heat transfer is dominated by thermal conduction and the temperature evolution can be calculated independently of the hydraulic and mechanical processes. In this case we input the heat load as shown in Figure 2.4 and then calibrated the transversely anisotropic thermal conductivity until a good agreement was obtained between simulated and measured temperature evolution at 31 locations in the rock mass. A good overall temperature match was obtained for thermal conductivity parallel to the bedding planes, $K_{\parallel}$ = 2.15 W/m-K, and perpendicular to bedding planes, $K_{\perp}$ = 1.19 W/m-K; a thermal conductivity anisotropy factor, $K_{\parallel}/K_{\perp}$ = 1.8. Figure 2.5 shows the simulated and measured temperature evolution near the heaters and the heat loss along the heater borehole towards niche HE-D. Moreover, an additional heating-system power loss of 5% was assumed for achieving the best overall match between simulated and measured temperature evolution.

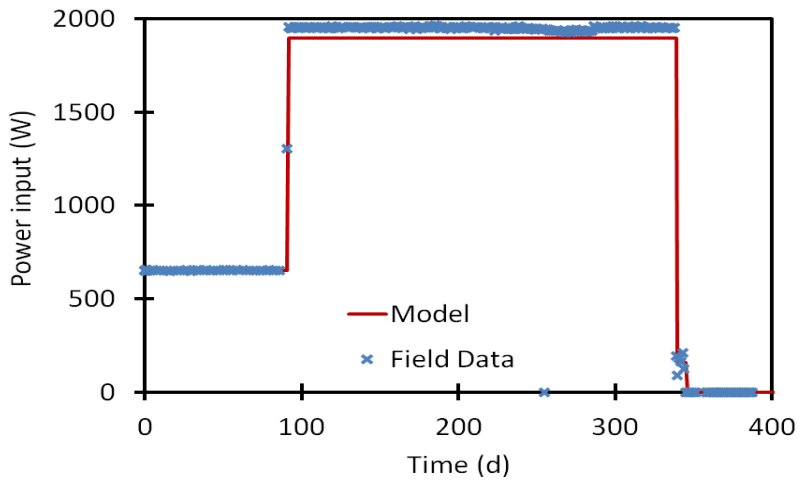

Figure 2.4. Modeled and measured power input for the HE-D experiment.

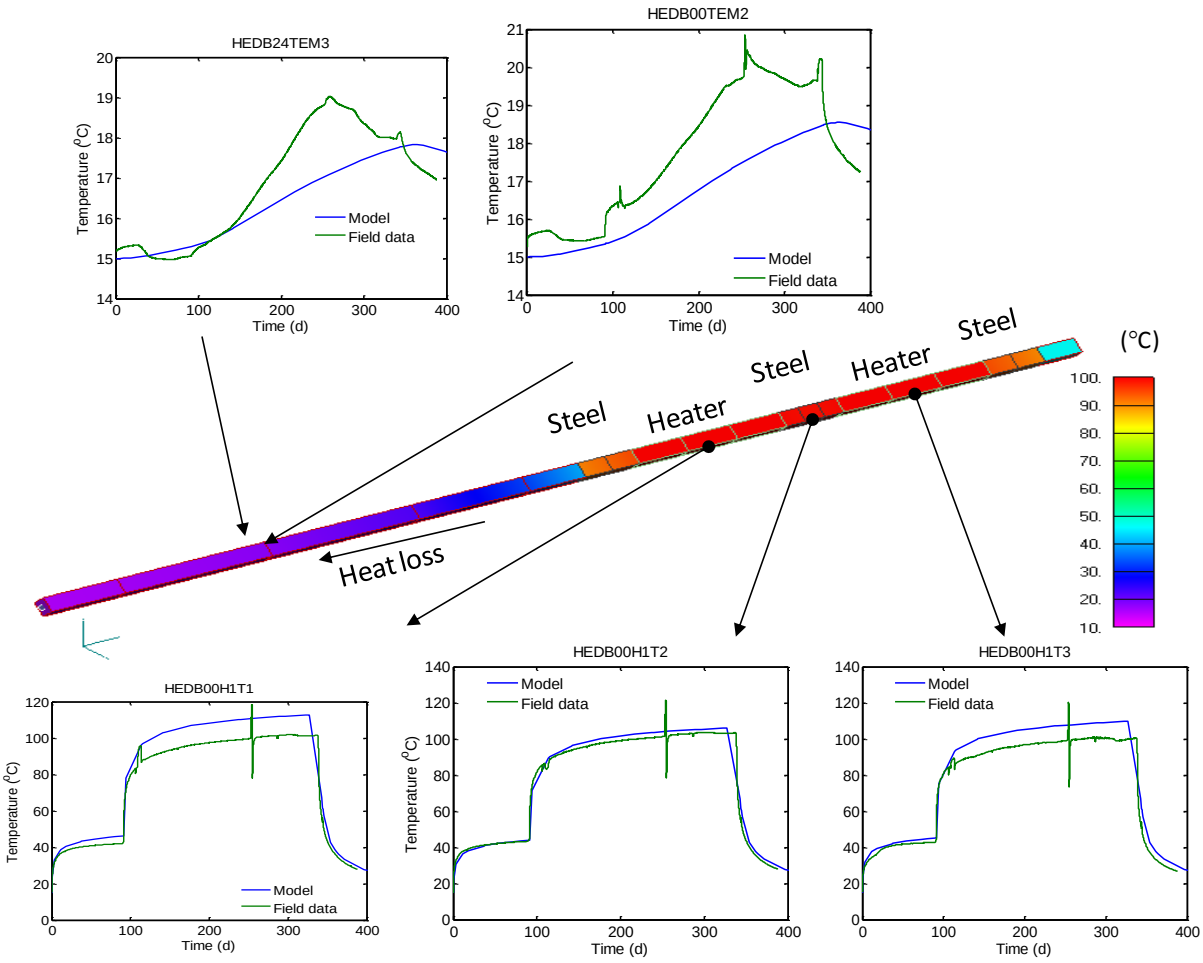

Figure 2.5. Simulated and measured temperature evolution near the heaters and heat loss along equipment in the boreholes toward niche HE-D.

Figure 2.6 presents 3D contour plots of temperature, volumetric strain and pressure after 300 days of heating. The figure shows that rock volumetric strain is up to 0.1% near the heaters whereas the fluid pressure increases to about 3.8 MPa. The change in temperature has a direct impact on the volumetric strain through thermal expansion. Considering free thermal expansion, the volumetric strain caused by a temperature increase from 15 to 50°C is expected to result in a maximum thermal expansion of $\Delta\varepsilon_V = 3 \times \Delta T \times \alpha_T = 3 \times 35 \times 1.4 \times 10^{-5} = 0.0015$, or 0.15%. In this case the thermal expansion is not free and some thermal strain will be taken up by the confined rock mass as thermal stress. The thermal expansion of the fluid inside the pores is the cause of the increasing fluid pressure, a process referred to as thermal pressurization. Such a pressure increase might also result in additional volumetric strain. However, using a simple analytic calculation we can estimate this for free strain from the pressure change ΔP and bulk modulus K as $\Delta\varepsilon_V = \alpha_{biot} \times \Delta P/K = 0.6 \times 2\times10^6 / 4\times10^9 = 0.0003$, or 0.03%. Thus, the volumetric strain is mainly thermal strain.

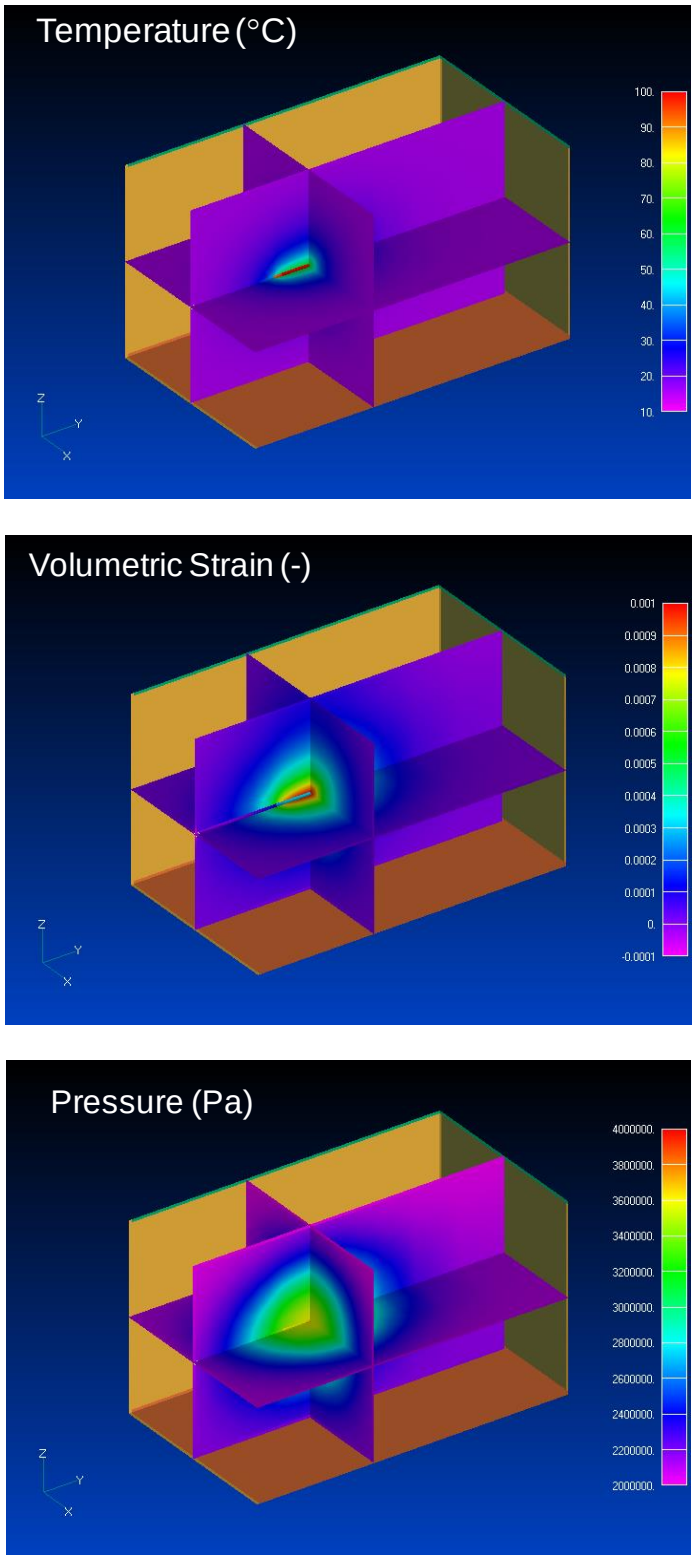

Figure 2.6. Simulated contours of (a) temperature, (b) volumetric strain and (c) pressure after 300 days of heating.

Figure 2.7 shows comparison of simulated and measured temperature and pressure at two monitoring points (B16 and B15), and strain at another location. The simulation shows a correlation between temperature and fluid pressure as a result of thermal pressurization, which occurs as a result of the differences in the coefficient of thermal expansion between the fluid and the solid rock. As previously mentioned, a good temperature agreement is achieved using an anisotropic thermal conductivity. A reasonably good agreement between simulated and measured pressure is achieved with the permeability set to 5×10^{-20} m^2 and a pore compressibility of 1×10^{-9} Pa^{-1}. This pore compressibility was estimated from the elastic properties of the rock assuming uniaxial strain conditions (Rutqvist et al., 2013a). The strain results shown in Figure 2.7 were measured from the relative displacement between two anchor points located about 1 m from each other and in the radial direction from the heater hole. The fact that these anchor points are located in the radial direction means that radial strain can be back-calculated from the relative displacements between these anchor points. The radial strain mainly shows a compression during heating as rock is expanded from the heated borehole.

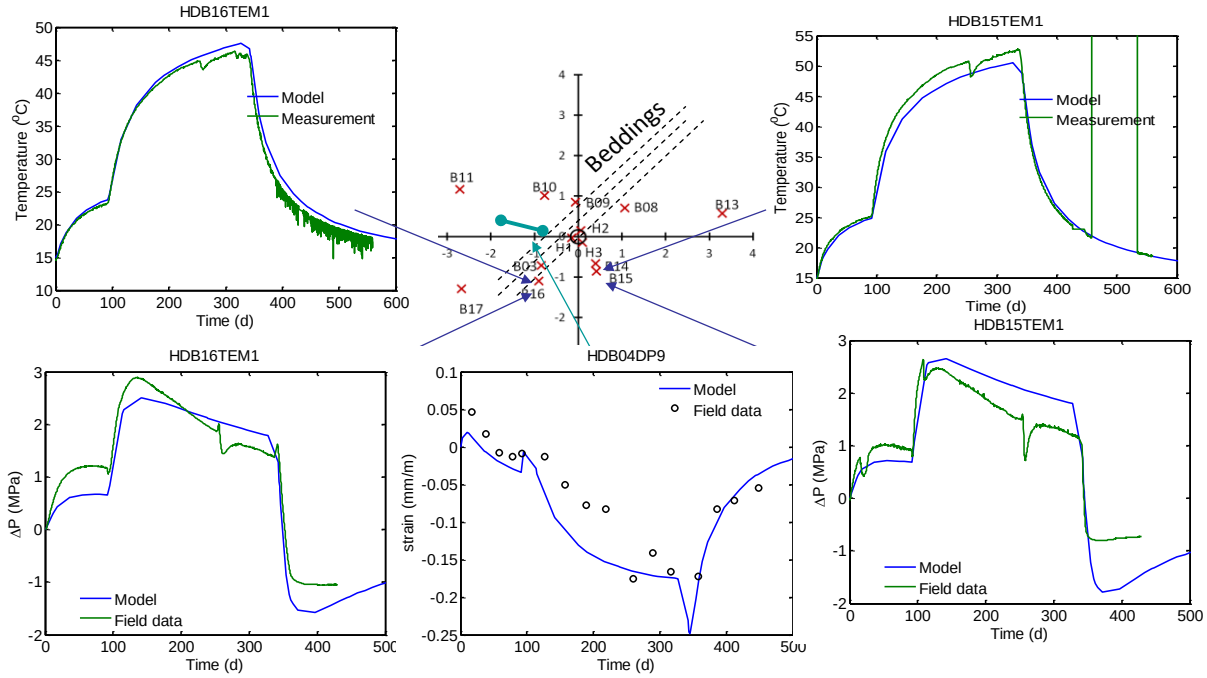

Figure 2.7. Comparison of simulated and measured temperature and pressure at two monitoring points (B15 and B16) and stain at another location close to the heater.

As previously mentioned, a total of eight modeling teams are involved in comparative calculations of the THM processes with different codes (Table 2.1). The comparison of the results for the temperature field shows a good agreement between the teams and the simulated temperatures are close to the measurements. One example is shown in Figure 2.8 for two temperature sensors. Sensor HEDB03 is located at a distance of 1.11 m away from the centre of the heater parallel to bedding, whereas sensor HEDB14 is located 0.775 m away perpendicular to bedding. Figure 2.8 shows a good agreement between the results of the different groups as well

as between simulations and observations. The comparison of these sensors also illustrates the effect of the anisotropic heat conductivity of Opalinus clay. Despite the different distance to the heater, both sensors show a similar temperature evolution over time. The largest disagreement shown is for one team at sensor HEDB14 in which the temperature was overestimated because the simulation was conducted with an axisymmetric model in which the thermal anisotropy could not be considered. The modelling of the HE-D heater test is now completed and detailed comparison of the simulation results of different research teams are underway within the DECOVALEX-2015 project.

Table 2.1. Modeling teams participating in Task B1 of DECOVALEX-2015 Graupner et al., 2013)

Team	Principal Investigator	F.O.	Country	Code	2D/ 3D	T-H-M	Heater
UFZ	W. Wang	BGR	Germany	OpenGeo Sys	3D	THM	int.
CAS	P. Pan	CAS	China	EPCA3D	3D	THM	Bc
LBNL	J. Rutqvist	DOE	USA	TOUGH-FLAC	3D	THM	int.
ENSI	B. Graupner	ENSI	Switzerland	OpenGeo Sys	3D	THM	int.
CNSC	S.T. Nguyen	IRSN	Canada/ France	COMSOL	3D	THM	Bc
JAEA	S. Nakama	JAEA	Japan	THAMES	3D	THM	Bc
KAERI	C. Lee	KAERI	South Korea	FLAC3D	3D	THM	int.
CNWRA	C. Manepally	NRC	USA	FLAC-xFlo	2D	TH(M)	Bc

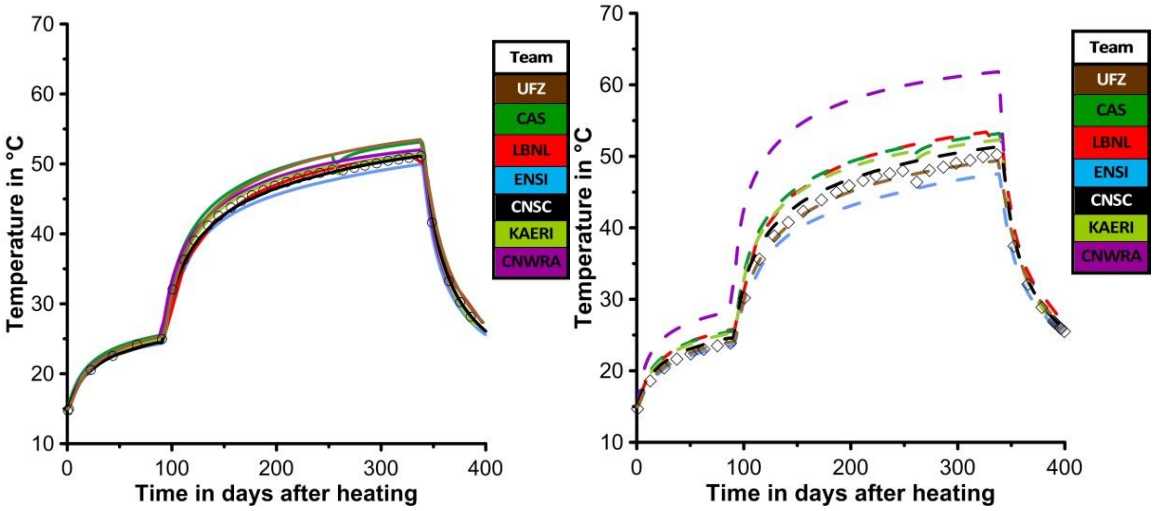

Figure 2.8. Comparison of measurements and model results of for the temperature evolution over time at sensors HEDB03 and HEDB14 (Graupner et al., 2013).

2.1.2 Buffer Material Study

The buffer material study within the DECOVALEX-2015 Task B1 mainly consists of modeling a column experiment on granular MX-80 bentonite. The experiment was conducted in a closed system where the bottom was heated to a high temperature and the top was kept at ambient temperature. Temperature and relative humidity at three points along the axis of the column were measured over time. The objective of this study is to calibrate the water retention curve, the dependency of thermal conductivity on water saturation, and the dependency of water relative permeability on degree of saturation against the relative humidity and temperature data measured in a laboratory column experiment. The model simulations reported here were conducted with the inverse modeling and optimization tool iTOUGH2 (Finsterle, 2007).

2.1.2.1 Description of the Column Experiment

Bentonite pellets were poured into the Teflon column without extra packing. The Teflon column was initially wrapped with a layer of foam, but the insulation layer was later replaced with wool. A heater was placed at the bottom of the column and the temperature of the heater was controlled by adjusting the power input using a digital relay. At the top of the column was a cooler where water was circulated through the inner channels of the cooler to maintain the temperature to be the ambient temperature. The packed portion of the column was 48.4 cm high, and sensors were installed with distances of 10 cm, 22 cm, and 40 cm from the heater. Temperature and relative humidity were measured during the experiment.

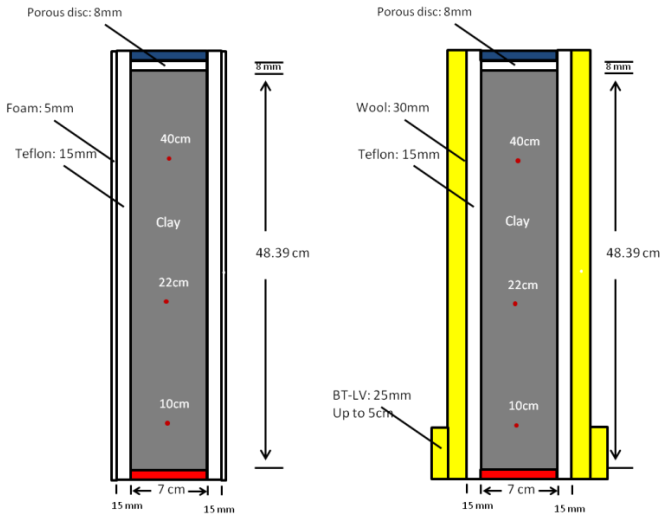

Figure 2.9. Schematic of experimental setups before and after changing insulation.

After the system was assembled, the data acquisition system was turned on and measured the relative humidity and temperature for 140 hours without heating the system. The measured results showed that the relative humidity was quite uniform along the column (~40%). The heater was turned on at t=0. After heating for 33 minutes, the temperature of the heater increased to the target temperature of 100 ºC. The heater temperature was maintained at 100 ºC, while the temperature of the cooler was kept at 21.5 ºC. After 1566 hours, the foam layer was replaced with wool of 30 mm thickness covering the entire column length and BT-LV of 25 mm thickness

covering the bottom 5 cm. After 3527 hours, the target temperature of the heater was adjusted to 140 ºC. The temperature increased to 140 ºC 17 minutes after the adjustment was made. The experiment was stopped after 5015 hours (209 days).

2.1.2.2 Model Development

A 2D radial symmetric mesh was created to simulate the column experiment. The mesh has 6 columns and 28 rows (Figure 2.10). Materials used in the model include Bentonite pellets (BENTL), porous disk (PORUS), heater (HEATR), cooler (COOLR), Teflon (TEFLN), foam (FOAMA), wool (WOOLA), BT-LV insulation (BTLVA), and air (AIRLT). The Bentonite pellets are represented by a column of elements (1×25 elements). Other elements represent the porous disk, heater, cooler, insulation materials, and air. The bentonite properties used in the model are as shown Table 2.2. The bentonite pellets have a solid grain density of 2700 kg/m^3, intrinsic permeability of 3.5×10^{-21} m^2, and porosity of 0.46. The thermal conductivity of bentonite is 1 W/m-K when saturated with water, in contrast to 0.3 W/m-K under dry conditions. The specific heat of the bentonite pellets is 950 J/kg-K. Before the experiment started, the pores of the bentonite pellets were initially saturated with 22% of water and the measured relative humidity was uniformly 40% along the column.

Table 2.2. Properties of Bentonite pellets used in the model

Solid grain density	2700 kg/m^3
Porosity	0.46
Intrinsic permeability	3.5×10^{-21} m^2
Saturated thermal conductivity	1 W/m-K
Unsaturated thermal conductivity	0.3 W/m-K
Specific heat	950 J/kg-K
Tortuosity	0.67

From laboratory experiments it has been observed that the gas permeability in unsaturated bentonite is about six orders of magnitude higher than the liquid permeability under saturated conditions (Olivella and Gens, 2000). To account for the increased gas permeability, we consider vapor and air diffusion and Klinkenberg effect in the model. A gas diffusion coefficient of 2.13×10^5 m^2/s is used for both components and a tortuosity of 0.67 is used in the model. A Klinkenberg parameter of 2.5×10^{11} Pa is used.

We use the van Genuchten formula to describe the water retention curve (van Genuchten, 1980).

$$P_c = -P_0\left[(s^*)^{-1/\lambda} - 1\right]^{(1-\lambda)} \quad (2.1)$$

$$s^* = \frac{(s_l - s_{lr})}{(s_{ls} - s_{lr})} \quad (2.2)$$

with the parameters given in Table 2.3.

Table 2.3. Capillary pressure parameters of bentonite pellets used in the model

λ	0.512
s_{lr}	0
$1/P_0$ (1/Pa)	3.5E-08
P_{max} (Pa)	3×10^9
s_{ls}	1.0

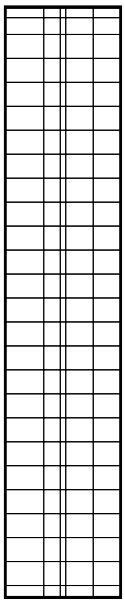

Figure 2.10. Model mesh of the column experiment.

A power law function is used to describe the relative permeability of liquid water at various water saturations and we assume the gas phase is perfectly mobile.

$$k_{rl} = {s_l}^5 \quad (2.4)$$

$$k_{rg} = 1 \quad (2.5)$$

Note that we are not explicitly simulating the dependency of unsaturated properties on swelling in this case. As previously mentioned, the intrinsic permeability for gas flow may be up to six orders of magnitude higher than the intrinsic permeability for liquid flow and the much higher intrinsic permeability is in this case simulated using a high value of the Klinkenberg parameter.

The thermal conductivities of other materials are shown in Table 2.4. In the model, we use all the measured thermal conductivity values from Villar (2012) except those for porous disk and wool. The thermal conductivity of porous disk is not available in Villar (2012). The thermal conductivity of wool is decreased slightly from 0.04 W/mK as reported in Villar (2012) to 0.03 to better match the temperature profile.

Table 2.4. Thermal conductivity of other materials used in the model

Thermal conductivity of porous disk	3.5 W/m-K
Thermal conductivity of Teflon	0.25 W/m-K
Thermal conductivity of foam	0.04 W/m-K
Thermal conductivity of wool	0.03 W/m-K
Thermal conductivity of BT-LV	0.034 W/m-K
Thermal conductivity of air	0.04 W/m-K

2.1.2.3 Initial and Boundary Conditions

As described in Villar (2012), the initial condition of the system is as follows: Bentonite pellets have an initial water saturation of 0.22; other materials are completely dry. The system is uniformly at the atmospheric pressure of 1.01325×10^5 Pa and an ambient temperature of 21.5 ºC. Villar (2012) reported that the relative humidity is 40% before the start of the heating test. The relative humidity is dependent on the water retention curve and temperature, which can be calculated using Kelvin's equation:

$$P_g^w = P_{gS}^w(T)R_H(P_c,T) = P_{gS}^w(T)\exp\left(\frac{-P_c m^w}{\rho_l RT}\right) \tag{2.6}$$

$$lnR_H = \frac{-P_c m^w}{\rho_l RT} \tag{2.7}$$

The calculated capillary pressure at $R_H = 0.4$ at 21.5 ºC is approximately 1.24×10^8 Pa. The water retention curve used in the model compared with the measured data with bentonite pellets MX-80 (Rizzi et al., 2011) is shown in Figure 2.11.

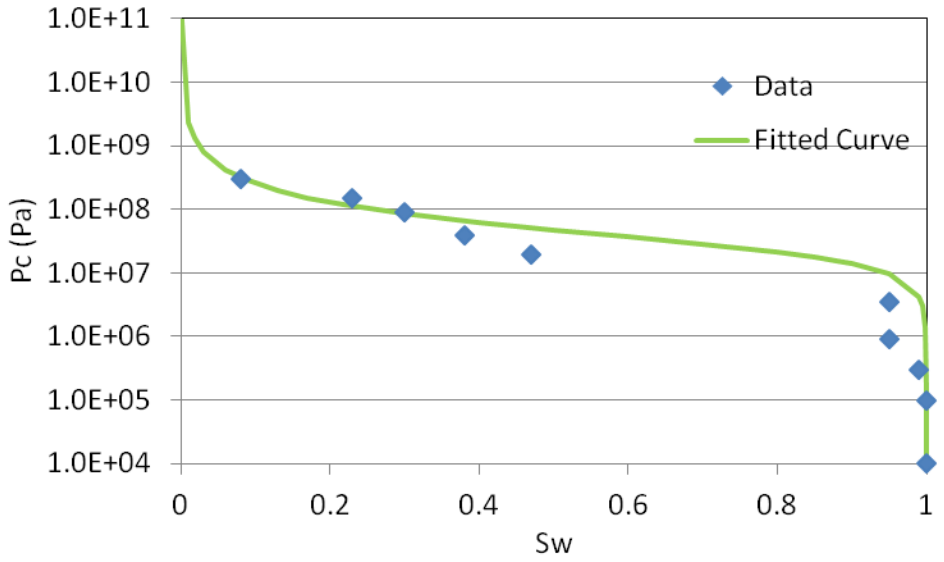

Figure 2.11. Water retention curve in model and measured water retention curve (MX80).

The experiment was conducted in a closed system. No-flow boundary conditions are used for the model. The heater, cooler, and air are simulated by assigning an extremely large specific heat (e.g., 0.5×10^{34} W/kg ºC). The increase of the temperature in the heater is simulated by injecting a large amount of heat to increase the temperature linearly to the target temperatures (e.g., 100 ºC and 140 ºC). The change of the insulation layer is represented in iTOUGH2 by stopping the forward simulation at the time and changing the material type followed by running the simulation using the state condition at the end of the previous run as initial condition.

2.1.2.4 Simulation Results

The simulated results are shown in Figure 2.12. The initial relative humidity was at 40% along the column. With the heater turned on, the simulated relative humidity at 10 cm increases within 200 hours and decreases gradually after that. The simulated relative humidity is lower than the measured relative humidity curve. At 22 cm, the model underestimates the relative humidity but shows similar pattern in relative humidity changes. The relative humidity at 40 cm increases almost linearly. The simulated relative humidity at 40 cm is in excellent agreement with the measured relative permeability. The simulated temperature profile is quite similar to the measured data except the overestimated temperature gradients after 3527 hours. Overall the simulated results are in a reasonable agreement with the measured data, although we will continue to improve the modeling of this experiment along with the DECOVALEX-2015 project.

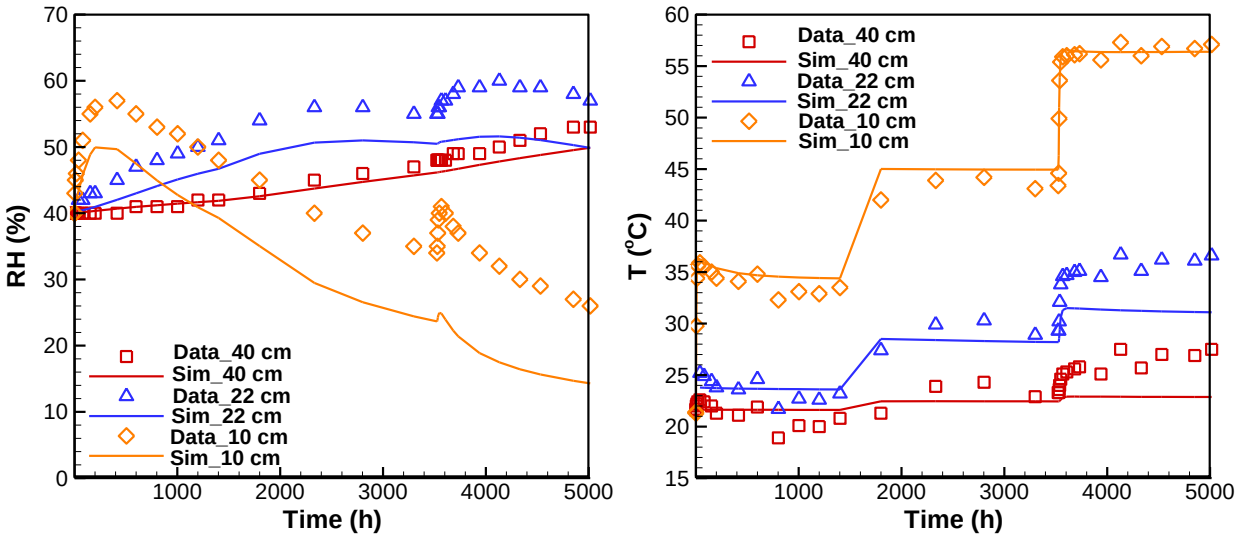

Figure 2.12. Left figure: simulated and measured relative humidity; Right figure: simulated and measured temperature

2.2 Task B2: Horonobe EBS experiment

This task focuses on coupled THMC modeling of a planned full-scale EBS experiment conducted by the Japan Atomic Energy Agency (JAEA) at the Horonobe URL, Hokkaido, Japan (Figure 2.13). The EBS experiment will be carried out at a depth of 350 m in a very porous and soft, siliceous mudstone with the following basic properties

- Porosity 35-60%
- Permeability 10^{-20} – 10^{-18} m^2
- UCS (Strength) 5-25 MPa
- Young's Modulus 1-4 GPa
- Thermal Conductivity 1.34-1.53 W/mK

Figure 2.14 show the experimental layout with a vertical heater emplacement installed in a test pit at the bottom of a experimental drift. The experimental drift will be backfilled after the installation of the heater and bentonite buffer into the test pit. The backfill and buffer material will be based on the Japanese Kunigel V1 bentonite. The experimental area will then be isolated by a concrete plug.

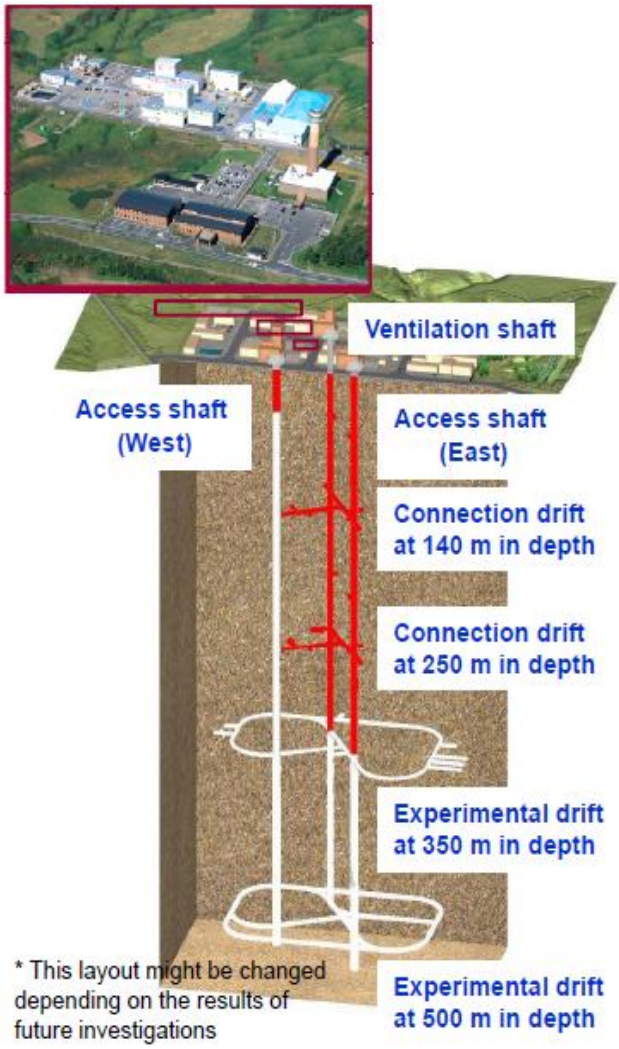

Figure 2.13. Layout of the Horonobe URL in Hokkaido, Japan.

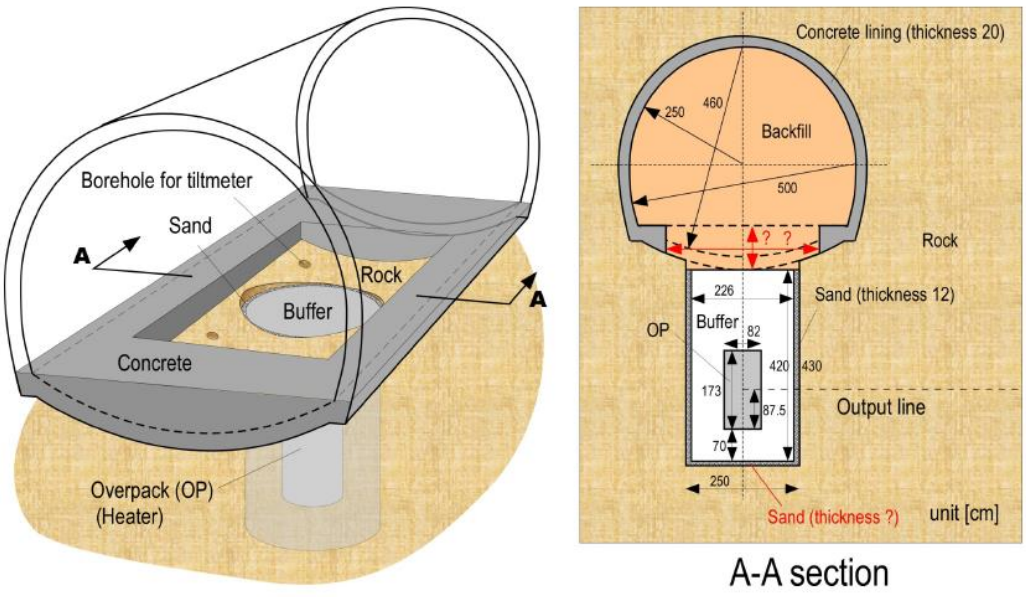

Figure 2.14. General description of the EBS experiment at the Horonobe URL Project in Japan.

Sensors will be installed in buffer, backfill and rock to monitor temperature, stress, strain, pore pressure, humidity, displacement, pH, resistivity, electric potential, and seismic velocity. The detailed layout is not yet fixed and may be changed depending on the initial modeling results.

The DECOVALEX Task B2 is divided into the following steps;

- Step 1 (1D benchmark test)
- Step 2 (prediction analysis 1 and proposal of the sensors layout)
- Step 3 (prediction analysis 2)
- Step 4 (calibration analysis)

The 1D benchmark test will first be performed with exact properties and boundary conditions given by the JAEA. This will be conducted for the teams to familiarize themselves with the problem and for precise comparison of computer codes before going into the more complex full-scale case. Thereafter, a model of the real experimental design will be constructed and a first predictive analysis will be performed for several years from the start of the heating. The results will then be used to guide the installation of sensors that is planned to begin by April 2014. The heating is planned to start in November 2014 and in April 2015 JAEA will provide the monitored data for the first six months of heating to the research teams. The research teams will calibrate their models against this first 6 months of field data and then carry out coupled numerical analysis for long term predictions (100 - 1,000 years) using the test conditions of the EBS experiment. If possible, research teams will also simulate chemical reactions in the buffer material, the rock mass and the groundwater. Output will be the pH and chemical species affected by the concrete lining material.

JAEA will provide reports from the investigations at the Horonobe URL for input parameters related to the mudstone host rock and buffer material properties for the Kunigel V1 bentonite from the previous H12 project, whereas properties for the backfill are still being investigated. The Task B2 started in May 2013 with Step 1. In the next section we present the preliminary LBNL results for this benchmark.

2.2.1 1D Benchmark Modeling

We first conduct the basic thermal hydrological simulation using the TOUGH2 code. Simulation example results have also been provided by JAEA for an initial comparison. One of the issues in this kind of benchmark is that properties may not be constants, but can for example be functions of temperature and saturation. Also, the properties given by JAEA are based on their modeling approach and their numerical model has been used to calibrate some properties by back-analysis of laboratory experiments. We also conduct simulations using ROCMAS, which uses an approach similar to that of the JAEA simulation model.

2.2.1.1 Problem set-up

A thermal-hydrologic model of DECOVALEX task B2 was conducted to make model predictions for temperature, degree of saturation, water content and hydraulic pressure for the system shown in Figure 2.15. The system is a one-dimensional slice of the heater, buffer, and rock from the center of the overpack (which is a heat source) out to 25 m. As shown in Figure 2.15, this includes 0.41 m of the overpack, 0.72 m of the bentonite buffer, and 23.87 m of the rock.

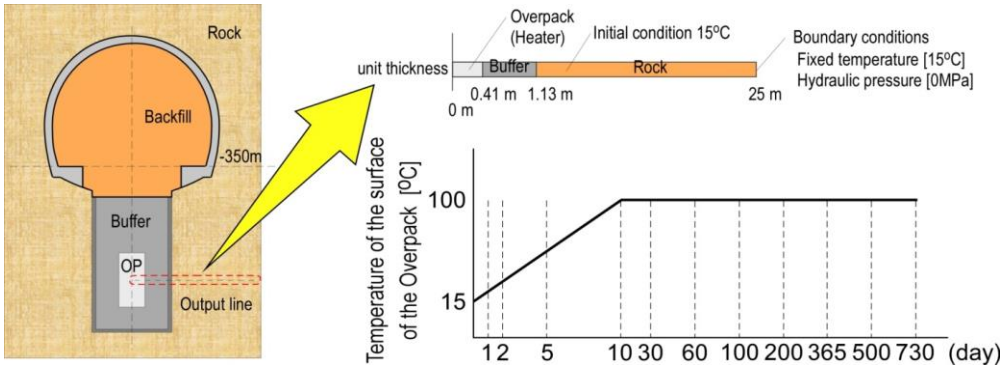

Figure 2.15. DECOVALEX-2015 Task B2 modeling domain and overpack temperature history.

The figure also shows some of the initial and boundary conditions. The initial system temperature is 15° C, and the boundary temperature in the rock is fixed at 15° C. The fixed pressure value at the boundary is 0.10142 MPa pressure, which is one atmosphere pressure and equivalent to a fixed hydraulic gauge pressure of zero. The overpack temperature rises over ten days from 15° C to 100° C and stays there for the duration of the period investigated, 730 days. In addition to the information available from the figure, the rock was also specified to be initially saturated with water and the buffer initially 50% saturated. The rock boundary was also assumed to remain at a fixed saturation of 100%.

2.2.1.2 Parameterization for TOUGH2 simulation

For the TOUGH2 simulation, the input parameters of the system are given in Table 2.5.

Table 2.5. Parameters for DECOVALEX Task B2 using TOUGH2

	Overpack	Buffer	Rock
Solids density (kg/m^3)	10,000.	2680.	2454.
Porosity	0.403	0.403	0.4482
Permeability (m^2)	5 x 10^{-51}	4 x 10^{-20}	1.33 x 10^{-15}
Thermal conductivity (saturated) (W/m)	20	1.986	1.231
Specific heat (solids)	10,000	341	626
Thermal conductivity (desaturated) (W/m)	20	0.444	0.579
Klinkenberg parameter (Pa)	8.47 x 10^{-10}	8.47 x 10^{-10}	8.47 x 10^{-10}
Water relative permeability parameter A, (Equation (2.8))	1.3	1.3	NA
Water relative permeability residual saturation, S_r (Equation (2.8))	0	0	NA
Water relative permeability maximum saturation, S_m (Equation (2.8))	1	1	NA
Water relative permeability parameter *m*, (Equation (2.9))	NA	NA	0.503
Water relative permeability residual saturation, S_r (Equation (2.9))	NA	NA	0
Water relative permeability maximum saturation, S_m (Equation (2.9))	NA	NA	1
Capillary pressure parameter, α (m^{-1}) (Equation (2.10))	8 x 10^{-3}	8 x 10^{-3}	9.928 x 10^{-3}
Capillary pressure parameter, *m*, (Equation (2.10))	0.375	0.375	0.503
Capillary pressure residual saturation, S_r (Equation (2.10))	0	0	0
Capillary pressure maximum saturation, S_r (Equation (2.10))	1	1	1
Vapor and air diffusion coefficients (m^2/s)	1.44 x 10^{-5}	1.44 x 10^{-5}	1.44 x 10^{-5}

The water relative permeability in the buffer (and overpack) is a power-law relationship given by

$$k_{rw}(S_w) = \left(\frac{S_w - S_r}{S_m - S_r}\right)^A \tag{2.8}$$

The water relative permeability in the rock is given by the van Genuchten relationship:

$$k_{rw}(S_w) = \left(\frac{S_w - S_r}{S_m - S_r}\right)^{1/2} \left[1 - \left\{1 - \left(\frac{S_w - S_r}{S_m - S_r}\right)^{1/m}\right\}^m\right]^2 \tag{2.9}$$

In the buffer (and overpack), the gas relative permeability is the Corey model,

$$k_{rg}(S_w) = \left\{1 - \left(\frac{S_w - S_r}{1 - S_r - S_{gr}}\right)^2\right\}\left\{1 - \left(\frac{S_w - S_r}{1 - S_r - S_{gr}}\right)\right\}^2 \tag{2.10}$$

In the rock, the gas relative permeability is

$$k_{rg}(S_w) = 1 - k_{rw}(S_w) \tag{2.11}$$

Capillary pressure in the buffer (and overpack) and rock are given by the van Genuchten relationship:

$$\psi(S_w) = \frac{1}{\alpha}\left\{\left(\frac{S_w - S_r}{S_m - S_r}\right)^{-1/m} - 1\right\}^{1-m} \tag{2.12}$$

Variations in thermal conductivity and specific heat with water saturation are assumed to be linear between the defined end points. The vapor diffusion coefficient is constant; there is no temperature dependence.

The thermal conductivity and specific heat functions given in the benchmark input were not followed exactly. The following two figures show the comparisons between the benchmark curves and what was used in our model. The maximum specific heat at a water content of about 33% for rock in zone 2 appears to be close to 1500 J/kg-K in the figure provided.

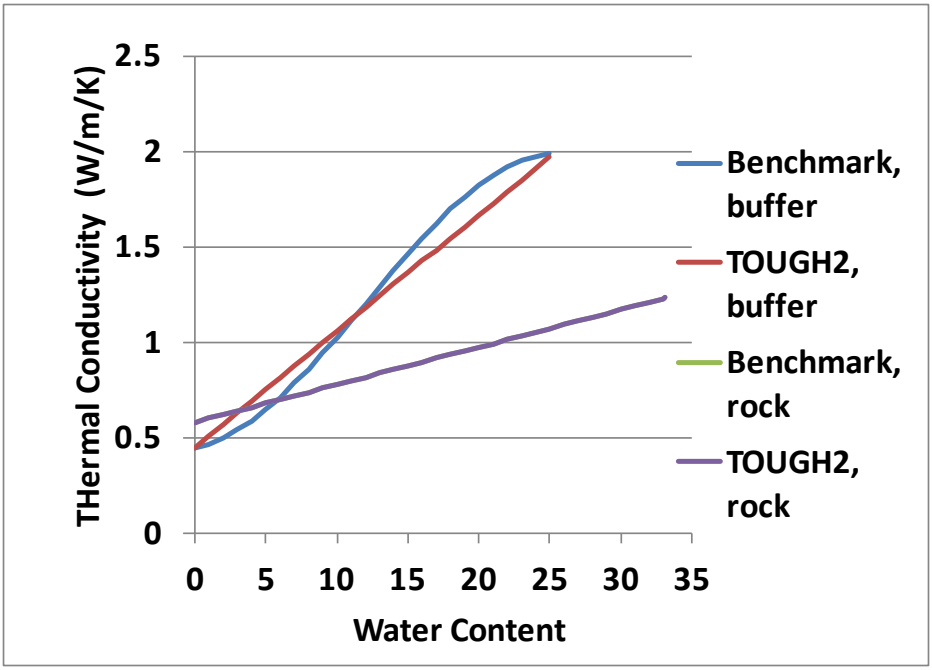

Figure 2.16. Thermal conductivities as functions of water content (the green curve is behind the purple curve).

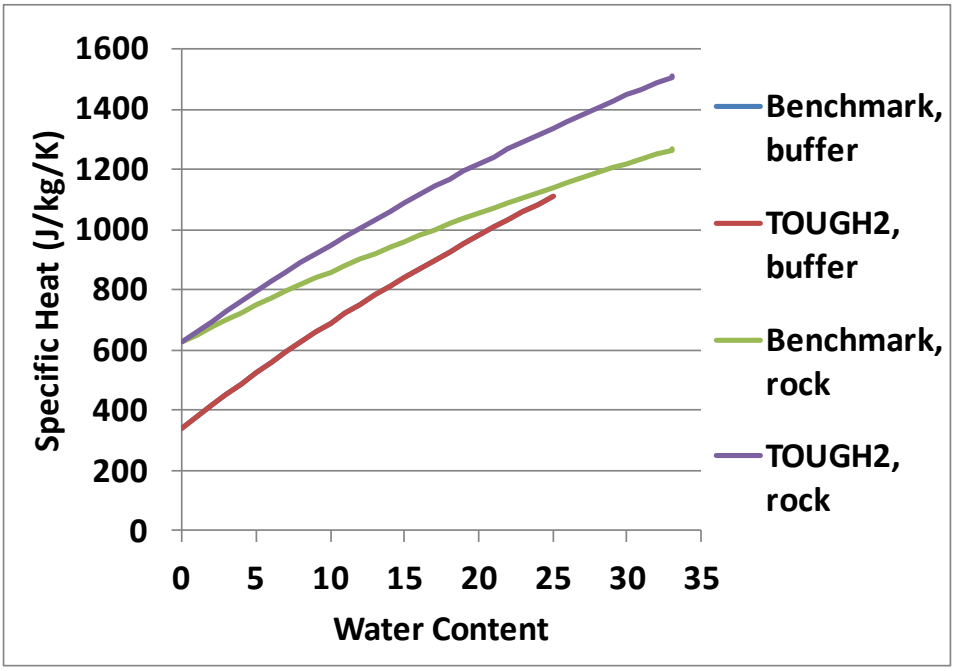

Figure 2.17. Specific heats as functions of water content (the blue curve is behind the red curve).

2.2.1.3 Numerical Model

The problem was solved using the EOS4 equation of state module available in TOUGH2. The following code modifications were implemented:

- In subroutine RELP the gas relative permeability was changed from a constant value of 1 to the relationship given in Equation (2.10) for the relative permeability selection IRP=2. This was done to follow the benchmark input.
- The tortuosity in subroutine MULTI was added as a multiplicative factor to the diffusion coefficient for cases in which the diffusion coefficient is input as a negative number. For this case, $\tau_0\tau_\beta = \tau_0 S_\beta$ instead of $\tau_0\tau_\beta = S_\beta$ in the original code. This was done to use tortuosity for the overpack (set to a small number, 10^{-11}) so that diffusion is suppressed in that material type. Tortuosity for the other material types was set to 1.
- The diffusion driving force in subroutine MULTI was changed from the mass fraction gradient times the phase density to the density gradient of the diffusing component. If the phase density is constant, these two methods give the same result. This was done to avoid instabilities in water saturation.

Table 2.6 gives the cell dimensions along the axis of the 1-D model. The other dimensions of each cell are 1m by 1m. A large-volume cell is also included at the end of the rock section to maintain constant thermodynamic conditions at the rock boundary. The temperature at the overpack was generated by injecting heat into the large-volume overpack cell at a constant rate that raised the temperature from 15 °C to 100 °C over the first 10 days followed by no heat injection over the remaining time period. Because of the large volume of the overpack cell, the temperature remained at 100 °C from 10 to 730 days.

Table 2.6. Numerical discretization

Component	Number of cells	Cell size (m)
Overpack	1	0.41
Buffer	72	0.01
Rock	87	0.01
Rock	50	0.1
Rock	90	0.2

2.2.1.4 Model Results

Model results are given in Figures 2.18, 2.19, and 2.20 for temperature, water saturation, and hydraulic pressure, respectively. The overpack-buffer interface is at x = 0.41 m, the buffer-rock interface is at x = 1.13 m and the far boundary is at 25 m. Time histories are given in Figure 2.21 for water saturation and temperature at the heater (x = 0.41 m) and near the outer edge of the buffer (x= 0.95 m).

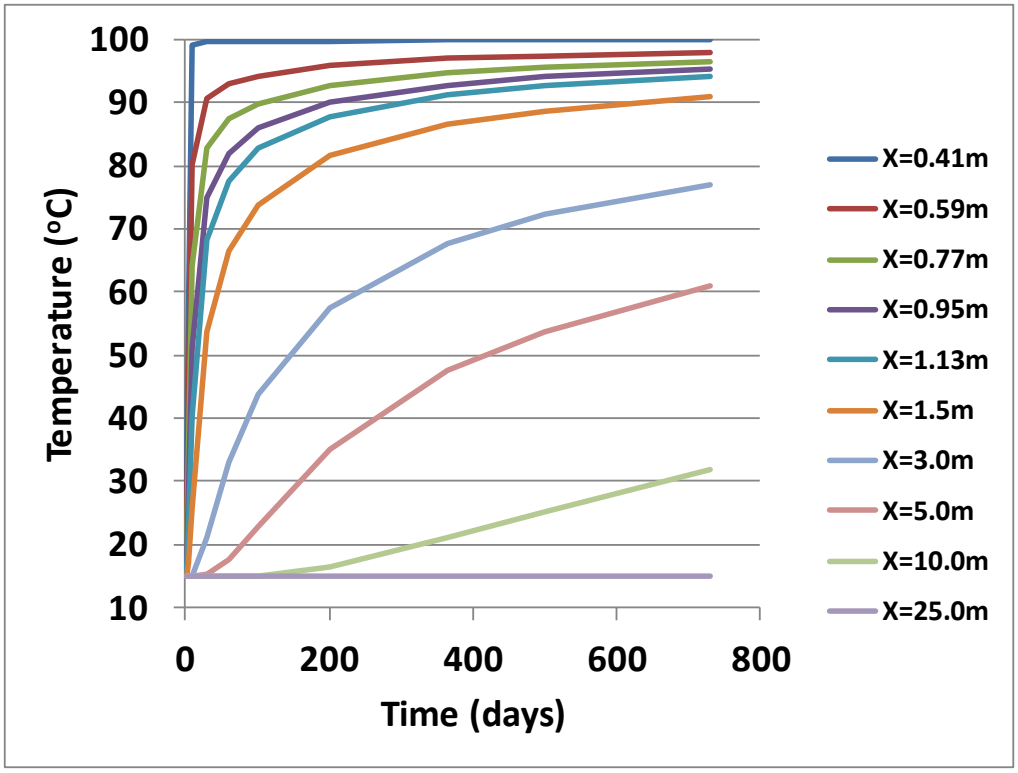

Figure 2.18. Temperature histories at different locations.

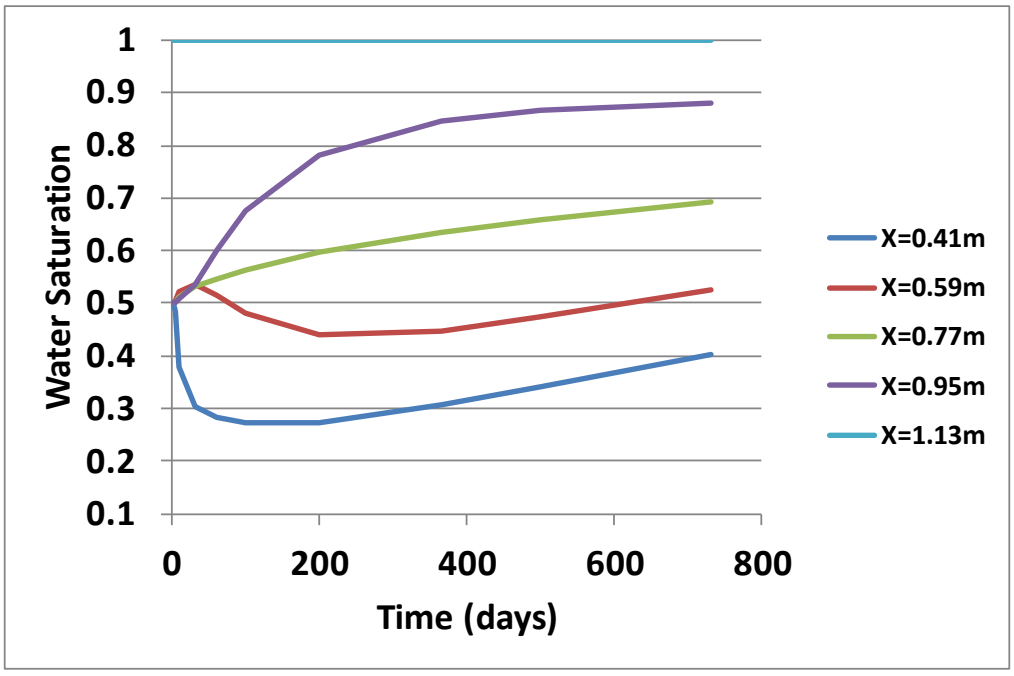

Figure 2.19. Saturation histories at different locations.

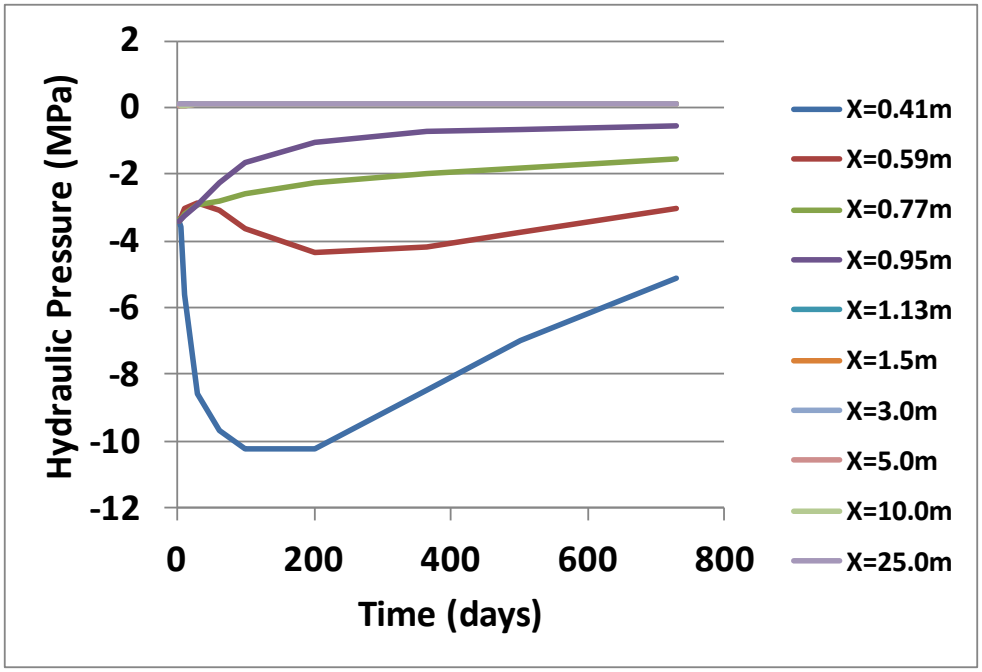

Figure 2.20. Hydraulic pressure histories at different locations.

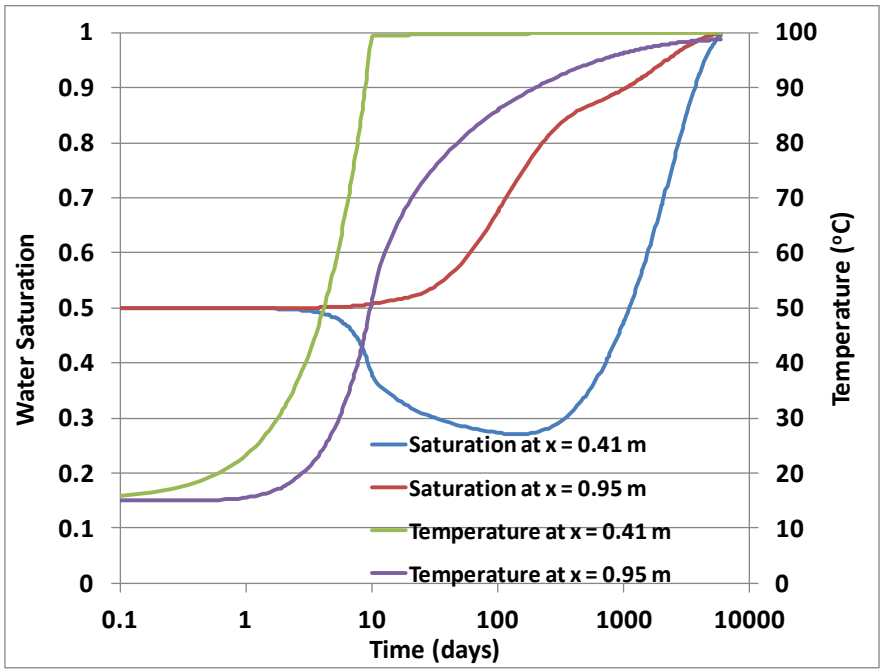

Figure 2.21. Time histories for temperature and saturation at two locations in the buffer.

Another case was also considered. This is where the gas relative permeability is increased by a factor of 10,000 for the buffer. This was implemented by multiplying the gas relative permeability by a factor of 10,000 in subroutine RELP for IRP=2. The results are not significantly different as shown in Figures 2.22 through 2.24, although there is a slight decrease

in the minimum water saturation at the x = 0.41 m in Figure 2.23, resulting in a lower hydraulic pressure at that location in Figure 2.24.

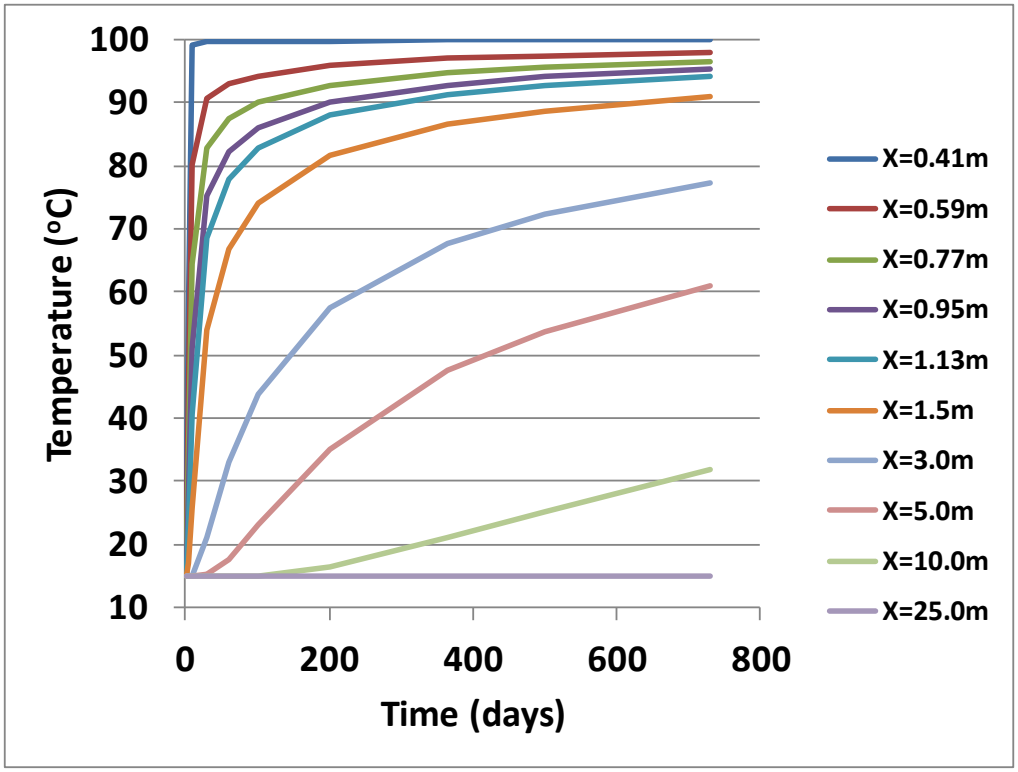

Figure 2.22. Temperature histories at different locations using the high k_{rg}.

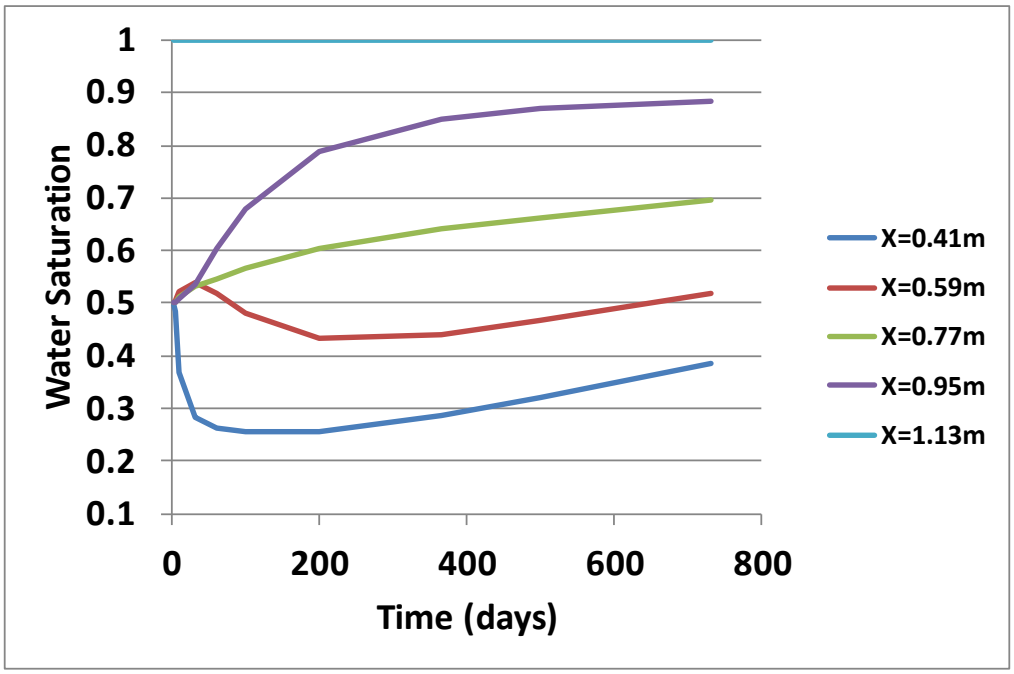

Figure 2.23. Saturation histories at different locations using the high k_{rg}.

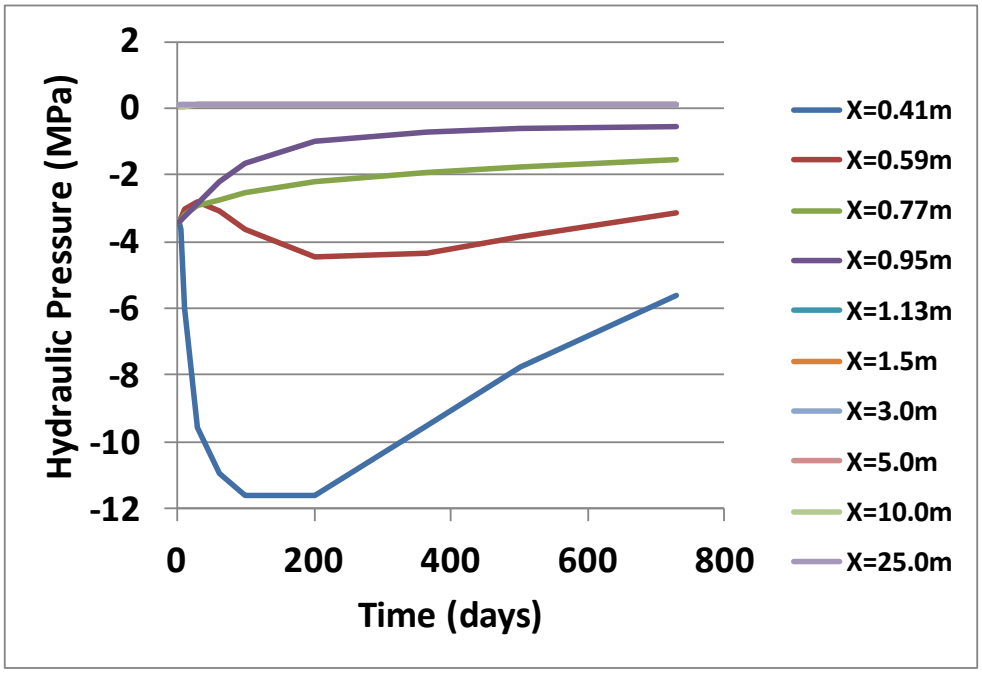

Figure 2.24. Hydraulic pressure histories at different locations using the high k_{rg}.

2.2.1.5 ROCMAS simulation

We conduct an alternative simulation using the ROCMAS code (Rutqvist et al., 2001a) for confidence building and code-to-code comparison. The ROCMAS code has been extensively used for modeling of coupled THM processes in rock-bentonite systems of previous DECOVALEX phases. For example, it was applied to model the Kamaishi Mine heater test in Japan (Rutqvist et al., 2001b). The ROCMAS code models coupled THM processes in partially saturated porous media with single phase liquid flow and vapor diffusion in a static gas phase. It is more similar to the approach used by the JAEA, which is also based on a single phase flow approach. In this approach, the gas phase pressure is assumed to be constant and equal to atmospheric pressure.

In the ROCMAS simulations we assign the exact values of all parameters given in Table 2.5. We do not need to assign parameters related to gas flow because the gas phase is assumed to be a passive spectator at constant pressure.

The simulation results shown in Figures 2.25 through 2.28 are very similar to corresponding TOUGH2 simulation results in Figures 2.18, through 2.21. The temperature evolution is practically identical, whereas some slight differences can be observed in the evolution of saturation and pressure. Such slight differences in saturation are not surprising considering the different approaches (full two-phase flow versus single phase flow) that are used. Considering the very good agreement it appears that the single phase approach used in ROCMAS is sufficient in this case.

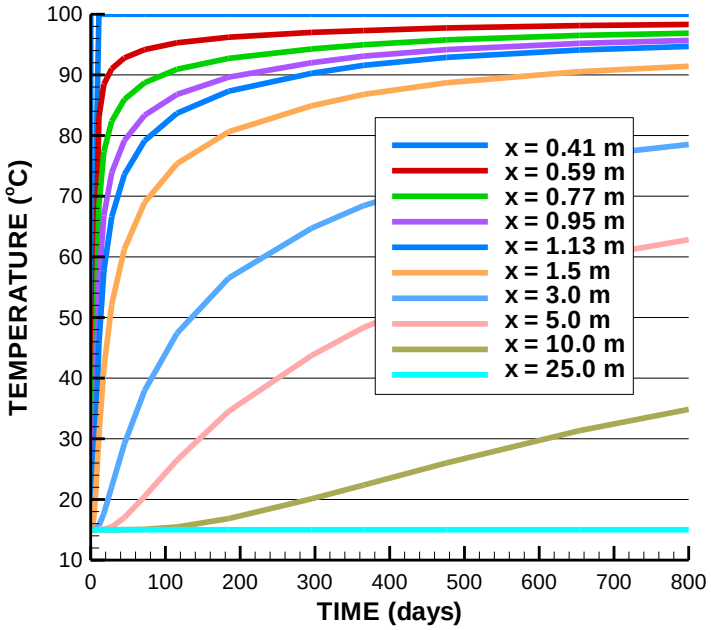

Figure 2.25. Temperature histories at different locations for ROCMAS simulation.

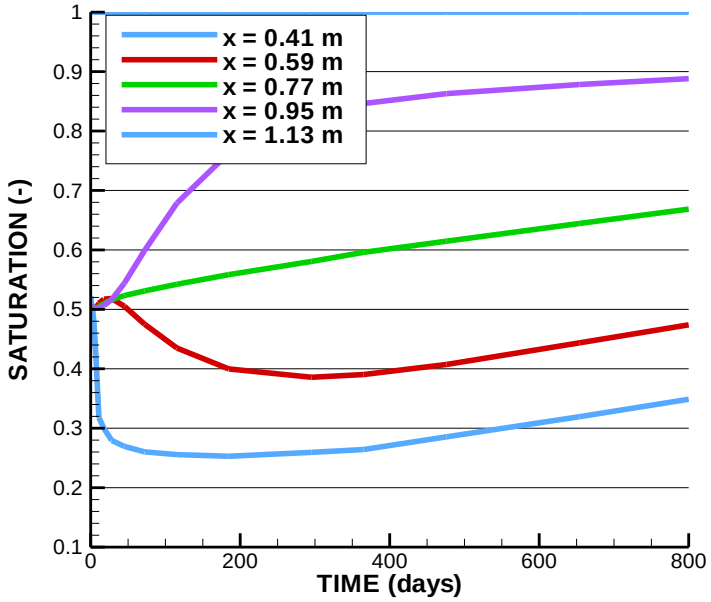

Figure 2.26. Saturation histories at different locations for ROCMAS simulation.

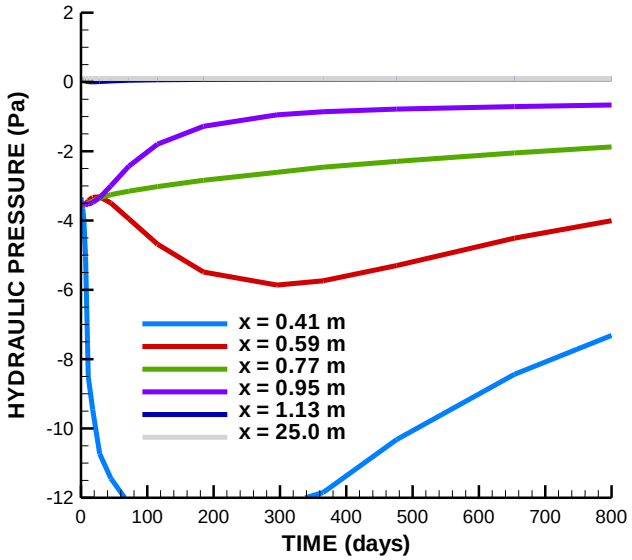

Figure 2.27. Hydraulic pressure histories at different locations for ROCMAS simulation.

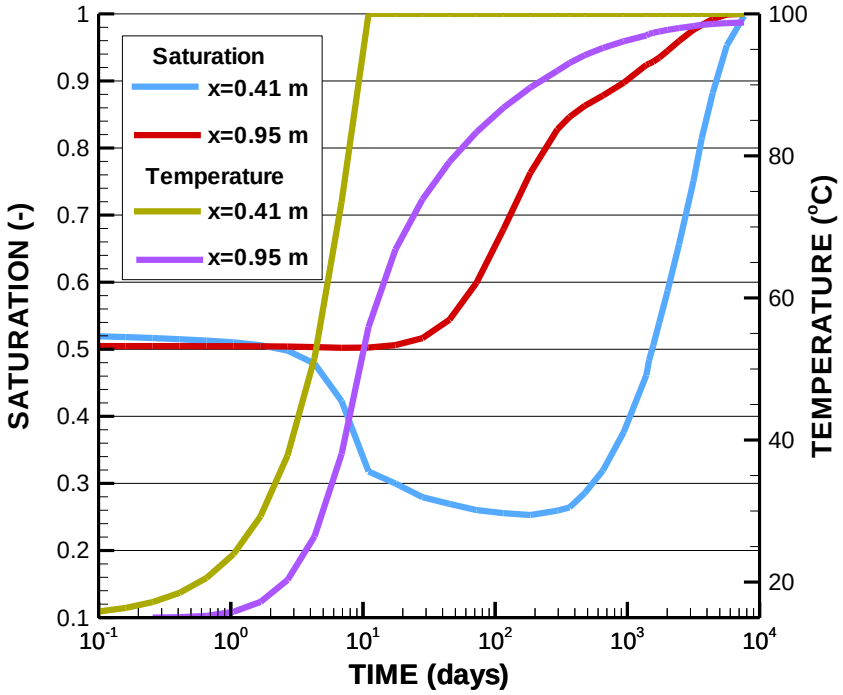

Figure 2.28. Time histories for temperature and saturation at two locations in the buffer for ROCMAS simulation.

2.3 THM MODELING STATUS AND PLANS

We are now one year into the participation of the DECOVALEX-2015 project. At the same time, we have conducted significant model developments related to the THM modeling of bentonite and clay rock. In this situation it is extremely valuable to have access to field and laboratory data for testing and validation of the newly developed models. In addition to the modeling of field experiments we are currently conducting a number of benchmark tests which enable us to compare our models to other models that are part of the DECOVALEX-2015 project. The modeling of the HE-D *in situ* heater test at Mont Terri has been completed showing good agreement with field data and with other models in the DECOVALEX-2015 project. We are currently focusing on parameterization of bentonite properties through modeling of laboratory experiments and benchmarks related to the modeling of the Mont Terri URL HE-E heater test and the Horonobe URL EBS experiment. This work was presented at the next DECOVALEX-2015 workshop at Mont Terri in November 2013. Thereafter, new model simulations will be performed related to both the Mont Terri URL HE-E experiment and the Horonobe URL EBS experiment.

3. MODELING REACTIVE DIFFUSIVE TRANSPORT

Clay-rich rock, like engineered clay barriers, have remarkable macro-scale properties such as high swelling pressure (Gonçalvès et al., 2007), very low permeability (Mammar et al., 2001), semi-permeable membrane properties (Malusis et al., 2003), and a strong coupling between geochemical, mechanical, and osmotic properties (Malusis and Shackelford, 2004; Gonçalvès et al., 2007). These properties are thought to arise from the distinct geochemical, transport, and mechanical properties of the interlayer nanopores of swelling clay minerals such as Na-montmorillonite and other smectites (Gonçalvès et al., 2007), as well as the non-swelling clays like illite. An important feature of the clays is the high negative charges typically present on the mineral surfaces, which results in a substantial Electrical Double Layer (EDL) that may make up a significant fraction of the porosity in the rock. This is certainly one of the reasons why clay-rich rocks like the Opalinus Clay in Switzerland are being considered as host rocks for geological nuclear waste repositories. The isolation potential of Opalinus Clay is determined by its physical and chemical properties. Hence, the main interest is in its permeability and capacity for self-sealing, as well as the diffusion behavior of radionuclides. The diffusion behavior of radionuclides and their retention potential are being investigated in the DR-A (diffusion and retention) experiment, for example. In a small borehole, an isolated test interval is saturated with water and a controlled amount of tracer material (e.g. tritium) is then introduced. After at least a year, the small borehole is overcored. In the new, larger core, investigations are then carried out to determine how far the tracer has penetrated into the rock. In the process, non-sorbing radionuclides (e.g. tritium) migrate more quickly than strongly sorbing radionuclides (e.g. cesium) that will be present in a high-level waste repository. In addition, as in engineered clay barriers, anion exclusion is an important effect that slows the rate of diffusion of the anions. The rate of diffusion is also monitored by tracking the chemistry of a borehole that is injected with a cocktail at a specified time. The rate of decrease of the constituents of the cocktail give an indication of the rate of diffusion of the anions, cations, and uncharged species through the Opalinus Clay, making it possible to assess the feasibility of using it as a natural barrier system for a geological nuclear waste repository.

This section describes a modeling approach for simulating the out-diffusion of tracers and ions from the DR-A borehole test in Opalinus Clay at Mont Terri site. Use is made of a new model for diffusive transport that includes an explicit Electrical Double Layer (EDL) model (CrunchEDL), which is described in detail below.

3.1 Mathematical and Numerical Formulation

Since the clays in rock like the Opalinus Clay typically possess a strong negative surface charge, the Electrical Double Layer (EDL) bordering the clays are enriched in cations and depleted in anions. The anions are said to be “excluded”, although only in the very smallest nanopores (typically less than 1 micron) are anions excluded altogether. Since the EDL porosity can constitute a significant fraction of the total porosity, it is important to have a mechanistic model to describe its behavior, especially the diffusive transport of ions within it. A rigorous model for

the electrical double layer (EDL) can be derived from the combination of several equations, including the Poisson equation describing the distribution of electrical potential, ψ, in water

$$\nabla^2\psi = -\frac{\rho_z}{\varepsilon}, \tag{3.1}$$

where ε is the permittivity and ρ_z is the volumetric charge density given by

$$\rho_z = e\sum_i z_i C_i. \tag{3.2}$$

In Equation 3.2, e is the elementary charge of the electron, z_i is the valence of the ion, and C_i is the concentration bulk solution. The Boltzmann distribution gives an expression for the concentration, $C_i^{EDL}(z)$, in the electrical double layer as a function of distance from the charge solid surface, z,

$$C_i^{EDL}(z) = C_i \exp\left(\frac{-z_i e\psi(z)}{k_B T}\right), \tag{3.3}$$

where k_B is the Boltzmann constant, and T is the absolute temperature. Combining Equation 3.3 with the Poisson equation (Equation 3.1) yields the Poisson-Boltzmann equation (Schoch et al., 2008)

$$\nabla^2\psi = \frac{-e}{\varepsilon}\sum_i z_i C_i \exp\left(\frac{-z_i e\psi(z)}{k_B T}\right) \tag{3.4}$$

which can be solved exactly for various simple formulations (e.g., the Gouy-Chapman model, which assumes a symmetric electrolyte).

Integrating the Poisson-Boltzmann equation over nanometer length scales from charged mineral surfaces, however, was not practical in the present version of CrunchEDL (a reactive transport simulator developed by Carl Steefel) because of the desire to consider larger length scales, so an alternative approach based on a Donnan Equilibrium model (Wersin et al., 2004; Leroy and Revil, 2004; Appelo et al., 2007; Leroy et al., 2007; Appelo et al., 2008; Birgersson and Karnland, 2009; Tournassat and Appelo, 2011) is used. The electrical double layer is conceptualized as consisting of two parallel layers of charge, one being the surface charge associated with direct sorption at the mineral surface (the Stern layer, typically divided into an inner and outer Helmholtz layer), and the second being the diffuse layer charge, a swarm of counterbalancing ions (Figure 3.1).

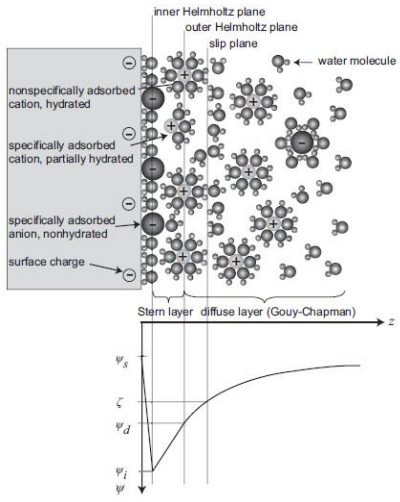

Figure 3.1. Schematic illustration of the Gouy-Chapman-Stern model of the solid-electrolyte interface, with the potential distribution $\psi(z)$ versus distance from the charged solid surface. The diffuse layer is defined beyond the outer Helmholtz plane (from Schoch et al., 2008).

In the approach taken in CrunchEDL, the chemical potentials of the species in the diffuse layer and the bulk solution are equated. Writing equations for the chemical potentials of the species *i* in the bulk solution (or macroporosity) (superscript "B") and electrical double layer (superscript "EDL") respectively, we have

$$\begin{aligned} \mu_i^B &= \mu_i^{B,0} + k_B T \ln a_i^B \\ \mu_i^{EDL} &= \mu_i^{EDL,0} + k_B T \ln a_i^{EDL} + q_i \psi_m \end{aligned} \tag{3.5}$$

where the superscript *0* (first term on the right-hand side) refers to the chemical potential at the reference state, a_i are the species activities, q_i, is the charge of an ion (the elementary charge of a particle, *e*, multiplied by the valence of the ion, z_i), and ψ_m is the mean electrical potential in the electrical double layer. The condition of Donnan Equilibrium implies that

$$\begin{aligned} \mu_i^{EDL} &= \mu_i^B \\ \mu_i^{EDL,0} &= \mu_i^{B,0} \end{aligned} \tag{3.6}$$

Combining Equations 3.3, 3.5, and 3.6 and assuming that the activity coefficients for the diffuse layer and bulk solution are the same gives the Boltzmann distribution for the ion activities in the electrical double layer, C_i^{EDL}:

$$C_i^{EDL} = C_i^B \exp\left(\frac{-z_i e \psi_m}{k_B T}\right). \tag{3.7}$$

The diffuse layer charge balances the charge within the Stern layer, Q^{SL}, which may consist in CrunchEDL of either a fixed mineral charge due to vacancies in the mineral structure (as in the case of classical ion exchange), or of fixed mineral charge modified by inner sphere and out

sphere complexes developed within the Stern layer calculated with a surface complexation model:

$$\phi^{EDL} \sum_i z_i C_i^{EDL} = Q^{SL} \tag{3.8}$$

where ϕ^{EDL} is the volume (or porosity) of the electrical double layer. The left-hand side of Equation 3.8 gives a volumetric charge density in units of charge equivalents per unit volume porous medium. The surface charge is given by

$$Q^{SL} = \sum_k^{Ns} z_k \Gamma_k \tag{3.9}$$

where Γ_k is the concentration in units of moles sorbed species per unit volume porous medium and z_k is the valence of the surface complex. In the CrunchEDL approach, therefore, one new equation is introduced (Equation 3.8), with one new unknown, the mean electrostatic potential of the diffuse layer, ψ_m. Note that in this formulation, the concentrations of the ions in the diffuse layer are dependent (or secondary) species that are calculated algebraically from the knowledge of the bulk solution composition and the mean electrostatic potential. A kinetic treatment of the diffuse layer ions would require that they be considered as primary unknowns.

Several approaches are available for calculating the fixed or Stern layer charge that is balanced by an electrical double layer. Even if the full Poisson-Boltzmann (PB) equation is used, special consideration needs to be given to the charge present in the Stern layer, a feature not always seen in the simpler implementations of the Poisson-Boltzmann equation. The starting point is the fixed mineral charge, which is normally given by the cation exchange capacity. If no Stern layer sorption occurred, the fixed mineral charge would provide a Dirichlet boundary condition for the electrostatic potential, ψ_f, at the solid surface,

$$\psi(0) = \psi_f \tag{3.10}$$

In the case of no Stern layer sorption, therefore, the PB equation can be integrated across the entire thickness *z* of the electrical double layer. In the case where the charged bentonite particles are bordered by bulk water, this would be the point in space where the local solution becomes electroneutral (where the electrostatic potential goes to zero). In the case of overlapping double layers, as considered by Gonçalvès et al. (2007) and Schoch et al. (2008), this would be the midpoint between the two charged clay (or solid) surfaces.

3.1.1 Dynamic Calculation of Electrical Double Layer Thickness

CrunchEDL also now includes a dynamic calculation of the electrical double layer porosity, ϕ^{EDL}, based on the diffuse layer thickness as a function of ionic strength according to

$$\phi^{EDL} = A_{clay}\lambda_{DL}D_L = A_{clay}\lambda_{DL}\frac{\beta_{DL}}{\sqrt{I}} \tag{3.11}$$

where D_L is the Debye length, λ_{DL} gives the multiples of the Debye length used in calculating the electrical double layer porosity (as in the approach of Tournassat and Appelo, 2011), β_{DL} is a temperature-dependent factor (= $2.15\text{x}10^{-10}$ meters at 25°C), I is the ionic strength of the bulk solution, and A_{clay} is the surface area of the charged mineral surfaces (normally clays). The Debye length provides an approximate measure of the width of the electrical double layer, although in their Donnan or mean electrostatic model, Tournassat and Appelo (2011) included as many as five Debye lengths to describe the EDL porosity.

Previously we have presented results in which the ionic strength is constant over the domain. It is also possible, however, to consider transient cases in which a salinity front propagates through the domain, changing the Debye length and thus the diffuse layer porosity dynamically. Note that in this case, the EDL thickness and thus the transport properties of the compacted bentonite are modified by the changing ionic strength. The effect is different from the swelling behaviour described in Section 2, and may in fact work in the opposite way.

In the CrunchEDL approach, in which solute mass is tracked in both the bulk porosity and the diffuse layer (EDL) porosity, this gives an accumulation term (neglecting liquid saturation) of

$$\frac{\partial\left[\phi^B C_i^B + \phi^{EDL} C_i^{EDL}\right]}{\partial t} = \frac{\partial\left[\phi^B C_i^B + \left(A_{clay}\lambda_{DL}\beta_{DL}\Big/\sqrt{I}\right)C_i^{EDL}\right]}{\partial t}. \tag{3.12}$$

In this case, the bulk porosity is treated as a constant, or at least as separately determined or fixed. Since the total porosity then can increase or decrease as the EDL thickness changes, special considerations need to be made to conserve mass in the system. Alternatively, it is preferred to treat the total porosity (bulk and EDL) as constant, in which case the bulk and EDL porosities would be updated according to:

$$\frac{\partial\left[\left(\phi^{Tot}-\phi^{EDL}\right)C_i^B+\phi^{EDL}C_i^{EDL}\right]}{\partial t} \tag{3.13}$$

where ϕ^{Tot} is the total porosity = $\phi^B+\phi^{EDL}$.

3.2 Application to the DR-A Diffusion Test at Mont Terri, Switzerland

To test the EDL transport model developed and described here, we have used it to simulate non-reactive and reactive transport processes in the DR-A experiment at Mont Terri in Switzerland. The Mont Terri site consists of Opalinus Clay, a primarily marly claystone with differing proportions of sand and carbonates, and is about 180 million years old. The stratigraphic section in which the Mont Terri site is located is shown in Figure 3.2. The Opalinus Clay is characterized by a very low permeability, which makes diffusion the dominant mode of solute transport (in this respect, similar to compacted bentonite under normal conditions).

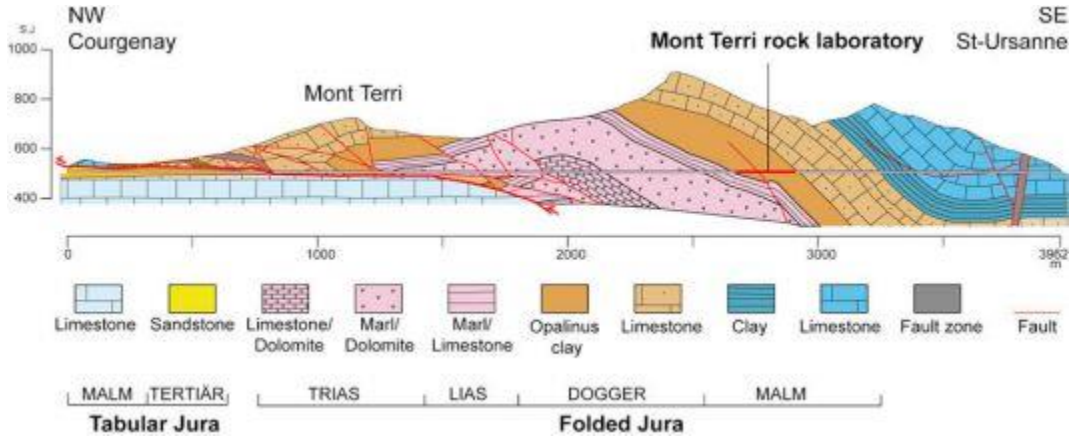

Figure 3.2. Stratigraphic section of the Jura Mountains in which the Mont Terri rock laboratory is located.

The DR-A test has consisted of a single borehole drilled in the Opalinus Clay that contains a constant ionic strength cocktail and anions, cations, and non-reactive tracers like tritium (HTO). Figure 3.3 shows the location of the DR-A niche in map view. Figure 3.4 shows the experimental setup used for the earlier DI-A test at Mont Terri, similar in setup to what has been used for the DR-A test. A volume of cocktail in excess of the actual cylindrical volume of the borehole is

used as reservoir. This is treated in CrunchEDL by defining a capacity factor, α (= 2.175), that represents the additional volume needed to accommodate the extra solution volume (11.2 L) available to the actual borehole volume. In the first stage through Day 189, the borehole cocktail is a 0.384 M ionic strength solution dominated by sodium (Table 3.2). At Day 189, a higher ionic strength solution (1.135M) was circulated in the borehole apparently without diluting the tracers (HTO, iodine, and bromine) in the cocktail. The higher ionic strength was made up of both Na^+ (0.50M) and K^+ (0.56M) and Cl^- (1.13M) and was allowed to diffuse out of the borehole through Day 412.

3.2.1 CrunchEDL Simulation of DR-A Test

3.2.1.1 DR-A Simulation Parameters

In the simulations, a total porosity of 0.15 was assumed for the Opalinus Clay. The total porosity was treated as fixed, with partitioning between the "bulk" and "EDL" porosities governed by the Debye length (determined by the ionic strength, and thus variable over the course of the 412 day experiment). For Case 1 (Figure 3.5), four Debye lengths were used to calculate the EDL porosity according to Equation 3.11. For Case 2 (Figure 3.6), six Debye lengths were assumed. The dynamic Debye length and result partitioning between bulk and EDL porosity was calculated using Equation 3.12. The additional volume needed to accommodate the extra solution volume (11.2 L) available to the actual borehole volume (Table 3.1) was treated in CrunchEDL by defining a capacity factor, α (= 2.175).

Table 3.1. Physical parameters for DR-A test

Length of injection interval	104 cm
Length of filter screen	67 cm
Volume of circulation system	11.2 L
Borehole diameter	76 mm
Filter, outer diameter	70 mm
Filter, inner diameter	62 mm
Filter, porosity	45%
Gap between filter and borehole wall	3 mm
Central tube, outer diameter	61 mm
Dip of bedding	32.5º
Porosity of Opalinus Clay	15%

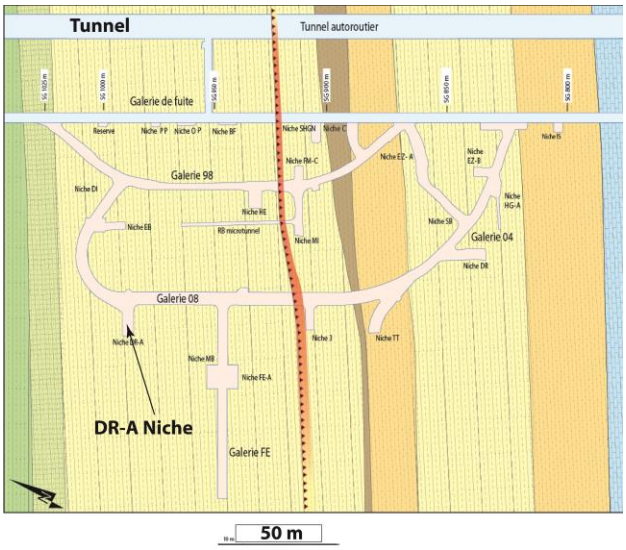

Figure 3.3. Plan view of the Mont Terri site showing location of DR-A niche.

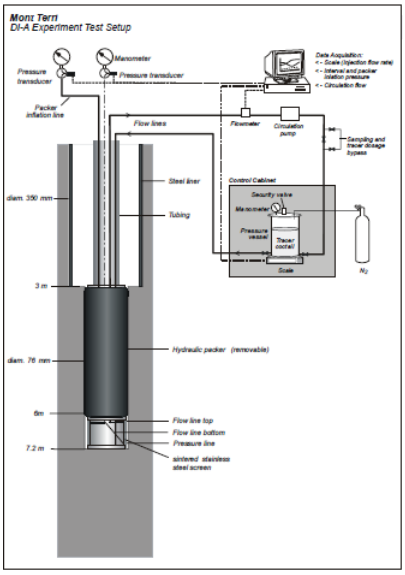

Figure 3.4. Schematic of the experimental setup from the DI-A test, similar in concept to the DR-A test.

Table 3.2. Geochemistry of borehole solution, with higher ionic strength used 189-413 days.

Species (Total)	0-189 Days	189-413 Days
	(M)	(M)
Ionic Strength	0.384	1.135
pH	4.16	7.60
Ca^{2+}	0.0188	0.0230
Mg^{2+}	0.0180	0.0147
Na^{+}	0.259	0.500
K^{+}	0.0016	0.560
Cl^{-}	0.300	1.113
SO_4^{2-}	0.0137	0.00024
HCO_3^{-}	0.00328	0.00050
Sr^{2+}	0.00051	0.00045
Cs^{+}	0.00027	0.0000062
I^{-}	0.0109	0.0109
Br^{-}	0.0109	0.0109
HTO	1.000	1.000

For the simulation, a preliminary estimate of the illite specific surface area (200 m2/g) and volume fraction (0.25) was made for the Opalinus Clay, which is the material expected to provide most of the retardation. A fixed mineral charge of 200 μequivalents/g illite was assumed, all of which is compensated by the electrical double layer (i.e., no Stern Layer sorption was allowed). Cylindrical coordinates were used in the simulations, with the assumption that the system was axisymmetric—thus, the system is modeled in a 1D plane.

3.2.1.2 DR-A Simulation Results

In both cases, a high value for the diffusion coefficient of solutes in the filter has been used to avoid a limitation on the rate of loss from the borehole due to this material. In Case 1 (Figure 3.5), a diffusion coefficient of 2.7×10^{-10} m^2/s was assumed for all of the species in the Opalinus Clay, with the exception of the anions, for which a value of 1.25×10^{-10} m^2/s was used. As an initial test, the same values for the diffusion coefficients were used in the bulk and EDL porosity, although this assumption abandoned in Case 2 (Figure 3.6) so as to optimize the fit to the ionic strength effect.

Results for Case 1, with the increase in ionic strength in the borehole-reservoir system at Day 189, are shown in Figure 3.5. It should be noted that the anion (iodide and bromide) breakthrough data shows a slight increase in the rate of loss from the borehole starting about Day 189, the time when the ionic strength was increased. There is a mismatch with the HTO data, but close inspection shows that it follows the same exponential decay curve (i.e., the slope of the

concentration versus time profile continuously decreases). Figure 3.6 shows that the HTO can be modeled as a single decaying curve. The simulation results in Figure 3.5 show only a very small increase in the rate of loss from the borehole (solid line red for iodide), apparently the result of the use of the same diffusion coefficients for the iodide and bromide in the EDL and bulk porosity. One expects that diffusion rates of anions in the EDL are smaller because of the greater tortuosity for the negatively charged ions versus the bulk fluid. Note that the data shows a stronger effect of the ionic strength, with the rate of loss from the hole increasing more dramatically for the anions at about Day 290. This effect is in keeping with a decrease in the thickness of the EDL, and thus an increase in bulk versus EDL porosity that follows from Equation 3.11. This is in contrast to some of the predictions based on swelling behavior alone that would have the effect of an increase in ionic strength reducing the bulk porosity. If the only effect of an increase in ionic strength was on the swelling behavior of the clays, then one would expect a less (not more) rapid loss of anions from the borehole.

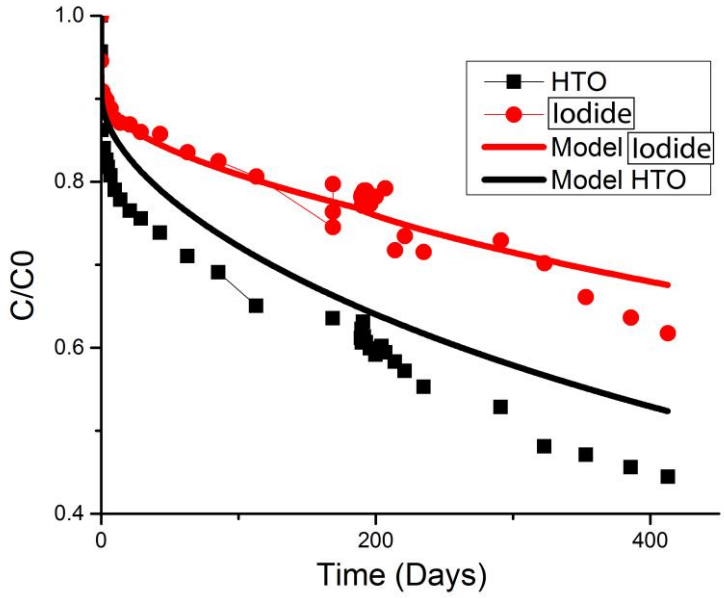

Figure 3.5. Data (symbols) versus simulation results (solid lines) for the DR-A test through Day 412 for Case 1 in which diffusion coefficients are the same in the bulk and EDL porosity and 4 Debye lengths make up the EDL porosity.

As a contrast, compare a simulation in which all species (anions, cations, and uncharged species) are characterized by diffusion coefficients of $4x10^{-10}$ m^2/s in the bulk porosity, while in the EDL porosity the cations and uncharged species have diffusion coefficients of $1x10^{-10}$ m^2/s and the anions have diffusion coefficients of $5x10^{-11}$ m^2/s (i.e., nearly an order of magnitude lower than in the bulk porosity). In order to get an improved fit with the data, it is also necessary to increase the number of Debye lengths considered as making up the EDL porosity to 6 from the value of 4

used in the simulations shown in Figure 3.5. When a value of 6 Debye lengths is used, then the EDL porosity makes up approximately 50% of the total porosity of the Opalinus Clay. As shown in Figure 3.6, with this model the increase in ionic strength results in an increase in the rate of out-diffusion in the simulation results (see change in slope at 189 days).

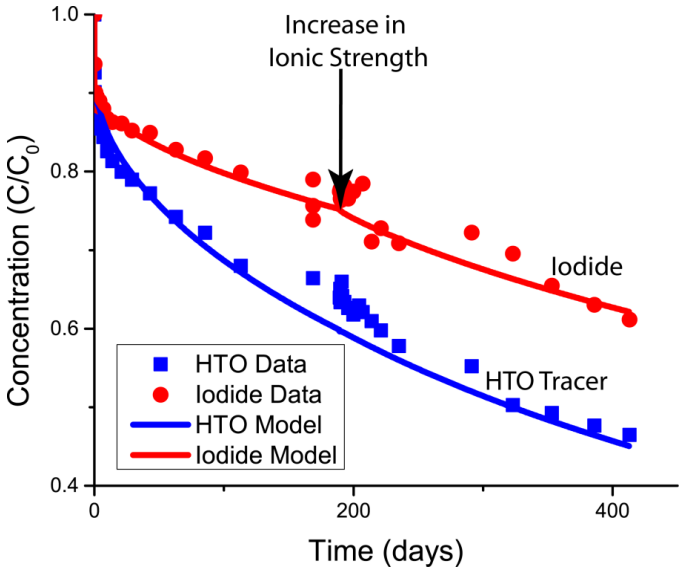

Figure 3.6. Data (symbols) versus simulation results (solid lines) for the DR-A test through Day 412 for Case 2 in which diffusion coefficients for anions are nearly one order of magnitude less in the EDL porosity than in the bulk porosity. 6 Debye lengths are considered for the EDL porosity in this case.

Table 3.3. Opalinus Clay Properties and Simulation Results

	Case 1 (Figure 3.5)		Case 2 (Figure 3.6)	
	0-189 Days	189-413 Days	0-189 Days	189-413 Days
Illite Specific Surface Area	200 m^2/g	200 m^2/g	200 m^2/g	200 m^2/g
Illite Volume Fraction	0.25	0.25	0.25	0.25
Fixed Charge of Illite	200 µeq/g	200 µeq/g	200 µeq/g	200 µeq/g
EDL Porosity (equilibrated w/ borehole)	0.076	0.049	0.113	0.074
Number of Debye lengths	4	4	6	6
Na^+ Concentration in EDL (equilibrated)	0.253	0.661	0.380	0.586
K^+ Concentration in EDL (equilibrated)	0.0029	0.335	0.0025	0.320
I^- Concentration in EDL (equilibrated)	0.0046	0.0049	0.0054	0.0051

4. Cement-Clay Interactions in Engineered Barrier Systems

4.1 Introduction

Cementitious materials are an integral part of the EBS, lining structures, and ground support in deep geological storage of nuclear waste. Engineered cement phases are also used for stabilization and encapsulation of intermediate and low level nuclear waste forms (Kosakowski and Berner, 2013; Pierce et al., 2010). Given the inherently contrasting pore-fluid chemistries between clay or other silicates (bentonite 'buffer' mix or clay rock) and cement, the interface between these two domains is chemically active and it is therefore an important boundary between the EBS and the natural barrier system (NBS). Therefore, cement reactivity can be a major factor in barrier performance within the repository safety assessment (Adler et al., 1999; Gaucher and Blanc, 2006; Gaucher et al., 2004; Kosakowski and Berner, 2013; Mäder and Adler, 2005; Pabalan et al., 2009; Savage, 2011; Savage et al., 2007).

In situ long-term experiments such as those at the ANDRA Meuse/Haute Marne (France) underground research laboratory (URL) (cement/shotcrete – claystone) (Gaboreau et al., 2012; Gaboreau et al., 2011) and the cement – Opalinus Clay interaction (CI) (Mader, 2012) experiment at the Mont Terri (Switzerland) URL have produced the much needed field-scale samples for phase characterization and geochemical studies at the clay-rock / cement interface. Other URL cement interaction studies includes those at the HADES site in Belgium (Read et al., 2001), the Tournemire site in France (Gaboreau et al., 2011), and the LOT project at the Äspö Hard Rock Laboratory site in Sweden (Karnland et al., 2009). Such URL sites provide a unique opportunity to conduct experiments and examine the extent at which alkaline fluids migrate across the EBS outer interface along with the mineralogical and multi-scale textural changes that accompany these interactions. These types of observations serve as the basis for the validation of reactive transport models and at the same time provides important information on the constraint of input parameters to these models. For example, accurate mineral phase characterization of clay rock and secondary mineral assemblage is crucial in defining the compositional system to be considered in the model.

4.2 Cement – Opalinus Clay Interaction (CI) Experiment at Mt Terri

The cement – Opalinus Clay interaction (CI) is a long-term experiment designed to supplement the current knowledge on the influence of cement on Opalinus Clay in a deep geological repository. Reactive transport simulations indicate that it will take decades before measurable alteration from an alkaline plume spread effectively beyond the confines of a concrete domain in contact with Opalinus Clay (OPA). Therefore, an extended time in the order of years motivated the inception of "phase 12" experiment so it can generate useful results in the planned time frame. The "phase 12" experiment started in 2007 by filling two boreholes with ordinary portland cement (OPC) with the purpose of measuring the extent of migration of an alkaline plume relative to the transport of a deuterated water tracer. Bentonite was also used as filling material to simultaneously evaluate the influence of cement on bentonite. In addition to OPC, two types of low-pH cement are also used as borehole filling material. The CI field experiment

configuration is depicted in Figure 4.1. Figure 4.2 showing the various sampling boreholes along the regions of interest transecting the interfaces between filling material and host rock. One of these samples of the interface between OPA and OPC was obtained by SNL and LANL to conduct small-angle neutron scattering (SANS) studies which are described in a later section. Table 4.1 describes the time schedule of the CI experimental program. The interface analysis and modeling steps in Table 4.1 map to the SANS study and reactive transport plus modeling activities, respectively. The current stage of the CI program is currently focused in the analysis of interfaces and material phase characterization from sampled core materials.

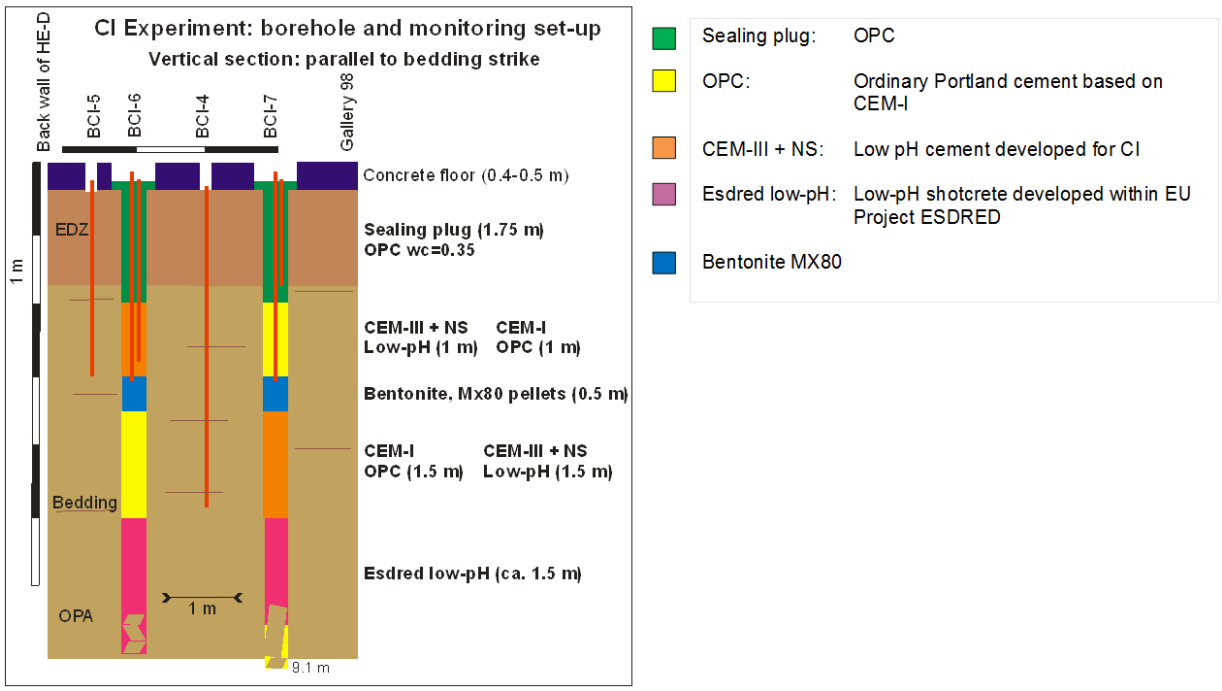

Figure 4.1. Schematic configuration of the cement – Opalinus Clay interaction (CI) experiment at Mont Terri URL, Switzerland.

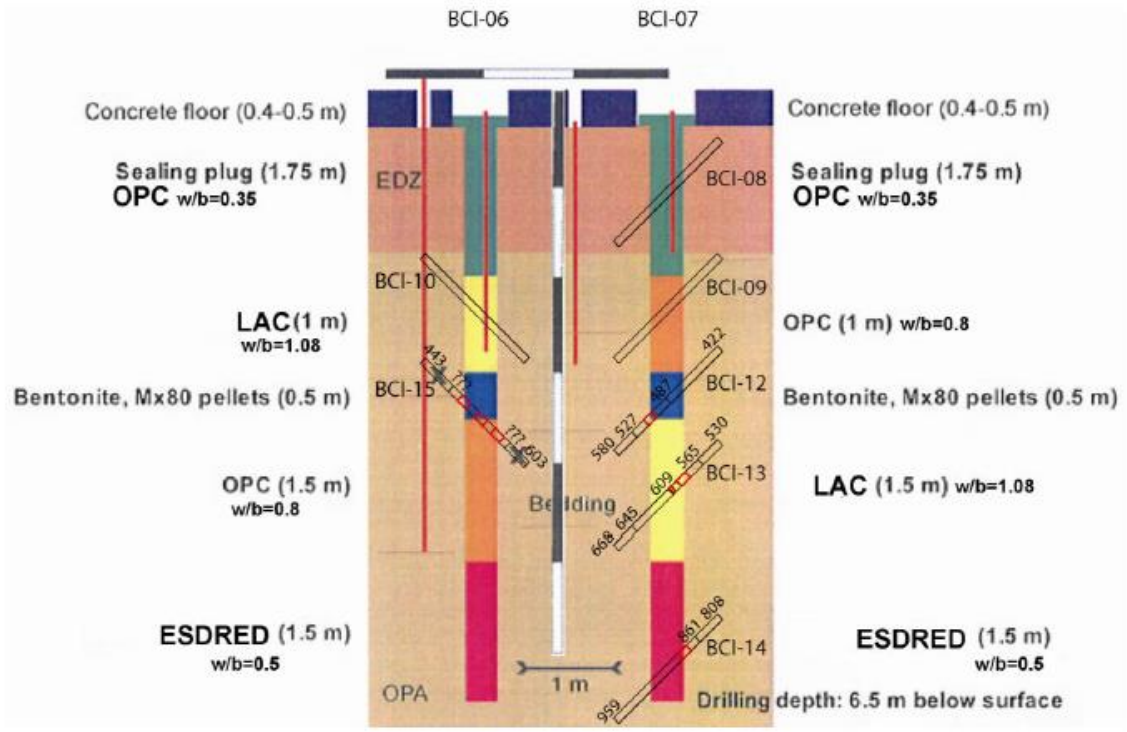

Figure 4.2. Schematic configuration of the cement – Opalinus Clay interaction (CI) experiment showing sampling boreholes transecting the interfaces between filling material and host rock. See legend in previous figure for labeling of backfilling materials. LAC corresponds to low-pH cement develop for the CI experiment.

Table 4.1. Time schedule of the CI experimental program. (program communication from Dr. Urs Mader)

Experiment **[CI]**	**20 12** I	II	III	IV	**20 13** I	II	III	IV	**20 14** I	II
	Phase 17		**Phase 18**				**Phase 19**			
Drilling Campaigns:										
Steps (Phase 18):										
Step 1: Maintenance / Logistics										
Step 2: Sampling (Phase 17)										
Step 3: Sample preparation (Phase 17 & 18)										
Step 4: Analysis of ^{2}HHO profile										
Step 5: Analyses of interfaces										
Step 6: Sampling of a mock-up barrel (option)										
Step 7: Modeling										

4.3 Cement –Clay Interaction and Reactive Transport: Brief Overview

Cement leaching has been a concern to the performance assessment deep geological repository concepts due to the potential development of hyperalkaline plumes and their aggressive interaction with silicate host rock. There is a rather extensive treatment of cement fluid-solid interactions in the scientific literature describing how these affect the concrete phase composition and leaching behavior (Gaucher and Blanc, 2006; Gaucher et al., 2004; Glynn and Reardon, 1990; Kersten, 1996; Kulik and Kersten, 2001; Lothenbach et al., 2010; Lothenbach and Gruskovnjak, 2007; Lothenbach et al., 2008; Lothenbach and Winnefeld, 2006; Pabalan et al., 2009). Clay host rock formation such as the Boom clay and their associated repository research program (ONDRAF/NIRAS) have conducted research on cement – clay interactions and behavior of cement as a buffer material in Belgian supercontainer engineered barrier design (Wang et al., 2010). Savage et al. (2007) and Dauzeres et al. (2010) provides a description of cement – clay interactions with emphasis on the characterization of secondary mineral assemblage and alteration processes at the interface. Gaucher and Blanc (2006) also provides an extensive synopsis of the past and current research conducted on clay-cement interactions applicable to the EBS in deep subsurface disposal of radioactive waste. These authors also describe key stages at which clay interaction with cementitious materials are subjected to and the anticipated changes to fluid chemistry:

- Interactions of cement (and associated pore fluid) with near-neutral pH pore water (host clay-rock)
- Dissolution of cement phases like portlandite resulting in pH increase
- Eventual attainment of equilibrium with respect to calcium-silicate-hydrate (CSH) phases and other secondary phases such as zeolites, clays, and oxy-hydroxides solids.

One of the salient consequences of clay-cement interactions is the clogging/sealing of pores and fractures near the cement-clay interfacial region largely as a result of secondary mineral precipitation. Such clogging is crucial to the long-term assessment of sealing performance at EBS interfaces and many studies ranging from URL field characterization to reactive transport modeling have advanced this process which is of course beneficial to the barrier capability. For example, the cement-clay domain in a disposal gallery will tend to be spatially associated with the excavated disturbed zone (EDZ). The EDZ is characterized by the presence of cracks that can become fast transport paths communicating the EBS with the host rock. Gaboreau et al. (2012) describes the filling of these cracks with gypsum in samples of the clay – cement interface. Even with all the artifacts involved in obtaining such samples (e.g., fracturing) and their preparation, this observation can be considered as a manifestation of crack healing in the EDZ. Although healing of cracks and openings has been observed in cement and clay media, such attribute can be considered as *sacrificial* in the evaluation of barrier performance on the basis of the extent of this zone in EBS design concepts. It should be noted that similar observations on cement healing of fractures has been reported by Carey et al. (2007) on borehole

samples borehole of cement casing from the SACROC (Scurry Area Canyon Reef Operators Committee) site for CO_2 flooding operations. The cement casing experienced carbonation producing a carbonate fracture filling. The cement casing sample studied in Carey et al. (2007) study was in contact with the shale caprock at this site which is a somewhat similar scenario as the cement – clay rock contact in URLs.

4.4 Thermodynamic Modeling of Clay-Cement Interactions

A description of thermodynamic data development for cement phases in the UFD campaign has been given in Jové Colón et al. (2010), Jové Colón et al. (2011), and Jové Colón et al. (2012). These reports provide descriptions of the development of thermodynamic data for cements from the Yucca Mountain Project (YMP) and more recent efforts. For completeness, a synopsis of these cement thermodynamic data description will be given in this section. It should be noted that the CI collaborative project has a modeling step in phase 18 (see Table 4.1). Although, the CI modeling activity hasn't been clearly defined, the thermodynamic modeling tool described in this section may be used to support this activity.

Thermodynamic modeling approaches are very powerful tools in the evaluation of chemical equilibrium between cement phases, aqueous solutions, and gases (Blanc et al., 2010b; Gartner and Jennings, 1987; Matschei et al., 2007; Reardon, 1990). However, these methods also have their limitations due in large part to the assumption of chemical equilibrium, their applicability to compositionally complex systems, and the overall scarcity of thermodynamic data. Jové-Colón et al. (2010) provided an example of a test case using reaction path modeling with the computer code EQ3/6 of Ordinary Portland Cement (OPC) leaching and compared the resulting mass transfer trends to experiments reported by Kienzler et al. (2000) and Metz et al. (2004). Comparison of these trends, although qualitative, shows good agreement supporting the key assumptions of chemical equilibrium in the complex interactions of cement with brine.

The sources described Jové Colón et al. (2010), Jové Colón et al. (2011), and Jové Colón et al. (2012) include multiple sources from U.S. and international nuclear waste research programs and emphasis is given to the most recent comprehensive efforts on the chemical and thermodynamic evaluation of cement phases (Wolery and Jové-Colón (2007), Taylor (1990); Reardon (1990); Bruton et al. (1993); Atkins et al. (1992); Neall (1996); Batchelor and Wu (1993); Sarkar et al. (1982); Atkins et al. (1993); Shaw et al. (2000); Glasser et al. (1987); Damidot et al. (1994); Bennett et al. (1992); Babushkin et al. (1985); Greenberg and Chang (1965); Fujii and Kondo (1983); Harvie et al. (1984); MacPhee et al. (1989); Berner (1987, 1990) Greenberg and Moller (1989); Perkins and Palmer (1999); Lothenbach et al. (2010; 2008); Balonis et al. (2010); Matschei et al. (2007); Blanc et al. (2010a, b)). The CEMDATA07 thermodynamic database is a recent compilation from the MPA institute, ETH, Switzerland, that represents a combined effort various authors to provide a comprehensive set of data (Matschei et al. (2007), Moschner et al. (2008), Blanc et al. (2010a, b), and Lothenbach et al. (2010; 2008; 2006).

Most compilations are centered on end-member compositions due to data availability and better constrains on the retrieval of thermodynamic data. However, incongruent dissolution behavior

(e.g., solubility as function of Ca/Si ratio) is a glaring limitation not only in obtaining the suitable data to model this phenomena but also adds complexity of the system (Berner, 1988, 1992; Greenberg and Chang, 1965; Greenberg et al., 1960; Soler and Mader, 2010). The treatment of CSH solid solutions has been mainly based on two approaches: Gibbs energy minimization and mass action law equations (e.g., Lippmann functions; binary non-ideal solid solutions) (Borjesson et al., 1997; Carey and Lichtner, 2007; Kersten, 1996; Kulik and Kersten, 2001; Lichtner and Carey, 2006; Lothenbach et al., 2010; Sugiyama and Fujita, 2006; Thomas and Jennings, 1998). Implementation of a Gibbs energy minimization model for CSH using the Cantera suite of codes (Moffat and Jové Colón, 2009) is given in Jové Colón et al. (2012).

Recent efforts in the development of thermodynamic data for cementitious phases have been fruitful in providing unified sources of data that have undergone a good level of scrutiny and analysis in terms of consistency and adopted methodologies for critical evaluation. Still, there are discrepancies (although within bounds) between databases including those for cements so there is a need to establish a common approach in their evaluation for usage and quality assessment compliance in repository science programs. An important part of such unifying effort should include tools to evaluate data and provide a centralized framework for data consistency and analysis. A proposed tool for such task is the open-source software library CHNOSZ (Dick, 2008). CHNOSZ is a package (in R language) that includes multiple functions and data to conduct chemical thermodynamic modeling covering large sets of chemical species for biochemistry and geochemistry at low temperatures. The package follows the approaches and methodologies developed by late Prof. Harold Helgeson (UC Berkeley) and students in the analysis and application of standard thermodynamic properties of aqueous, solids, and gases. It also includes a comprehensive set of data for organic species and biomolecules. The CHNOSZ package is developed in R (http://www.r-project.org/) which is an open-source language and computational environment for statistical analysis with a wide variety of graphics resources. The advantages of R as a language platform lie in its rich set of integrated capabilities for graphics, statistical computations, and data manipulation. A key capability of the CHNOSZ package is the ability to calculate thermodynamic properties of aqueous species using the Helgeson-Kirkham-Flowers (HKF) EoS and the generation of activity phase diagrams as a function of temperature, pressure, and species activities. An example of this is the construction of an activity phase diagrams for cementitious phases. Such diagrams are very useful in the mapping of phase relations with respect to aqueous species activities and gas fugacities. Also, given the thermodynamic database content (e.g., EoS parameters and Cp data) and input structure in CHNOSZ it allows the constructions of these phase diagrams as a function of pressure and temperature. There are other types of calculations with CHNOSZ such as those conducted using the code SUPCRT92 for single species or reactions, mass transfer calculations, and generation of speciation diagrams. Moreover, the package also exploits the capabilities of R to conduct parameter regressions and multidimensional optimization which are essential tools in the evaluation of thermodynamic data particularly for multiphase multicomponent systems.

Figure 4.3 shows an activity phase diagram of log activity of H_2O vs. the log activity of Ca^{++} in the system Ca-Al-SO_4-H_2O. This system was chosen to allow comparisons with the work of Albert et al. (2006) on the stability of cement phases with respect to the chemical potential or activity of water. As with the construction of any activity phase diagram, there are assumptions on the considered solids in the phase assemblage and the fixing of species activities. In Figure 4.4a, the logarithm of activities of Al^{+++} and H^+ are fixed to values of -6 and -11.3, respectively. Logarithmic values of the activities for the remaining species (Ca^{++}, SO_4^{--}, and O_2) are set to zero. Changes in the activities of these latter species (with the exception of SO_4^{--}) do not affect the overall topology of the diagram. Comparisons of equilibrium phase relations and invariant points generated in this diagram with those from the analysis of Albert et al. (2006) show a good level of agreement even with the use of different sources of thermodynamic data. All activity phase diagrams are constructed 25°C and 1 bar. The analysis of Albert et al. (2006) is based on the concept of thermodynamic "affigraphy" to predict the structure of phase relations in a multicomponent chemographical representation (Guy and Pla, 1997). This approach is similar to that adopted by mineralogist and petrologists to graphically represent stable mineral assemblages in P-T diagrams (e.g., Schreinemakers Rules).

Changes on the fixed activity values for the basis species in this system will change the topology of activity phase relations in the diagram. For example, a change in the log activity of H^+ towards lower values (e.g., -10.3) modifies the overall mapping of invariant point relations and the size of the stability fields of the cement phases (see Figure 4.4b). Fixing the activity of H^+ to near-neutral or acid concentrations will destabilize the cement phases and would expand the gibbsite and anhydrite stability fields. Another feature of constructing activity phase diagrams with CHNOSZ is the ease at which the component axis can be changed (say SO_4^{--} instead of Ca^{++} for the x-axis) to produce another phase diagram with different invariant point relations (see Figure 4.5). Similarly, adding or changing specified components and phases to a system is straightforward as with the addition of $SiO_{2(aq)}$ as a variable to evaluate the equilibria of cement and silicate phases such as kaolinite (clay) and laumontite (Ca-zeolite). Figure 4.6 show the stability relations of ettringite-Al with respect to kaolinite and laumontite with the log activity of H^+ is set to -9.3. Notice that an invariant point is clearly defined between these three phases suggesting the stable coexistence of secondary clay and zeolite at pH values within the range of low-pH cement pore solutions. The coexistence of these secondary minerals has been suggested in cement alteration studies. It should be noted that commercial software packages like Geochemist's Workbench® (GWB) (Bethke, 2008) can also generate similar type of activity phase diagrams and other types of graphical representation commonly used in geochemical analysis. However, GWB is not open-source and it's not directly linked to a computational environment that allows for computation of thermodynamic properties of chemical species and reactions, and statistical evaluation of thermodynamic data.

Given the versatility of CHNOSZ as an evaluation tool of thermodynamic data and graphic analysis for the generation of activity of phase diagrams, future work will include:

- Inclusion of the current cement thermodynamic database compilation into OrganoBioGeoTherm (OBIGT) database format for use with the CHNOSZ package. Such approach would provide a solid consistency basis using accepted critically-assessed data for the thermodynamic analysis of aqueous and solid species.
- Analyze chemograhic relations of cement phase stability with comparison to leaching and solubility data as a function of temperature. Comparisons of chemographic phase equilibria relations with outputs from solid-solution interaction models (reaction path and reactive transport calculations) are very useful in mapping predictive alteration trends in the alteration of barrier materials.
- Expand the number of phases to include clay and zeolite minerals to evaluate the coexistence of these phases in scenarios of cement-clay interactions. Although the OBIGT database already contains kaolinite and some zeolites, the list of relevant minerals to cement alteration needs to be expanded for a more comprehensive set of silicate solids.
- Following the above item, CHNOSZ could serve as a key tool for the wide-ranging analysis and development of thermodynamic data consistent with the guidelines adopted in other database efforts (e.g., NEA-OECD).

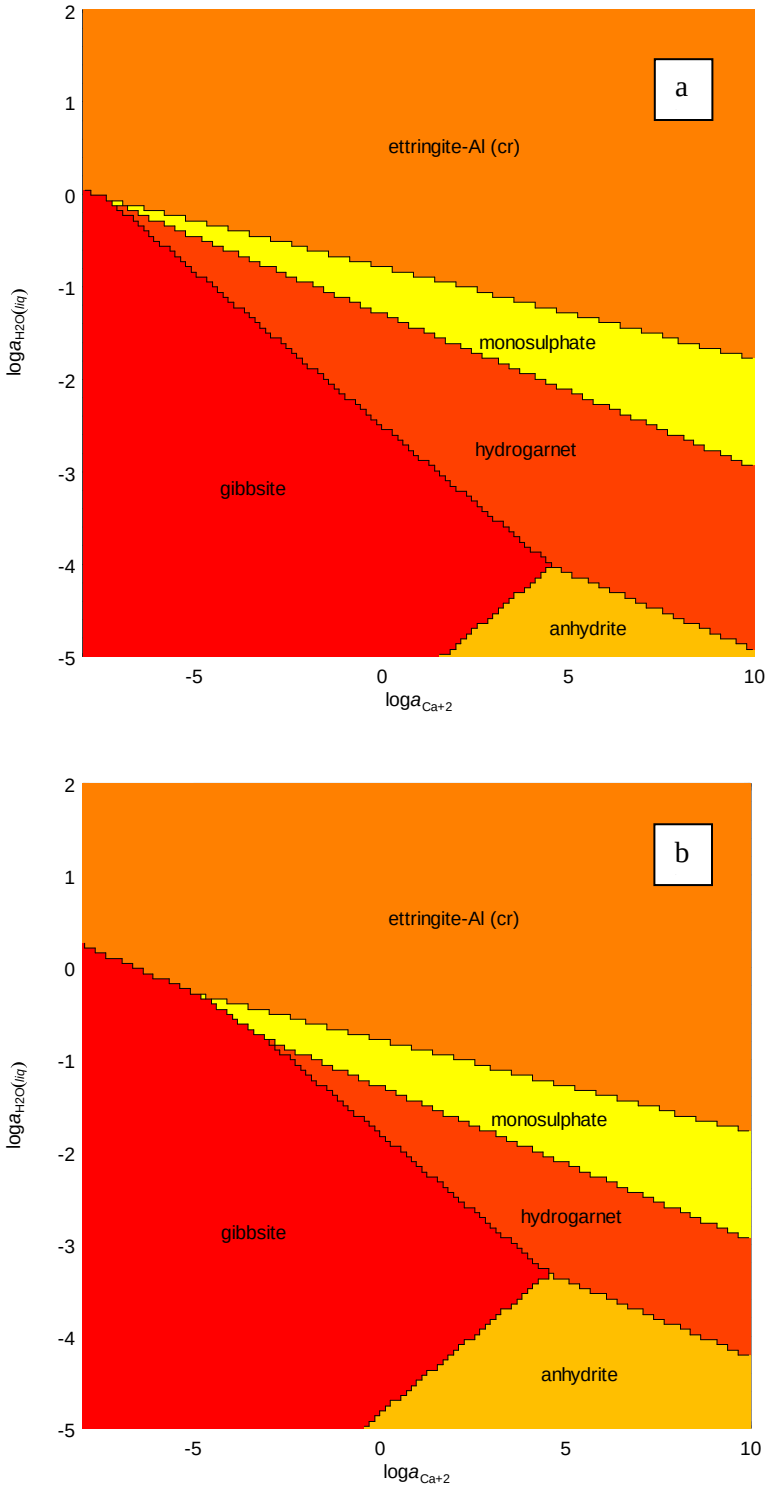

Figure 4.3. Activity phase diagram of log $aH_2O(liq)$ vs. log aCa^{++} for the system Ca-Al-SO_4-H_2O: a) logarithms of the activities of Al^{+++} and H^+ are fixed to -6 and -11.3, respectively; b) logarithms of the activities Al^{+++} and H^+ are fixed to -6 and -10.6, respectively. The logarithms of activity values of remaining species are set to zero. The diagrams are constructed at 25°C and 1 bar.

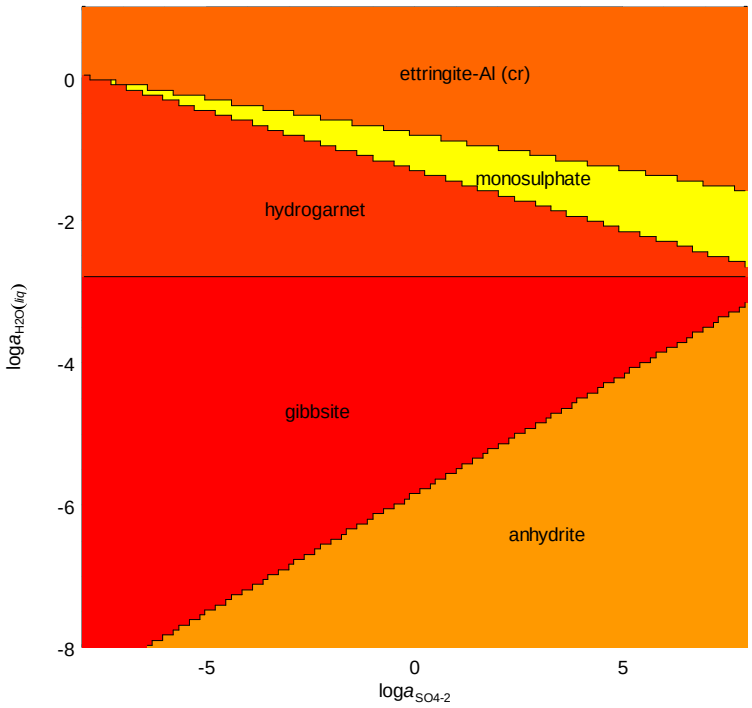

Figure 4.4. Activity phase diagram of log $aH_2O(liq)$ vs. log aSO_4^{--} for the system Ca-Al-SO_4-H_2O. The logarithms of the activities of Al^{+++} and H^+ are fixed to -6 and -11.6, respectively. The diagrams are constructed at 25°C and 1 bar.

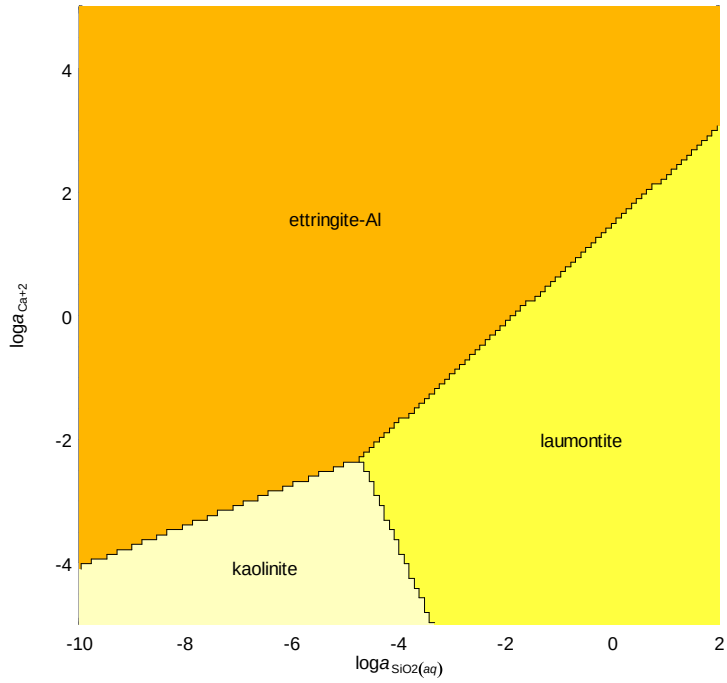

Figure 4.5. Activity phase diagram of log $aH_2O(liq)$ vs. log aCa^{++} for the system Ca-Al-SiO_2-SO_4-H_2O. The logarithms of the activities of Al^{+++} and H^+ are fixed to -6 and -9.3, respectively. The diagrams are constructed at 25°C and 1 bar.

4.5 Reactive Transport Modeling at Clay-Cement Interfaces

Reactive transport modeling of clay-cement interactions have been studied through observations in field scale experiments at clay rock media URLs and laboratory experiments. The works of Gaucher and Blanc (2006), Dauzeres et al. (2010), Savage (2011), and Gaboreau et al. (2012) among others provide a very good description of these types of investigations and some ideas on the needs to enhance the state of knowledge of this type of research. As explained in previous sections, interest on cement-clay interactions has been expanded towards studying the effects at the clay rock / cement interface given the wide-ranging use of cementitious materials in deep geological repositories. The use of cement spans from applications to support structures, barrier backfilling to cementitious waste forms. For this reason, reactive transport modeling tools has been used in the evaluation of spatio-temporal occurrence of engineered barrier alteration phases, their effects on the porous barrier (engineered and natural) transport properties, and fluid chemistry evolution. All these pieces of information are key to the assessment of EBS concepts and are considered in the establishment of confidence on the design and material behavior for short- and long-term performance. The CI collaborative project has a modeling step in phase 18 targeting simulation of cement – clay interactions and hyperalkaline plume migration (see Table 4.1). Therefore, the simple test case described in this section using the PFLOTRAN code could be used in support of this activity.

The aggressive nature of alkaline fluids generated by cementitious materials with clay and other silicates has been well documented and reviewed (Berner et al., 2013; Gaboreau et al., 2012; Kosakowski and Berner, 2013; Soler, 2012; Soler and Mader, 2010; Yang et al., 2008). The alteration parageneses of cement-bentonite coupled interactions has been outlined by Savage (2011; 2007). Cementitious materials can be present in many forms ranging from aggregates (concrete and mortar), shotcrete, and grouts. Cement aggregates can be mixed with siliceous or calcareous materials in some cases complicating the behavior of an already "complex" material assemblage. Such variability in cement materials has also motivated the tailoring of reactive transport computational schemes to closely represent the form of these phases targeted for use in a repository repository (Kosakowski and Berner, 2013).

Various reactive transport modeling investigations have focused on the effects of alkaline fluid interactions at the clay – cement interface (De Windt et al., 2004; Fernandez et al., 2009; Kosakowski and Berner, 2013; Marty et al., 2009; Trotignon et al., 2007; Trotignon et al., 2006; Trotignon et al., 1999; Wang et al., 2010). Other reactive transport studies evaluated the long-term interactions of alkaline fluids in contact with a marl formation as a natural analogue case (Shao et al., 2013; Soler, 2005; Steefel and Lichtner, 1998). These studies outline the effect of clogging or pore sealing due to secondary mineral formation, which is important to assessment of barrier performance. Even when these authors used different computer codes (CRUNCH(Flow), OpenGeoSys-GEM, HYTEC, CORE^{2D}), their overall results are quite similar in terms of the expected changes in fluid chemistry and the decrease of mass transfer across the interface due to pore occlusion. Some differences in modeling results are mainly on the

predicted time needed for the clogging process to effectively seal the interfacial domain and the choice of phase thermodynamic data.

The purpose of this study is to provide and test a tool to conduct reactive transport modeling of fluid-solid interactions at the cement – clay interface. The selected tool is PFLOTRAN, an open source, state-of-the-art massively parallel subsurface flow and reactive transport code (Lichtner et al., 2013). One major feature of PFLOTRAN lies in its performance on massively parallel computing architectures but also in its portability to workstations and laptops. Parallelization is achieved through domain decomposition using the PETSc (Portable Extensible Toolkit for Scientific Computation) libraries. The code is capable of performing calculations with the Richards equation, thermo-hydrological-chemical (THC), multiphase water and supercritical CO_2, surface flow, discrete fracture network, aqueous complexation, sorption (surface complexation and ion exchange), solid precipitation and dissolution, and subsurface flow-reactive transport coupling. PFLOTRAN has been chosen to conduct repository scale transport simulations in performance assessment modeling.

A simple 1D diffusion problem has been created to represent the reactive transport phenomena of cement – clay interactions using the reactive transport code PFLOTRAN. 1D simulations of cement – clay interactions to represent an interfacial domain has been reported by Wang et al. (2010) for the Boom Clay host rock formation, and Kosakowski and Berner (2013) on Opalinus Clay host rock in Switzerland. In the current study, the cement and clay domains are represented by a rectangular geometry divided by an interface. The cement and clay "blocks" have a porosity of 0.1 and tortuosity equal to 1. The diffusion coefficient is set to 1.5 E-12 m^2/s for all solute species to be consistent with the effective diffusion coefficient values adopted in the study of Kosakowski and Berner (2013) after scaled to porosity. The code runs were set for 10,000 years. It should be noted that the diffusive fluxes are computed according to changes in porosity and tortuosity as a result of updates in the solid volume fractions affected by reaction with fluids. Therefore, the choice of unity tortuosity is to keep track of the effective diffusion changes mainly from porosity updates. The cement and clay "blocks" have horizontal dimensions of 0.75 and 1.25 meters, respectively, vertical dimension of 1 meter, and a grid spacing of 1 cm (see Figure 4.6). The clay is a Na-smectite with thermodynamic data from 'Hanford.dat' database used by PFLOTRAN. The selected calcium-silicate-hydrate (CSH) cement phase is "CSH0.97" also from the 'Hanford.dat' database. The choice of the CSH phase composition is at this point arbitrary and the main purpose is just to have a cement solid to build the simulation case. No carbonate phases were considered in this case and this is a topic of future work. The 'Hanford.dat' database contains other CSH phases that can be used if analysis of other cement compositions is pursued. At this point, this simulation case is simple in the sense that no secondary precipitates are being considered so the process of porosity occlusion was not assessed. The next stage of in this evaluation is to include a larger set of phases similar to other reactive transport studies dealing with hyperalkaline interactions involving cementitious materials.

Initially, the Na-smectite phase domain is equilibrated with a dilute solution with a pH 7.5. Similarly, the CSH0.98 phase is also equilibrated with a relatively dilute solution with pH 11.5. PFLOTRAN allows for dissolution rates to be defined for each phase where in this case are 2.75E-12 and 6.0E-12 mol/m^2 sec for cement and clay, respectively. The dissolution rate value for clay under alkaline pH conditions is from Bauer and Berger (1998). The dissolution rate value for the CSH phase was obtained from Baur et al. (2004) for pH 11-12. Previous studies (Soler, 2005) have outlined the importance of kinetic rate data of the various phases and its treatment in reactive transport simulations of cement.

Preliminary results of these simulations are depicted in Figures 4.7 through 4.9. Figure 4.7 shows a profile of pH vs. time at various locations: very near (from both sides) to the cement – clay interface, and leftmost (clay) and rightmost (cement) boundaries. Figure 4.8 show snapshots of the reaction front evolution delineated by pH at various simulated time periods. Notice the sharp reaction front evolving towards the clay phase and the increase in pH for the clay pore water. In the span of 10,000 years simulation time, the pH diffusion front moves towards the clay side from the interface rather unimpeded due to the reactivity of the clay silicate phase as a result of the highly alkaline pH. Total aqueous silica concentration (not shown) indicates a similar behavior with a sharp diffusion front similar to that of pH. Since no secondary mineral precipitation was considered (i.e., no clogging), this could explain the further migration of the diffusion front relative to those reported in other reactive transport simulation studies and deduced from field observations. Overall, the changes in pH and steady-state behavior are consistent with other studies. Figure 4.9 illustrates the diffusion front evolution represented by the Ca concentration at various times. Notice that different from pH, the Ca reaction front is not sharply defined and remains nearly stationary for tenths of years but diffusing from both sides of the interface. Again, such behavior may change significantly with the precipitation of a secondary phase such as calcite which was not considered in this case. The porosity change in these simulations was negligible within the simulated time span. The extent of porosity occlusion near the cement – clay interface determines how the system will progress (Wang et al. 2010; Kosakowski and Berner 2013). As noted by Kosakowski and Berner (2013), once the clogging effectively seals the interfacial domain the chemical evolution of the system is drastically reduced or halted. These authors also remarked that in the opposite case where porosity clogging was not conisdered the extent of alteration due to mineralogical changes can spread more. Such observation is consistent with the result obtained in the modeling presented here regarding the extent of the pH diffusion front migration. Kosakowski and Berner (2013) also cautioned on the impact of diffusion and kinetic parameters on the evolution of reaction fronts. Therefore, further analysis of this type of simulations with an expanded set of minerals allowing for secondary mineral precipitation along with evaluations of sensitivities to diffusion parameters and rate constants is needed to evaluate porosity occlusion and the evolution of reaction fronts. Overall, this simple case of 1D diffusive transport using PFLOTRAN illustrates a behavior that is consistent with the chemical changes observed in other modeling studies.

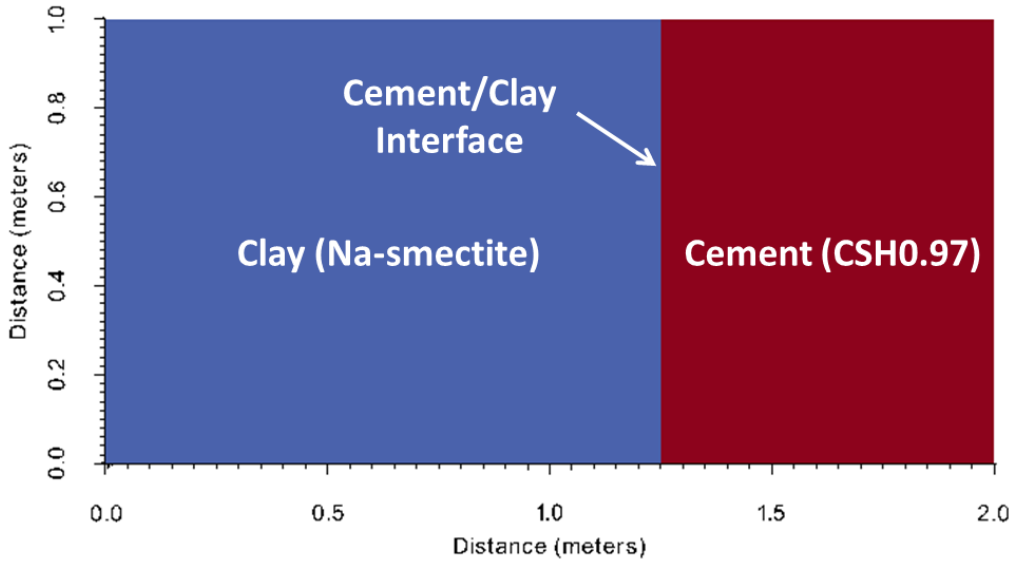

Figure 4.6. Overall configuration for cement and clay domains for the 1D reactive transport problem in PFLOTRAN.

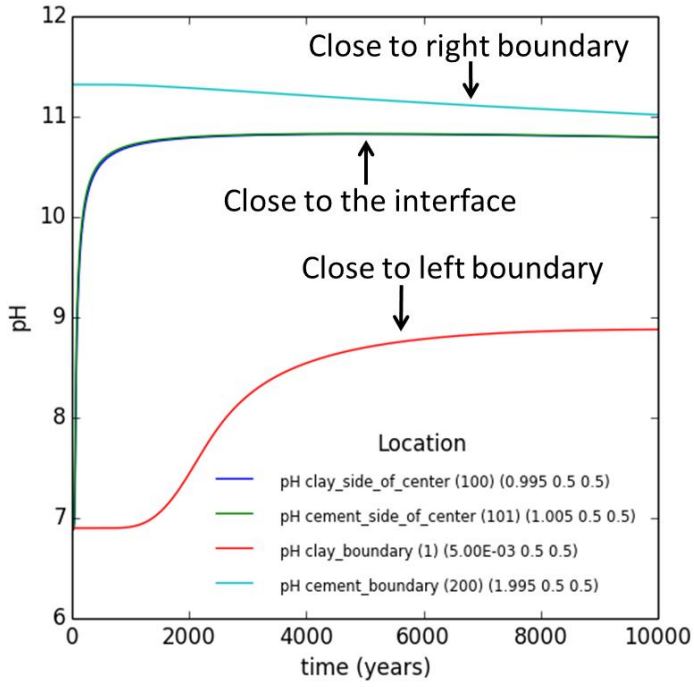

Figure 4.7. Temporal profile for pH predicted by PFLOTRAN at different locations of the domain geometry given in Figure 4.6: Left boundary, right boundary, and close to the interface.

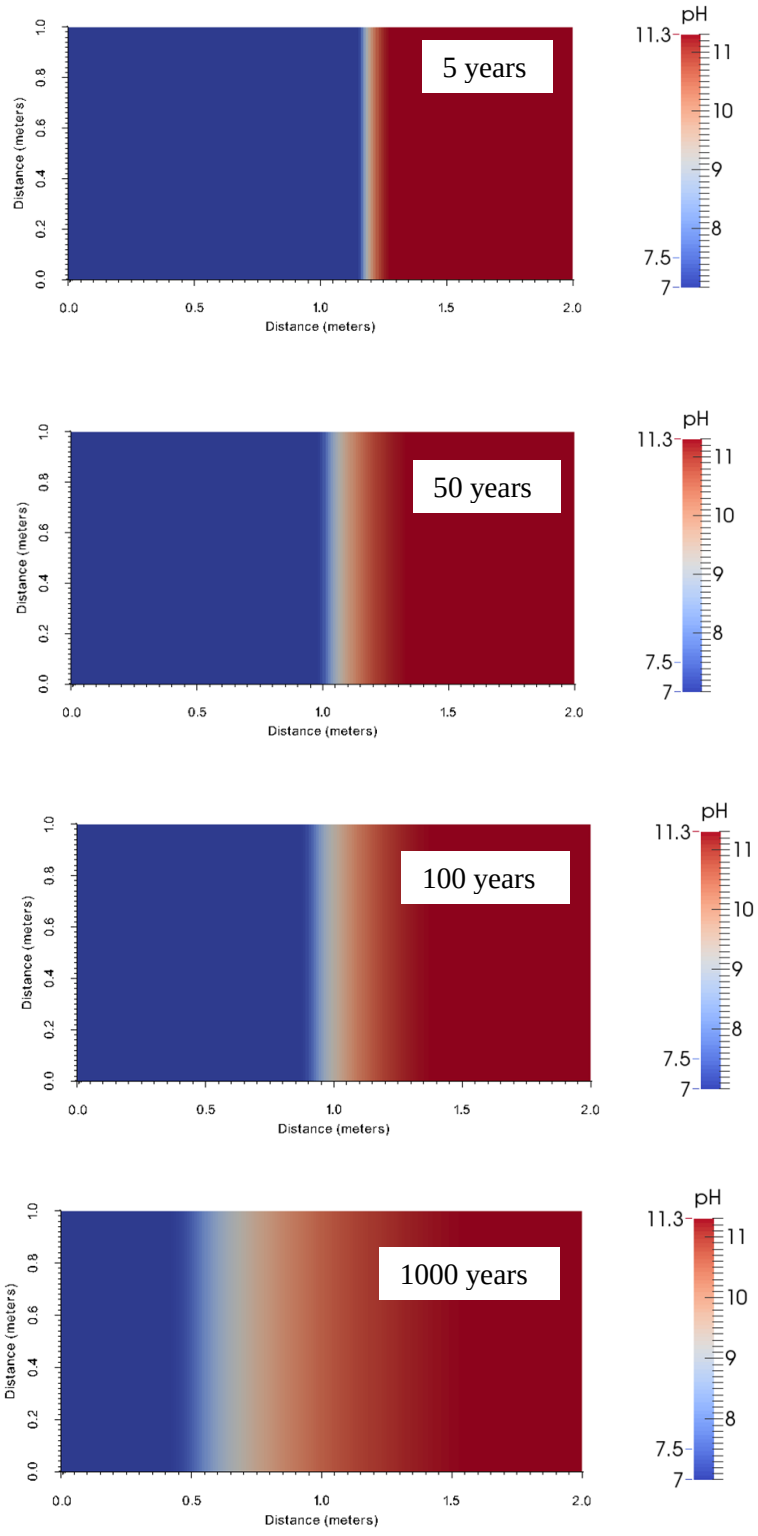

Figure 4.8. PFLOTRAN 1D reactive transport predictions of pH for the diffusion front near cement – clay interface. This case does not account for secondary mineral formation and porosity occlusion (see text).

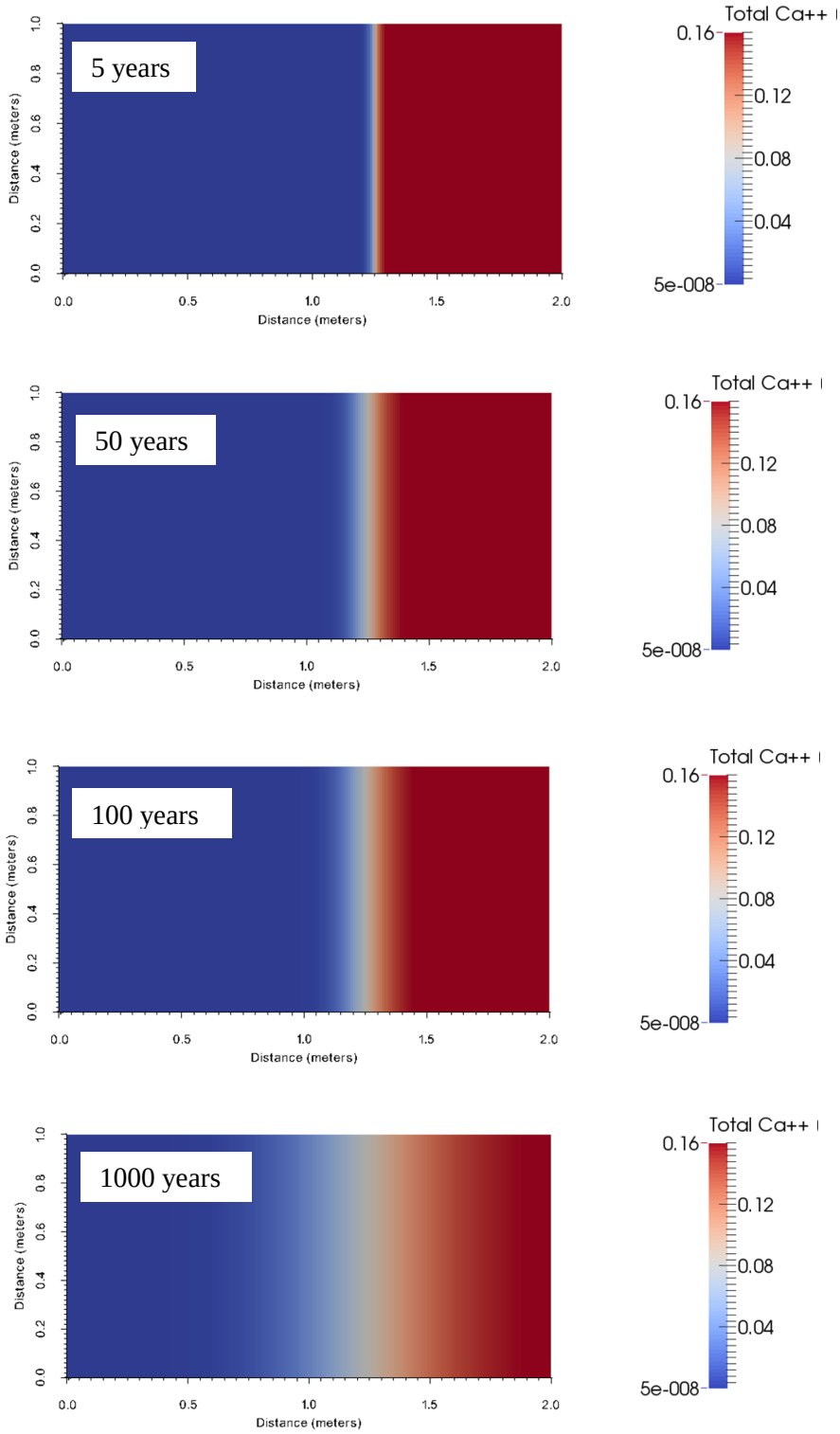

Figure 4.9. PFLOTRAN 1D reactive transport predictions of Ca concentration for the diffusion front near the cement – clay interface. Notice the near-stationary diffusion front spreading on both sides of the interface (see text).

It is anticipated that expansion of this work will evaluate:

- The effect of using a more sophisticated kinetic rate treatment (e.g., transition state theory in PFLOTRAN) to evaluate solid dissolution and precipitation. There is a need for improvement of kinetic rate data and model testing at the alkaline pH range applicable to cement fluid interactions. Also, to include the effect of cation exchange reactions which is possible in PFLOTRAN.
- The use of a larger assemblage of solids and clay-rock pore water compositions to accurately represent the effects on secondary phase formation. This is important in assessing the effects of pore clogging and fluid chemistry where also buffering effects can be important (e.g., carbonate precipitation). Porosity reduction through occlusion is a beneficial attribute from cement – clay hyperalkaline interactions to barrier sealing performance (Soler, 2005; Wang et al., 2010). Therefore, reactive transport simulations are crucial to resolve the extent of these reaction zones under variable conditions.
- Evaluate the effects of porous medium saturation on reactive transport. Experimental and natural analogue studies indicate that the hyperalkaline reactive fronts don't extend far from the interface domain not only due to mineral precipitation but are also influenced by fluid saturation. Most reactive transport studies assume fully saturated media but other studies like Yang et al. (2008) consider the effects of saturation.

The purpose of this preliminary work is not only to add another reactive transport simulation code to the existing suite but to advance and exploit the application of a powerful tool that has been selected for integration with performance assessment modeling. The use of these types of advanced simulation tools is crucial to the evaluation of barrier material alteration and stability that can indeed impact the barrier design and thus repository long-term performance. Moreover, the ongoing research on this subject has elucidated the need to improve models to better assess the simulation approaches and their inputs to accurately represent experimental and field observations. This calls for model validation and verification exercises that should include benchmarks for code-to-code comparisons and identify discrepancies that could impact modeling approaches utilized in safety assessment.

4.6 SANS Study of Opalinus Clay – Cement Core Sample

The microstructural characterization of pore space is crucial to the analysis of fluid transport behavior in deep geological porous formations. This is particularly important to sealing performance at the interface regions between the engineered and natural barrier systems. This need becomes even more critical when low permeability clay rock such as argillite is a candidate target for a subsurface nuclear waste repository. Small-angle neutron scattering (SANS) is a canonical technique well suited for probing the inner structure of disordered systems in the 1 to 1000 nm. Such capability allows for the statistical characterization of pores from nano- to micron-scale provides in systems with inhomogeneities such as fine-grained indurated clay rock or aggregated materials. The neutron beam diameter can vary from 2 to 8 mm. A major advantage of SANS is the ability to spatially resolve the fine-scale pore structure dimensions

with minimal sample preparation that could damage regions of interest such as interfaces between materials. Given the aggregated and/or potentially brittle behavior of these samples when exposed to ambient conditions, material recovery from sampling boreholes and cores in an intact state or with minimal damage can be complex and very difficult. Therefore, characterization studies need to be equally non-damaging to accurately analyze the preserved intact state of the sample.

The neutron scattering intensity provides information on the system inhomogeneity from which pore structure and surface area can be determined. Details concerning the theory and practice of SANS are outside the scope of this report. However, some basic background is given to briefly explain this technique. The scattering intensity observed in a SANS measurement is directly related to the structure of the sample, characterized by a scattering length density ρ (r). At any position, r, within the sample, the scattering length density is equal to the sum of the atomic and isotopic neutron scattering amplitudes in a small volume around that position (Zaccai and Jacrot, 1983):

$$\rho = \frac{\sum n_i b_i}{V_m} \qquad (4.1)$$

where b_i is the atomic neutron scattering length, n_i designates the number of atomic nuclei of a given type in a molecule, and V_m stands for the molecular volume. A fraction of the incident neutrons will be scattered into a scattering vector, Q, of magnitude $Q=(4\pi/\lambda)\sin\theta$, where λ is the wavelength of the incident neutron and θ represents half of the scattering angle, from fluctuations in the scattering length density. ρ(r) reflects the microscale structure in the sample in density, chemical, and isotopic composition.

The scattering intensity, I(Q), is measured as the absolute, differential cross section per unit scattering mass (cm^2g^{-1}) as a function of the magnitude of Q. For elastic scattering events, I(Q) is proportional to the squared Fourier transform of ρ (r) expressed as (Zaccai and Jacrot, 1983):

$$I(Q) = K\langle|\int \rho(r)\exp(-ir\cdot Q)\,dr|^2\rangle = KP(Q)S(Q) \qquad (4.2)$$

Here, P(Q) is the normalized particle form factor, which contains the particle shape information and K is a constant. S(Q) is the structure factor, which takes into account distance correlations between particles.

The interpretation of I(Q) in terms of the sample structure involves careful comparison with calculations of the scattering expected from model structures. Various transformations are also commonly used to interpret the data. The first tool used to analyze SANS data consists of a set of standard transformation plots that yield direct results after data reduction.

For example, based on the Porod-law, which is expressed as (Zaccai and Jacrot, 1983):

$$I(Q) = 2\pi S\Delta\rho^2 Q^{-4} \qquad (4.3)$$

where S is the interfacial area per gram of material. We can use the Porod transform (plotting I(Q) as function of Q^{-4}) to calculate the surface area of a material.

4.6.1 SANS Analysis of CI Experiment Sample Material

The OPC concrete – Opalinus Clay sample in this study is a cored piece from the CI experiment taken from sampling borehole BCI-15 as shown in Figure 4.10. The OPC concrete sample contains aggregates phases as seen in Figure 4.10. Figure 4.11 shows a thin section of core fragment with marked areas indicating the spatial location for the SANS analysis. The core sample was kindly provided by Dr. Urs Mäder from the University of Bern, Switzerland.

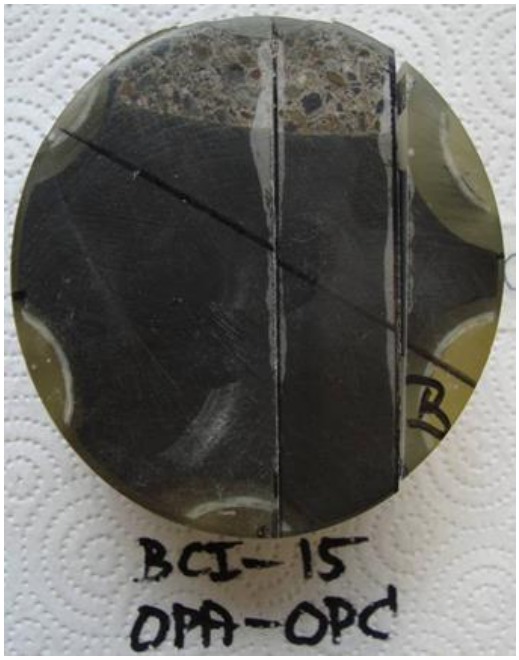

Figure 4.10. OPC concrete – Opalinus Clay sample used in this SANS study. The top part of the sample shows the OPC concrete – Opalinus Clay interface. The lens shaped features surrounding the core are the resin + fiber-glass reinforcements that were inserted parallel to the drilling direction to stabilize the interface region. The photo and core sample were kindly provided by Dr. Urs Mäder.

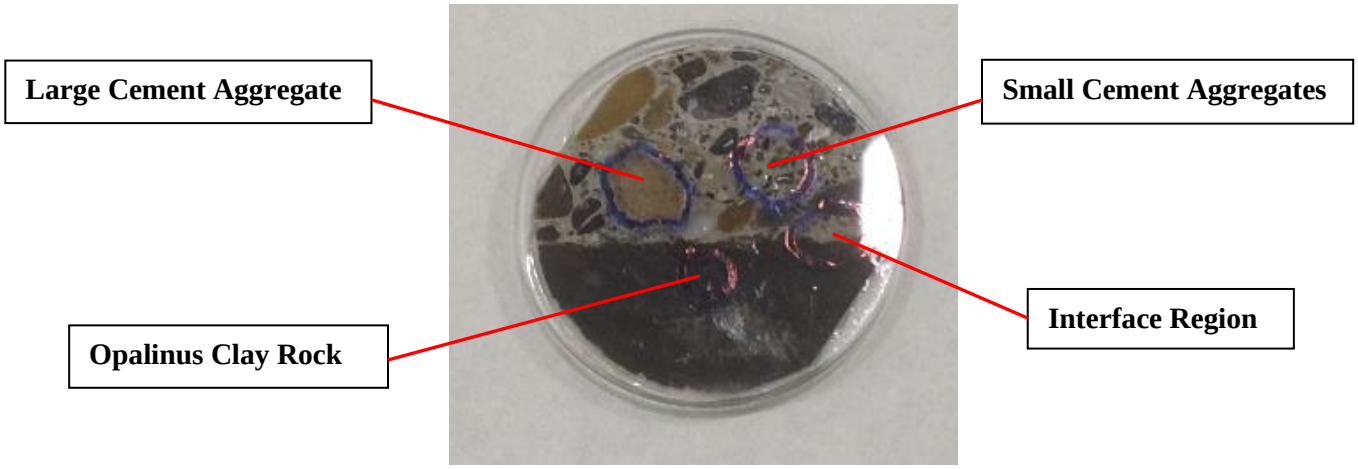

Figure 4.11. Thin-section of the OPC concrete – Opalinus Clay interface region. The marked circles in the figure are measurements spots.

The SANS measurement were conducted at the Manuel Lujan Jr. Neutron Scattering Center, Los Alamos National Laboratory (LANL) using the Low-Q Diffractometer (LQD) (http://lansce.lanl.gov/lujan/instruments/LQD.shtml). The neutron wavelengths range from 1 to 16 Å. The range of scattering vectors (Q) at LQD is 0.003-0.5 $Å^{-1}$, where $Q=4\pi\lambda^{-1}\sin\theta$. The pore size may be estimated from Bragg's law $\lambda=2R\sin\theta$. This law provides an approximated relationship between the scattering vector Q and the pore size R: $R=2\pi/Q$. This relationship was used in this work to relate Q-values with pore size R. Figure 4.12 show a schematic view of Flightpath 10(LQD) at the LANL Manuel Lujan, Jr. Neutron Center. The neutron beam diameter used in this study is 4 mm but it can be varied from 2 to 8 mm.

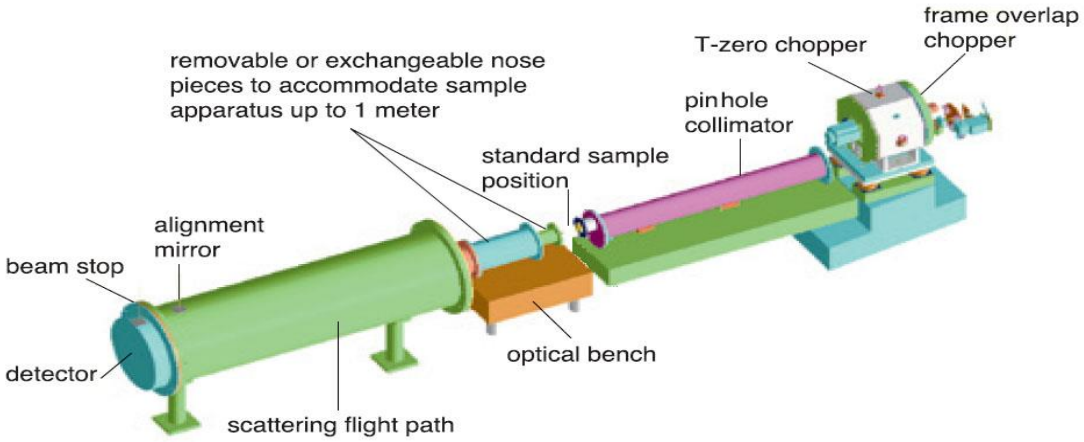

Figure 4.12. Schematic view of Flightpath 10(LQD) at the LANL Manuel Lujan, Jr. Neutron Center.

Figure 4.13 shows the SANS scattering profiles of the three representative spots of the cement-clay sample depicted in Figure 4.11. The curve for the Opalinus Clay rock indicates a distinctly different character from the OPC concrete and Opalinus Clay interface region, showing two potentially different pore structures. This is indicated by the change in slope within the pore size range between about 5-10 nm. For a pore size smaller than 10 nm, the Opalinus Clay rock display a mass fractal characteristic suggesting more contribution from porous structural features. For a pore size greater than 10 nm, the pore structure corresponding to a fractal characteristic is similar to those of the OPC concrete and Opalinus Clay interface, and small-cement aggregates. The curves for the interface and small-cement aggregates are similar for pore sizes greater than 10 nm, indicating a similarity in their pore structure with regards to their fractal characteristics. This is indicative of surface fractal features mainly contributed by the aggregates within these two regions. It should be noted that the SANS probing region is relatively large (4 mm) so it incorporates heterogeneities from various components in the concrete and clay rock. Detailed pore size distribution can be further derived from these scattering curves.

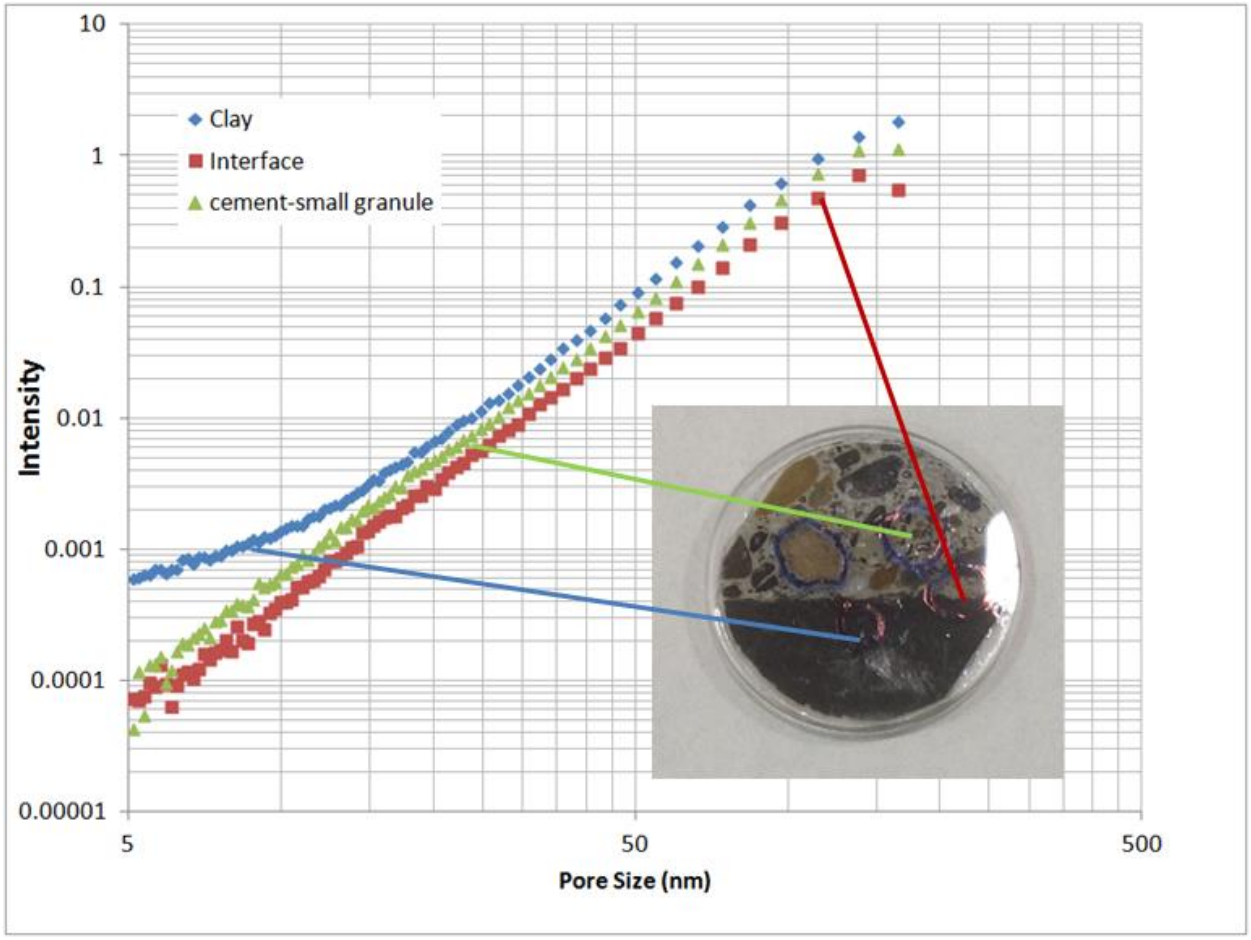

Figure 4.13. SANS scattering curves from three spot measurements: Opalinus Clay rock, OPC – OPA interface, and small cement granules.

The main goal of this study is to evaluate the feasibility of this technique on a natural intact sample and ensure the obtained results support the desired resolution required to retrieve pore structure information. Therefore, only raw SANS data and preliminary interpretations of these data are presented in this report. Analysis of the data to retieve pore size distributions and surface area will be assessed later or depending on the ability to continue the CI collaboration study. Even without going into a sophisticated analysis of the observed spectra, these results indicate that there is sufficient difference in the pore structure of this complex media to probe the effects of cement-clay interactions. Our results demonstrate that SANS is a powerful tool for use in the characterization of pore features and surface area of intact complex porous media. Pore structure characteristics and surface area are important parameters to the description of reactive transport and its assessment within models for the performance assessment of engineered and natural barrier systems. Moreover, SANS can quantitatively provide *in situ* measurements of fine-scale pore features with minimal sample preparation under controlled environmental conditions such as temperature, pressure, and relative humidity. It should be noted that this CI collaboration project will not continue in FY14. Nevertheless, serious consideration should be given to the

applications of SANS in the canonical pore characterization of samples with low porosity and permeability such as clay and salt obtained from field and laboratory experiments.

5. CONCLUDING REMARKS

LBNL, SNL, and LANL international activities related to EBS such as THM and reactive transport model development currently include modeling of field experiments at the Mont Terri URL, Switzerland, and Horonobe URL, Japan. It is DOE's participation in international projects such as DECOVALEX and Mont Terri that enable us to test our new model against relevant field and laboratory data.

Related to THM modeling of EBS components, we are currently focusing on parameterization of bentonite properties through modeling of laboratory experiments and benchmarks; both related to the modeling of the Mont Terri URL HE-E heater test and the Horonobe URL EBS experiment. This work was presented at the DECOVALEX-2015 workshop at Mont Terri in November 2013. Thereafter, new model predictions will be performed related to both the Mont Terri URL HE-E experiment and the Horonobe URL EBS experiment.

Related to reactive diffusive transport modeling, we have carried out preliminary simulations of the DR-A test, including the increase in ionic strength at Day 189. The anion exclusion effect seems to lessen (the rate of out-diffusion thus increases) when the ionic strength is increased, although this is not currently fully captured by the simulations. It appears that lower diffusion coefficients in the EDL for the anions are required to capture this effect. The objective of the FY14 work will be to refine the EDL-explicit model to the current DR-A experiment, out through 412 days. The major focus will be to establish the effect of the increase in ionic strength and its effect on anion exclusion, since the data suggests that the increase does contribute to a more rapid out-diffusion of the iodide and bromide. The sensitivity to EDL thickness and ion-specific diffusivity will be investigated.

Regarding the cement – clay interactions, the primary goal of testing the SANS technique on a cement (OPC) – Opalinus Clay (OPA) sample from the CI field experiment was successful. Sufficient differences were observed, allowing us to resolve distinct pore structures in the CI sample for the three main regions of interest (OPC, OPA, and interface), and showing that this technique may be very useful to provide a statistical description of heterogeneous media in an intact core sample. In addition, computational tools for the thermodynamic analysis of equilibrium phase relations and reactive transport modeling applicable to cement clay – clay systems have been tested using the open-source software CHNOSZ and PFLOTRAN. The CHNOSZ is a versatile tool for the evaluation of thermodynamic data and provides graphic capabilities for the generation of activity phase diagrams to map solid-fluid phase equilibria. PFLOTRAN is an open-source state-of-the-art massively parallel code with a mature development history and multiple applications to reactive transport problems. Overall, the 1D simulation results presented here are in good agreement with those reported elsewhere and are consistent with the expected change in pH for cement – clay pore water interactions. This simple 1D case is a preamble study to compare results with those reported in the literature and test the code ability to accurately represent the extent of the diffusion front as function of time. The

level of complexity in this 1D problem can be expanded to include a larger set of solids to represent secondary phase alteration, mineral precipitation/dissolution kinetics, ion exchange reactions, surface complexation, variable saturation, and conduct simulations in 2D or 3D. It should be noted that the CI international collaboration activity will not continue in FY14. However, some of the planned activities in the Argillite Work Package can leverage use of the tools such as CHNOSZ and PFLOTRAN for thermodynamic analysis and clay interactions. Preliminary results demonstrate that SANS is a promising tool for the canonical characterization of pore structure in an heterogeneous clay rock sample. Therefore, further consideration should be given to this technique for the pore structure analysis of low porosity / low permeability repository host rocks such as clay and salt.

6. REFERENCES

Adler, M., Mader, U.K., Waber, H.N. (1999) High-pH alteration of argillaceous rocks: an experimental study. Schweizerische Mineralogische Und Petrographische Mitteilungen, 79(3): 445-454.

Albert, B., Guy, B., Damidot, D. (2006) Water chemical potential: A key parameter to determine the thermodynamic stability of some hydrated cement phases in concrete? Cement and Concrete Research, 36(5): 783-790.

Appelo, C.A.J., Wersin, P. (2007) Multicomponent diffusion modeling in clay systems with application to the diffusion of tritium, iodide, and sodium in Opalinus Clay. Environmental Science and Technology 41, 5002-5007.

Appelo, C.A.J., Vinsot, A., Mettler, S., Wechner, S. (2008) Obtaining the porewater composition of a clay rock by modeling the in- and out-diffusion of anions and cations from an in-situ experiment. Journal of Contaminant Hydrology 101, 67-76.

Atkins, M., Bennett, D.G., Dawes, A., Glasser, F., Read, D. (1992) A thermodynamic model for blended cements. DoE/HMIP/RR/92/005, Department of the Environment, London, England.

Atkins, M., Glasser, F.P., Moroni, L.P., Jack, J.J. (1993) Thermodynamic modelling of blended cements at elevated temperatures (50-90°C), DoE/HMIP/RR/94/011. Aberdeen University, Aberdeen, United Kingdom.

Babushkin, V.I., Matveyev, G.M., Mchedlov-Petrossyan, O.P. (1985) Thermodynamics of silicates. Springer-Verlag, Berlin, Germany.

Balonis, M., Lothenbach, B., Le Saout, G., Glasser, F.P. (2010) Impact of chloride on the mineralogy of hydrated Portland cement systems. Cement and Concrete Research, 40(7): 1009-1022.

Batchelor, B., Wu, K. (1993) Effects of Equilibrium Chemistry on Leaching of Contaminants from Stabilized Solidified Wastes. In: Spence, R.D. (Ed.), Chemistry and Microstructure of Solidified Waste Forms. Lewis Publishers, Boca Raton, Florida.

Bauer, A., Berger, G. (1998) Kaolinite and smectite dissolution rate in high molar KOH solutions at 35 degrees and 80 degrees C. Applied Geochemistry, 13(7): 905-916.

Baur, I., Keller, P., Mavrocordatos, D., Wehrli, B., Johnson, C.A. (2004) Dissolution-precipitation behaviour of ettringite, monosulfate, and calcium silicate hydrate. Cement and Concrete Research, 34(2): 341-348.

Bennett, D.G., Read, D., Atkins, M., Glasser, F.P. (1992) A thermodynamic model for blended cements. II: Cement hydrate phases; thermodynamic values and modelling studies. Journal of Nuclear Materials, 190: 315-325.

Berner, U., Kulik, D.A., Kosakowski, G. (2013) Geochemical impact of a low-pH cement liner on the near field of a repository for spent fuel and high-level radioactive waste. Physics and Chemistry of the Earth, Parts A/B/C, 64(0): 46-56.

Berner, U.R. (1987) Modeling porewater chemistry in hydrated Portland cement. In: Bates, J.K., Seefeldt, W.B. (Editors), Scientific Basis for Nuclear Waste Management X Symposium Material Research Society, Boston, Massachusetts, 319-330.

Berner, U.R. (1988) Modelling the Incongruent Dissolution of Hydrated Cement Minerals. Radiochimica Acta, 44/45: 387-393.

Berner, U.R. (1990) A Thermodynamic description of the evolution of pore water chemistry and uranium speciation during the degradation of cement, PSI-Bericht 62. Paul Scherrer Institute, Wurenlingen und Villigen, Switzerland.

Berner, U.R. (1992) Evolution of Pore Water Chemistry During Degradation of Cement in a Radioactive Waste Repository Environment. Waste Management, 12: 201-219.

Bethke, C., 2008. Geochemical and biogeochemical reaction modeling. Cambridge University Press Cambridge, UK.

Birgersson, M., Karnland, O. (2009) Ion equilibrium between montmorillonite interlayer space and an external solution - Consequences for diffusional transport. Geochimica et Cosmochimica Acta 73, 1908-1923.

Birkholzer, J.T. (2012) Status of UFD Campaign International Activities in Disposal Research. Report prepared for U.S. Department of Energy Used Fuel Disposition Campaign, FCRD-UFD-2012-000295.

Birkholzer, J., Asahina, D., Chen, F., Gardner, P., Houseworth, J., Jove-Colon, C., Kersting, A., Nair, P., Nutt, M., Li, L., Liu, H.H., Painter, S., Reimus, P., Rutqvist, J., Steefel, C., Tynan, M., Wang, Y., Zavarin, M. (2013) An overview of US disposal research activities linked to international URLs. Proceedings of the 2013 International High-Level Radioactive Waste Management Conference (IHLRWM), April 28 – May 2, 2013, Albuquerque, New Mexico.

Blanc, P., Bourbon, X., Lassin, A., Gaucher, E.C. (2010a) Chemical model for cement-based materials: Temperature dependence of thermodynamic functions for nanocrystalline and crystalline C-S-H phases. Cement and Concrete Research, 40(6): 851-866.

Blanc, P., Bourbon, X., Lassin, A., Gaucher, E.C. (2010b) Chemical model for cement-based materials: Thermodynamic data assessment for phases other than C-S-H. Cement and Concrete Research, 40(9): 1360-1374.

Borjesson, S., Emren, A., Ekberg, C. (1997) A thermodynamic model for the calcium silicate hydrate gel, modelled as a non-ideal binary solid solution. Cement and Concrete Research, 27(11): 1649-1657.

Bruton, C.J., Meike, A., Viani, B.E., Martin, S., Phillips, B.L. (1993) Thermodynamic and structural characteristics of cement minerals at elevated temperature, Topical Meeting on Site Characterization and Model Validation, FOCUS '93, Las Vegas, Nevada, 150-156.

Carey, J.W., Lichtner, P.C. (2007) Calcium silicate hydrate (C-S-H) solid solution model applied to cement degradation using the continuum reactive transport model FLOTRAN. In: Mobasher, B., Skalny, J. (Eds.), Transport Properties and Concrete Quality: Materials Science of Concrete. John Wiley & Sons, Inc., 73-106.

Carey, J.W., Wigand, M., Chipera, S.J., WoldeGabriel, G., Pawar, R., Lichtner, P.C., Wehner, S.C., Raines, M.A., Guthrie, G.D. (2007) Analysis and performance of oil well cement with 30 years Of CO_2 exposure from the SACROC Unit, West Texas, USA. International Journal of Greenhouse Gas Control, 1(1): 75-85.

Corkum A.G., Martin C.D. (2007) The Mechanical Behaviour of Weak Mudstone (Opalinus Clay) at Low Stresses, International Journal of Rock Mechanics and Mining Sciences, 44, 196-209.

Damidot, D., Stronach, S., Kindness, A., Atkins, M., Glasser, F.P. (1994) Thermodynamic Investigation of the CaO-Al_2O_3-$CaCO_3$-H_2O Closed-System at 25^oC and the Influence of Na_2O. Cement and Concrete Research, 24(3): 563-572.

Dauzeres, A., Le Bescop, P., Sardini, P., Coumes, C.C.D. (2010) Physico-chemical investigation of clayey/cement-based materials interaction in the context of geological waste disposal: Experimental approach and results. Cement and Concrete Research, 40(8): 1327-1340.

Davis, J., Rutqvist, J., Steefel, C., Tinnacher, R., Viarrasa, V., Zhen, L., Bourg, I., Liu, H.H., Birkholzer, J. (2013) Investigation of reactive transport and coupled THMC processes in the EBS: FY13 Report (FCRD-UFD-2013-000216), U.S. DOE Used Fuel Disposition Campaign.

De Windt, L., Pellegrini, D., van der Lee, J. (2004) Reactive transport modelling of a spent fuel repository in a stiff clay formation considering excavation damaged zones, Radiochimica Acta/International journal for chemical aspects of nuclear science and technology, p. 841.

Dick, J.M. (2008) Calculation of the relative metastabilities of proteins using the CHNOSZ software package. Geochemical Transactions, 9.

Fernandez, R., Cuevas, J., Mader, U.K. (2009) Modelling concrete interaction with a bentonite barrier. European Journal of Mineralogy, 21(1): 177-191.

Finsterle, S. (2007) iTOUGH2 User's Guide. Report LBNL-40040, Lawrence Berkeley National Laboratory, Berkeley, CA.

Fujii, K., Kondo, W. (1983) Estimation of thermochemical data for calcium silicate hydrate (C-S-H). Journal of the American Ceramic Society, 66(12): C220-C221.

Gaboreau, S., , Lerouge, C., Dewonck, S., Linard, Y., Bourbon, X., Fialips, C.I., Mazurier, A., Pret, D., Borschneck, D., Montouillout, V., Gaucher, E.C., Claret, F. (2012) In-Situ Interaction of Cement Paste and Shotcrete with Claystones in a Deep Disposal Context. American Journal of Science, 312(3): 314-356.

Gaboreau, S., , Pret, D., Tinseau, E., Claret, F., Pellegrini, D., Stammose, D. (2011) 15 years of *in situ* cement-argillite interaction from Tournemire URL: Characterisation of the multi-scale spatial heterogeneities of pore space evolution. Applied Geochemistry, 26(12): 2159-2171.

Garitte, B. (2012) HE-E experiment - *In situ* Heater Test, Presentation given at 1th DECOVALEX 2015 workshop, April 2012, Berkeley.

Garitte, B., Gens, A., Vaunat, J., Armand, G. (2013) Thermal Conductivity of Argillaceous Rocks: Determination Methodology Using *In Situ* Heating Tests. In Rock Mechanics and Rock Engineering DOI 10.1007/s00603-012-0335-x.

Gartner, E.M., Jennings, H.M. (1987) Thermodynamics of Calcium Silicate Hydrates and Their Solutions. Journal of the American Ceramic Society, 70(10): 743-749.

Gaucher, E.C., Blanc, P. (2006) Cement/clay interactions - A review: Experiments, natural analogues, and modeling. Waste Management, 26(7): 776-788.

Gaucher, E.C., Blanc, P., Matray, J.M., Michau, N. (2004) Modeling diffusion of an alkaline plume in a clay barrier. Applied Geochemistry, 19(10): 1505-1515.

Gens, A., Garitte, B., Wileveau, Y. (2007) *In situ* Behaviour of a Stiff Layered Clay Subject to Thermal Loading: Observations and Interpretation, Geotechnique, 57, 207-228.

Gens, A., Sanchez, M., Guimaraes, L.D.N., Alonso, E.E., Lloret, A., Olivella, S., Villar, M.V., Huertas, F. (2009) A full-scale *in situ* heating test for high-level nuclear waste disposal: observations, analysis and interpretation. Geotechnique 59, 377–399.

Glasser, F.P., Lachowski, E.E., MacPhee, D.E. (1987) Compositional Model for Calcium Silicate Hydrate (C-S-H) Gels, Their Solubilities, and Free Energies of Formation. Journal of the American Ceramic Society, 70(7): 481-485.

Glynn, P.D., Reardon, E.J. (1990) Solid-Solution Aqueous-Solution Equilibria - Thermodynamic Theory and Representation. American Journal of Science, 290(2): 164-201.

Gonçalvès, J., Rousseau-Gueutin, P., Revil, A. (2007) Introducing interacting diffuse layers in TLM calculations: A reappraisal of the influence of the pore size on the swelling pressure and the osmotic efficiency of compacted bentonites. *J. Colloid Interface Sci.*, **316**, 92-99.

Graupner, B.J., Lee, C., Manepally, C., Pan, P., Rutqvist, J., Wang, W., Garitte, B. (2013) The Mont Terri HE-D Experiment as a Benchmark for the Simulation of Coupled THM Processes. Extended abstract for the European Association of Geoscientists & Engineers (EAGE) International Workshop Geomechanics & Energy, Lausanne, Switzerland, 26-28 November, 2013.

Greenberg, J.P., Moller, N. (1989) The prediction of mineral solubilities in natural waters: A chemical equilibrium model for the Na-K-Ca-Cl-SO_4-H_2O system to high concentration from 0 to 250°C. Geochimica et Cosmochimica Acta, 53: 2503–2518.

Greenberg, S.A., Chang, T.N. (1965) Investigation of the Colloidal Hydrated Calcium Silicates. II. Solubility Relationships in the Calcium Oxide-Silica-Water System at 25^{o}C. Journal of Physical Chemistry, 69(1): 182-188.

Greenberg, S.A., Chang, T.N., Anderson, E. (1960) Inestigation of Colloidal Hydrated Calcium Silicates: I. Solubility Products. Journal of Physical Chemistry, 64(9): 1151-1157.

Guy, B., Pla, J.M. (1997) Structure of phase diagrams for n-component (n+k)-phase chemical systems: the concept of affigraphy. Comptes Rendus De L Academie Des Sciences Serie Ii Fascicule a-Sciences De La Terre Et Des Planetes, 324(9): 737-743.

Harvie, C.E., Moller, N., Weare, J.H., 1984. The Prediction of Mineral Solubilities in Natural Waters: The Na-K-Mg-Ca-H-Cl-SO_4-OH-HCO_3-CO_3-CO_2-H_2O System to High Ionic Strengths at 25°C. Geochimica et Cosmochimica Acta, 48(4): 723-751.

Itasca (2009) FLAC3D V4.0, Fast Lagrangian Analysis of Continua in 3 Dimensions, User's Guide. Itasca Consulting Group, Minneapolis, Minnesota.

Jové Colón, C.F. Caporuscio, F.A., Levy, S.S., Blink, J.A., Greenberg, H.R., Halsey, W.G., Fratoni, M., Sutton, M., Wolery, T.J., Rutqvist, J., Liu, H.H., Birkholzer, J., Steefel, C.I., Galindez, J. (2011) Disposal Systems Evaluations and Tool Development - Engineered Barrier System (EBS) Evaluation, Sandia National Laboratories, U.S. Department of Energy, 192 pp.

Jové Colón, C.F. C.F., Caporuscio, F.A., Levy, S.S., Xu, H., Blink, J.A., Halsey, W.G., Buscheck, T., Sutton, M., Serrano de Caro, M.A., Wolery, T.J., Liu, H.H., Birkholzer, J., Steefel, C.I., Rutqvist, J., Tsang, C.-F., Sonnenthal, E. (2010) Disposal Systems Evaluations and Tool Development - Engineered Barrier System (EBS) Evaluation, Sandia National Laboratories, U.S. Department of Energy, 200 pp.

Jové Colón, C.F. C.F., Greathouse, J.A., Teich-McGoldrick, S., Cygan, R.T., Hadgu, T., Bean, J.E., Martinez, M.J., Hopkins, P.L., Argüello, J.G., Hansen, F.D., Caporuscio, F.A., Cheshire, M., et al. (2012) Evaluation of Generic EBS Design Concepts and Process Models: Implications to EBS Design Optimization (FCRD-USED-2012-000140), Sandia National Laboratories, U.S. Department of Energy, 250 pp.

Karnland, O. Olsson, S., Dueck, A., Birgersson, M., Nilsson, U., Hernan-Håkansson, T., Pedersen, K., Nilsson, S., Eriksen, T.E., Rosborg, B. (2009) Long term test of buffer material at the Äspö Hard Rock Laboratory, LOT project. Swedish Nuclear Fuel and Waste Management Co, Stockholm, Sweden, 279 pp.

Kersten, M. (1996) Aqueous solubility diagrams for cementitious waste stabilization systems .1. The C-S-H solid solution system. Environmental Science & Technology, 30(7): 2286-2293.

Kienzler, B., Vejmelka, P., Herbert, H.J., Meyer, H., Althenhein-Haese, C. (2000) Long-term leaching experiments of full-scale cemented waste forms: Experiments and modeling. Nuclear Technology, 129: 101-118.

Kosakowski, G., Berner, U. (2013) The evolution of clay rock/cement interfaces in a cementitious repository for low- and intermediate level radioactive waste. Physics and Chemistry of the Earth, 64: 65-86.

Kulik, D.A., Kersten, M. (2001) Aqueous solubility diagrams for cementitious waste stabilization systems: II, end-member stoichiometries of ideal calcium silicate hydrate solid solutions. Journal of the American Ceramic Society, 84(12): 3017-3026.

Lichtner, P.C., Carey, J.W. (2006) Incorporating solid solutions in reactive transport equations using a kinetic discrete-composition approach. Geochimica et Cosmochimica Acta, 70(6): 1356-1378.

Lichtner, P.C., Hammond, G.E., Lu, C., Karra, S., Bisht, G., Andre, B., Mills, R.T., Kumar, J. (2013) PFLOTRAN User Manual, http://www.pflotran.org.

Liu, H.H., Houseworth, J., Rutqvist, J., Zheng, L., Asahina, D., Li, L., Vilarrasa, V., Chen, F., Nakagawa, S., Finsterle, S., Doughty, C., Kneafsey, T., Birkholzer, J. (2013) Report on THMC modeling of the near field evolution of a generic clay repository: Model validation and demonstration. (FCRD-UFD-2013-000244), U.S. DOE Used Fuel Disposition Campaign.

Leroy, P., Revil, A. (2004) A triple-layer model of the surface electrochemical properties of clay minerals. Journal of Colloid and Interface Science 270, 371-380.

Leroy, P., Revil, A., Altmann, S., Tournassat, C. (2007) Modeling the composition of a pore water in a clay-rock geological formation (Callovo-Oxfordian, France). Geochimica et Cosmochimica Acta 71, 1087-1097.

Lothenbach, B., Damidot, D., Matschei, T., Marchand, J. (2010) Thermodynamic modelling: state of knowledge and challenges. Advances in Cement Research, 22(4): 211-223.

Lothenbach, B., Gruskovnjak, A. (2007) Hydration of alkali-activated slag: Thermodynamic modelling. Advances in Cement Research, 19(2): 81-92.

Lothenbach, B., Matschei, T., Moschner, G., Glasser, F.P. (2008) Thermodynamic modelling of the effect of temperature on the hydration and porosity of Portland cement. Cement and Concrete Research, 38(1): 1-18.

Lothenbach, B., Winnefeld, F. (2006) Thermodynamic modelling of the hydration of Portland cement. Cement and Concrete Research, 36(2): 209-226.

MacPhee, D.E., Luke, K., Glasser, F.P., Lachowski, E.E. (1989) Solubility and aging of calcium silicate hydrates in alkaline solutions at 25ºC. Journal of the American Ceramic Society, 74(4): 646-654.

Mäder, U. (2012) CI Experiment: Cement – Opalinus Clay Interaction, Project Description to Carlos F. Jove Colon from Dr. Urs Mäder, University of Bern, Switzerland.

Mäder, U., Adler, M., 2005. Mass balance estimate of cement - clay stone interaction with application to a HLW repository in Opalinus Clay, ECOCLAY II Project - Final Report, Effects of Cement on Clay Barrier Performance – Phase II. The European Commission, p. 188-197.

Malusis M.A., Shackelford C.D. Explicit and implicit coupling during solute transport through clay membrane barriers. *J. Contam. Hydrol.*, **72**, 259-285 (2004).

Malusis M.A., Shackelford C.D., Olsen H.W. Flow and transport through clay membrane barriers. *Eng. Geol.*, **70**, 235-248 (2003).

Mammar N., Rosanne M., Prunet-Foch B., Thovert J.-F., Tevissen E., Adler P.M. Transport properties of compact clays. I. Conductivity and permeability. *J. Colloid Interface Sci.*, 240, 498-508 (2001).

Marty, N.C.M., Tournassat, C., Burnol, A., Giffaut, E., Gaucher, E.C. (2009) Influence of reaction kinetics and mesh refinement on the numerical modelling of concrete/clay interactions. Journal of Hydrology, 364(1-2): 58-72.

Matschei, T., Lothenbach, B., Glasser, F.P. (2007) Thermodynamic properties of Portland cement hydrates in the system CaO-Al_2O_3-SiO_2-$CaSO_4$-$CaCO_3$-H_2O. Cement and Concrete Research, 37(10): 1379-1410.

Metz, V., Schussler, W., Kienzler, B., Fanghanel, T. (2004) Geochemically derived non-gaseous radionuclide source term for the Asse salt mine – assessment for the use of a $Mg(OH)_2$ – based backfill material. Radiochimica. Acta, 92: 819-825.

Moffat, H.K., Jové Colón, C.F. (2009) Implementation of Equilibrium Aqueous Speciation and Solubility (EQ3 type) Calculations into Cantera for Electrolyte Solutions. SAND2009-3115, Sandia National Laboratories, Albuquerque, N.M.

Moschner, G., , Lothenbach, B., Rose, J., Ulrich, A., Figi, R., Kretzschmar, R. (2008) Solubility of Fe-ettringite ($Ca_6[Fe(OH)_6]_2(SO4)_3$*****$26H_2O$). Geochimica Et Cosmochimica Acta, 72(1): 1-18.

Neall, F.B. (1996) Modelling the long-term chemical evolution of cement-groundwater systems. In: Murphy, W.M., Knecht, D.A. (Editors), Scientific Basis for Nuclear Waste Management XIX, Symposium. Materials Research Society, Pittsburgh, Pennsylvania, 483-490.

Nutt, M. (2011) Used Fuel Disposition Campaign Disposal Research and Development Roadmap (FCR&D-USED-2011-000065 REV0), U.S. DOE Used Fuel Disposition Campaign.

Olivella, S., Gens A. (2000). Vapour transport in low permeability unsaturated soils with capillary effects. Transport in porous Media 40: 219–241.

Pabalan, R.T. et al. (2009) Review of Literature and Assessment of Factors Relevant to Performance of Grouted Systems for Radioactive Waste Disposal (CNWRA 2009-001), Report prepared for the U.S. Nuclear Regulatory Commission by the Center for Nuclear Waste Regulatory Analyses, San Antonio, Texas, 359 pp.

Perkins, R.B., Palmer, C.D. (1999) Solubility of Ettringite ($Ca_6[Al(OH)_6]_2(SO_4)_3 \cdot 26H_2O$) at 5–75°C. Geochimica et Cosmochimica Acta, 63(13/14): 1969-1980.

Pierce, E.M., Mattigod, S.V., Westsik, J.H., Serne, R.J., Icenhower, J.P., Scheele, R.D., Um, W., Qafoku, N. (2010) Review of Potential Candidate Stabilization Technologies for Liquid and Solid Secondary Waste Streams, Pacific Northwest National Laboratory (PNNL), Richland, WA (US), Environmental Molecular Sciences Laboratory (EMSL).

Pruess, K., Oldenburg, C.M., Moridis, G. (2011) TOUGH2 User's Guide, Version 2.1, LBNL-43134(revised), Lawrence Berkeley National Laboratory, Berkeley, California.

Rizzi, M., Seiphoori, A., Ferrari, A., Ceresetti, D., Laloui, L. (2011) Analysis of the Behaviour of the Granular MX-80 bentonite in THM-processes; Orders No 7'928 and 5'160; Swiss Federal Institute of Technology: Lausanne, 2011.

Read, D., Glasser, F.P., Ayora, C., Guardiola, M.T., Sneyers, A. (2001) Mineralogical and microstructural changes accompanying the interaction of Boom Clay with ordinary Portland cement. Advances in Cement Research, 13(4): 175-183.

Reardon, E.J. (1990) An Ion Interaction-Model for the Determination of Chemical-Equilibria in Cement Water-Systems. Cement and Concrete Research, 20(2): 175-192.

Rutqvist, J., Börgesson, L., Chijimatsu, M., Kobayashi, A., Nguyen, T.S., Jing, L., Noorishad, J., Tsang, C.-F. (2001a) Thermohydromechanics of partially saturated geological media – Governing equations and formulation of four finite element models. Int. J. Rock Mech. & Min. Sci. 38, 105-127.

Rutqvist J., Börgesson L., Chijimatsu M., Nguyen T. S., Jing L., Noorishad J., Tsang C.-F. (2001b) Coupled Thermo-hydro-mechanical Analysis of a Heater Test in Fractured Rock and Bentonite at Kamaishi Mine – Comparison of Field Results to Predictions of Four Finite Element Codes. Int. J. Rock Mech. & Min. Sci. 38, 129-142.

Rutqvist J., WuY.-S., Tsang C.-F., Bodvarsson G. (2002) A modeling approach for analysis of coupled multiphase fluid flow, heat transfer, and deformation in fractured porous rock. *International Journal of Rock Mechanics and Mining Sciences*, 39, 429-442.

Rutqvist J., Ijiri Y., Yamamoto H. (2011) Implementation of the Barcelona Basic Model into TOUGH–FLAC for simulations of the geomechanical behavior of unsaturated soils. *Computers &Geosciences*, 37, 751-762.

Rutqvist J., Zheng L., Chen F, Liu H.-H, Birkholzer J. (2013a) Modeling of Coupled Thermo-Hydro-Mechanical Processes with Links to Geochemistry Associated with Bentonite-Backfilled Repository Tunnels in Clay Formations. *Rock Mechanics and Rock Engineering*, (In Press, January 2013).

Rutqvist, J., Chen F., Birkholzer J., Liu H.-H., Müller H., Garitte B., Vietor T. (2013b) Modeling of coupled thermo-hydro-mechanical processes at Mont Terri heater experiment in Opalinus Clay, using TOUGH-FLAC. Proceedings of the 2013 International High-Level Radioactive Conference (IHLRWM), April 28 – May 2, 2013.

Sarkar, A.K., Barnes, M.W., Roy, D.M. (1982) Longevity of borehole and shaft sealing materials: Thermodynamic properties of cements and related phases applied to repository sealing, ONWI-201. Battelle Memorial Institute, Office of Nuclear Waste Isolation, Columbus, Ohio.

Savage, D. (2011) A review of analogues of alkaline alteration with regard to long-term barrier performance. Mineralogical Magazine, 75(4): 2401-2418.

Savage, D., C. Walker, R. Arthur, C. Rochelle, C. Oda and H. Takase (2007). Alteration of bentonite by hyperalkaline fluids: A review of the role of secondary minerals. Physics and Chemistry of the Earth, 32(1-7): 287-297.

Schoch, R.B., Han, J., Renaud, P. (2008) Transport phenomena in nanofluidics. Reviews of Modern Physics 80, 840-883.

Shao, H., G. Kosakowski, U. Berner, D. A. Kulik, U. Mäder and O. Kolditz (2013) Reactive transport modeling of the clogging process at Maqarin natural analogue site, Physics and Chemistry of the Earth, Parts A/B/C, 64(0): 21-31.

Shaw, S., Henderson, C.M.B., Komanschek, B.U. (2000) Dehydration/recrystallization mechanisms, energetics, and kinetics of hydrated calcium silicate minerals: An *in situ* TGA/DSC and Synchrotron Radiation SAXS/WAXS Study. Chemical Geology, 167(1-2): 141-159.

Soler, J.M. (2005) Interaction Between Hyperalkaline Fluids and Rocks Hosting Repositories for Radioactive Waste: Reactive Transport Simulations. Nuclear Science and Engineering, 151(1): 128-133

Soler, J.M. (2012) High-pH plume from low-alkali-cement fracture grouting: Reactive transport modeling and comparison with pH monitoring at ONKALO (Finland). Applied Geochemistry, 27(10): 2096-2106.

Soler, J.M., Mader, U.K. (2010) Cement-rock interaction: Infiltration of a high-pH solution into a fractured granite core. Geologica Acta, 8(3): 221-233.

Steefel, C.I., Lichtner, P.C. (1998) Multicomponent reactive transport in discrete fractures: II: Infiltration of hyperalkaline groundwater at Maqarin, Jordan, a natural analogue site. Journal of Hydrology, 209(1–4): 200-224.

Sugiyama, D., Fujita, T. (2006) A thermodynamic model of dissolution and precipitation of calcium silicate hydrates. Cement and Concrete Research, 36(2): 227-237.

Taylor, H.F.W. (1990) Cement Chemistry. Academic Press Limited, San Diego, California.

Thomas, J.J., Jennings, H.M. (1998) Free-energy-based model of chemical equilibria in the CaO-SiO_2-H_2O system. Journal of the American Ceramic Society, 81(3): 606-612.

Tournassat, C., Appelo, C.A.J. (2011) Modelling approaches for anion-exclusion in compacted Na-bentonite. Geochimica et Cosmochimica Acta 75, 3698-3710.

Trotignon, L., Devallois, V., Peycelon, H., Tiffreau, C., Bourbon, X. (2007) Predicting the long term durability of concrete engineered barriers in a geological repository for radioactive waste. Physics and Chemistry of the Earth, 32(1-7): 259-274.

Trotignon, L., Peycelon, H., Bourbon, X. (2006) Comparison of performance of concrete barriers in a clayey geological medium. Physics and Chemistry of the Earth, 31(10-14): 610-617.

Trotignon, L., Peycelon, H., Cranga, M., Adenot, F. (1999) Modelling of the interaction between an engineered clay barrier and concrete structures in a deep storage vault. Scientific Basis for Nuclear Waste Management Xxii, 556: 607-614.

UFD (2012) Office of Used Fuel Disposition International Program — Strategic Plan (2013) April 2012, U.S. Department of Energy.

van Genuchten, M.T. (1980) A closed-form equation for predicting the hydraulic conductivity of unsaturated soils. Soil Sci Soc Am J 1980, 44, 892-898.

Villar, M.V. (2012) THM Cells for the HE-E Test: Setup and First Results; PEBS Report D2.2.7a. CIEMAT Technical Report CIEMAT/DMA/2G210/03/2012; Euratom 7th Framework Programme Project: PEBS: Madrid, Spain.

Wang, L., Jacques, D., De Cannière, P. (2010) Effects of an alkaline plume on the Boom Clay as a potential host formation for geological disposal of radioactive waste, External Report SCK•CEN-ER-28, SCK•CEN, Belgium, 194 pp.

Wang, Y., Gardner, P., Reimus, S., Painter, S., Makedonska, N., Pollack , A., Houseworth, J., Rutqvist, J., Asahina, D., Chen, F., Vilarrasa, V., Liu, H. H., Birkholzer, J., Begg, J. D., Zavarin, M., Kersting, A., Kim, G.-Y. (2013) Natural System Evaluation and Tool Development - International Collaborations: FY13 Progress Report, FCRD-UFD-2013-000628, Sandia National Laboratories, U.S. Department of Energy, 153 pp.

Wersin, P., Curti, E. Appelo, C.A.J. (2004) Modelling bentonite-water interactions at high solid/liquid ratios: swelling and diffuse double layer effects. Applied Clay Science 26, 249-257.

Wileveau, Y. (2005) THM behaviour of host rock: (HE-D experiment): Progress Report September 2003 – October 2004. Mont Terri Project, TR 2005-03.

Wileveau, Y., Rothfuchs, T. (2007) THM behaviour of host rock (HE-D) Experiment: Study of Thermal effects on Opalinus Clay. Mont Terri Project, TR 2006-01.

Wolery, T.J., Jové Colón, C.F. (2007) Qualification of Thermodynamic Data for Geochemical Modeling of Mineral–Water Interactions in Dilute Systems (ANL-WIS-GS-000003 REV 01). Sandia National Laboratories; OCRWM Lead Laboratory for Repository Systems, Las Vegas, Nevada, 412 pp.

Yang, C., Samper, J., Montenegro, L. (2008) A coupled non-isothermal reactive transport model for long-term geochemical evolution of a HLW repository in clay. Environmental Geology, 53(8): 1627-1638.

Zaccai, G., Jacrot, B. (1983) Small Angle Neutron Scattering. Annual review of biophysics and bioengineering, 12(1): 139-157.